Higher partial wave and dipolar confinement-induced resonances

Dissertation

zur Erlangung des Doktorgrades

des Department Physik

der Universität Hamburg

vorgelegt von

Panagiotis Giannakeas

aus Athen

Hamburg

2013

Gutachter der Dissertation:	Prof. Dr. P. Schmelcher Prof. Dr. R. Santra
Gutachter der Disputation:	Prof. Dr. P. Schmelcher Prof. Dr. H. Moritz
Datum der Disputation:	12. August 2013
Vorsitzender des Prfungsausschusses:	Dr. habil. M. Martins
Vorsitzender des Promotionsausschusses:	Prof. Dr. P. Hauschildt
Dekan der Fakultt fr Mathematik, Informatik und Naturwissenschaften:	Prof. Dr. H. Graener

Zusammenfassung

In dieser Arbeit werden binäre Kollisionen ultrakalter unpolarer sowie ultrakalter dipolarer Atome in quasi-eindimensionalen Wellenleitern mit harmonischen Fallenpotential in den transversalen Richtungen studiert. Hierzu wurde ein nicht-perturbativer Formalismus für die Behandlung von Vielkanal-Kollisionen in quasi-eindimensionalen Fallengeometrien entwickelt. Dieser Zugang basiert auf dem K-Matrix Formalismus, wobei auch höhere Drehimpulseigenzustände und deren direkte Kopplung berücksichtigt werden. Mit Hilfe dieses Formalismus wurden binäre Kollisionen zwischen ultrakalten unpolaren Atomen unter Berücksichtigung höherer Partialwellen studiert. Hierbei wurde das Phänomen der l-Wellen "confinement-induced resonances" beobachtet, welches zu einer - verglichen mit reinen s-Wellen confinement-induced resonances - reichhaltigeren Resonanzstruktur führt. In analoger Weise wurden für binäre Kollisionen ultrakalter Dipole in harmonischen Wellenleitern eine Reihe von dipolaren confinement-induced resonances gefunden, welche verschiedenen l-Wellen Zuständen zugeordnet werden können. Darüber hinaus wurde die Auswirkung der Anisotropie der dipolaren Wechselwirkung auf confinement-induced resonances charakterisiert. Unser theoretischer Zugang zu den beiden obigen Systemen geht weit über die bisherigen Studien hinaus, da die Restriktionen, die mit der sonst üblichen Pseudopotential-Theorie einhergehen, vermieden werden. Insbesondere erlaubt uns der Zugang, analytisch die Resonanzbedingungen herzuleiten. Die analytischen Resultate für beide Systeme stehen in exzellenter Übereinstimmung mit den korrespondierenden exakten numerischen Simulationen.

Abstract

In this thesis ultracold atom-atom and dipole-dipole collisions in the presence of a transversally harmonic waveguide are studied. A non- perturbative theoretical framework for multichannel collisions within quasi-one-dimensional geometries is developed. This treatment is based on K-matrix formalism where we included higher angular momentum states and their direct couplings. Within this framework we investigate atomic collisions with higher partial wave interactions, where the effect of ℓ-wave confinement-induced resonances is observed. This provides us with a richer resonance structure, which may attribute new properties to ultracold gases, i.e. many-body systems. Similarly, for dipolar collisions in the presence of a harmonic waveguide we observed sequences of dipolar confinement-induced resonances, which are attributed to different ℓ-wave states. Moreover, we unravel the impact of the anisotropy of the dipolar interactions on confinement-induced resonances. In both systems our study provides us

with analytically derived resonance conditions going beyond previous studies, since our framework avoids the limitations of pseudopotential theory. The obtained analytical results for both systems are in excellent agreement with the corresponding exact numerical simulations.

To my family and Eleni

Contents

Introduction

Breaking the silence of an ancient pond, a frog jumped into water - A deep resonance. "Matsuo Bashô: Frog Haiku (1686)"

Leucippus and Democritus[1] conceived the idea that matter is structured by elementary building blocks, the so-called atoms. Even more, they assumed that between atoms there is only empty space where the atoms have the property of motion. This fascinating idea lead them to the assumption that the moving atoms collide with each other structuring in this manner the matter that surrounds us.

This thought provoking idea may lead us to the consideration that the collision properties are essentially crucial in order to understand the underlying physics or even to manipulate large atomic ensembles. In the recent years ultracold atomic physics proved to be a suitable "playground" in order to test or exploit such ideas. More specifically, the highly sophisticated experimental techniques allow us to cool down the motion of atoms to nanokelvin temperatures [1]. At these ultra-low temperatures an atomic gas of bosons[2] become quantum degenerate since the de-Broglie wavelength of the bosons exceeds their interparticle distance and therefore all the atoms of bosonic symmetry behave collectively as one "super atom". This state of matter is the so-called Bose-Einstein condensate (BEC), which was theoretically predicted by Satyendra Nath Bose and Albert Einstein in 1924-25 [2] for the case of a non-interacting and homogeneous[3] gas of bosons. The first BEC of ultracold bosonic atoms was realized seventy years later, in 1995 [3]. The experiments are performed in a harmonic trapping potential which spatially confines the cloud and the bosons interact with each other by performing collisions. The interactions have a twofold role in the formation of a BEC. Firstly, they allow the thermalization of the atomic cloud which is important in order to cool it down. Secondly, the BEC might be lost either because of attractive interactions among the bosons yielding the collapse of the atomic cloud or because of strong interactions enhancing inelastic collisions which result into loss of atoms from the trap. However, by means of magnetic Fano-Feshbach resonances [4] the experimentalists

[1] Lecippus leaved the first half of 5th century BCE and was one of the earliest Greek philosophers who developed the idea of atomism, which was analyzed in further detail by his student, Democritus.

[2] Bosons (fermions) are atoms where the total number of nucleons (protons and neutrons) and electrons is even (odd).

[3] Homogeneous means that the particles move freely in the three-dimensional space without any external potential being applied.

are able to tune the the strength and the sign atom-atom interactions controlling in this manner their collisional properties.

Nowadays, these pioneering experiments have evolved into the next generation of quantum technologies which experimentally allow us to create and manipulate low dimensional ultracold gases [5, 6] either of bosonic or fermionic symmetry [7]. An excellent paradigm constitutes the Tonks-Girardeau gas which was theoretically predicted by L. Tonks and M.D. Girardeau [8]. The Tonks-Girardeau gas is a one dimensional gas of bosons which infinitely repel each other. A fundamental property of the Tonks-Girardeau gas is the fermionization of the bosons, where they cannot interchange places due to infinite repulsion and therefore they behave like non-interacting fermions with respect to local observables. Although the momentum distribution of this gas of impenetrable bosons differ from the corresponding distribution of non-interacting fermions.

One might reasonably think that this exotic system can be experimentally realized in quasi-one-dimensional confining potentials which effectively restrict the bosonic ensemble to one dimension. However, from this consideration two important points arise: (i) what is the impact of the reduced dimensionality on the collisional properties of such a system and (ii) how are the effective interparticle interactions affected. Answering these questions Olsanii and Bergeman *et al.* in their seminal works [9, 10] studied two-body bosonic and elastic[4] collisions in quasi-one-dimensional geometries, namely in transverse harmonic waveguides. Due to the external confining potential the scattering process is modified yielding the effect of confinement-induced resonances (CIRs). This particular type of resonances fulfill a Fano-Feshbach scenario, which occur when the s-wave scattering length (a_s) becomes comparable to the length of the transversal confinement ($a_\perp$), namely $a_s/a_\perp = 0.68$. This means that for a given scattering length the two-body interactions can become infinitely strong simply by adjusting the confinement. Moreover, it was shown that this system can be described effectively by a one dimensional Hamiltonian where the two-body interactions are modeled by a one-dimensional δ function multiplied with a coupling constant g_{1D}. This coupling constant, $g_{1D} = 2\hbar^2 a_s/[\mu a_\perp(a_\perp - 0.68a_s)]$[5] , defines the strength and the sign of the interactions containing all the relevant scattering information of the quasi-one-dimensional Hamiltonian. In fact, by means of the CIR effect the Tonks-Girardeu gas was experimentally realized in 2004 [11]. Even more, Haller *et al.* utilized the CIR effect in order to realize experimentally the excited many-body state of the Tonks-Girardeau gas, the so-called super Tonks-Girardeau gas phase [12]. In the super Tonks-Girardeau gas the bosons interact with infinite attraction without collapsing.

In view of the importance of CIR effect for the bosonic gases, a plethora of theoretical efforts are concentrated the recent years on unraveling the underlying collisional physics of indistinguishable or distinguishable atoms in confinement-induced processes for various setups such as collisions which involve inelastic processes that alter the character of CIRs [13, 14, 15, 16], scattering in anharmonic waveguides or lattices which

[4]Elastic collisions here means that during the collisions the bosons do not populate any of the excited modes of the transverse confinement.

[5]The quantity μ refers to the reduced mass of the two bosons.

couple the center of mass and relative degrees of freedom [17, 18, 19, 20, 21, 22, 23] or atom-dimer and dimer-dimer collisions [24, 25, 26] within a harmonic waveguide. The concept of CIRs has also been investigated in collisional systems in the presence of two-dimensional harmonic waveguides [27, 28], in mixed dimensions [29] or an arbitrary transversal potential [30]. A lot of attention has attracted also collisional systems which involve interactions beyond the s-wave yielding the generalization of CIR physics [31, 32, 33, 34, 35, 36]. Apart from atom-atom collisions, the theoretical studies have focused also on the case of dipolar scattering within either a harmonic quasi-one-dimensional [37, 38] or a quasi-two dimensional waveguides [39], where now the long-range and anisotropic dipolar interactions yield new properties in CIRs.

In addition, the immense experimental progress permitted to explore the corresponding physics of CIRs. Haller *et al.* realized experimentally bosonic collisions within anisotropic waveguides, where it was observed that the CIR effect split into two components [40]. More recently, a detailed experimental investigation was provided regarding the mechanism which induces the splitting of CIRs [41]. According to the theoretical and experimental observations the split of CIR arises due to the weak anharmonicity of the trapping potential which in turn couples the center of mass and relative degrees of freedom. Confirming the theoretical predictions p- and s-wave CIRs in quasi-one and two-dimensional waveguides have been also explored in experiments [42, 43]. Apart from waveguide-like confining potentials, Lamporesi *et al.* observed CIRs in optical lattices as well [44]. The extra handling of the scattering processes due to the confinement allowed the experimentalists to realize ultracold gases of reactive polar molecules [45, 46, 47]. This is achieved by the specific confining trap geometry, which suppresses the chemical reactions among the polar molecules.

It becomes evident that the understanding of the collisional physics of the low-dimensional ultracold gases provides us with essential insights in order to manipulate or even to design new many-body phases by means of the confinement. Hence, in this thesis the main goal is the development of a non-perturbative theoretical framework for multichannel scattering processes within a quasi-one-dimensional waveguide geometry. This framework is based on the K-matrix formalism and the idea of local frame transformations, which incorporates contributions from higher angular momentum states avoiding the limitations of pseudopotential theory. We applied this treatment on higher partial wave scattering with two-body isotropic interactions and on dipolar collisions yielding the prediction of ℓ-wave CIRs and dipolar CIRs, respectively. Transition diagrams are developed as well which provide us with a classification of virtual processes that the atoms or dipoles undergo during the collision contributing to the corresponding resonant mechanisms. The rigorousness of this approach deepens the theoretical understanding on the collisional properties of the corresponding systems and its quantitative results, i.e. their resonance conditions, may constitute a key ingredient in order to probe new strongly correlated many-body phases in low-dimensional gases.

Outline

In chapter 1 we discuss the aspects of two-body collisions in the free space and its main objective is to overview the various concepts of the two-body scattering theory which we will use in the rest of the thesis.

In chapter 2 we discuss the scattering theory within quasi-one-dimensional waveguides and we analyze in detail the effect of CIRs and its interpretation. Moreover, we provide an overview on theoretical and experimental efforts on CIR physics. In sections 2.3 and 2.4 we consider a system of atoms within a harmonic waveguide, which scatter with higher partial wave interactions. More specifically, in section 2.3 we investigate this system numerically and in section 2.4 we analyze its modeling within the pseudopotential theory. By comparing the exact numerical calculations with the results of the pseudopotential theory a qualitative agreement is observed for the case of weak confinement. In the case of strong confinement however the pseudopotential theory breaks down.

In view of these theoretical difficulties, in chapter 3 we discuss and thoroughly analyze the development of a non-perturbative theoretical framework that avoids the shortcomings of pseudopotential theory. This treatment as we mentioned above is based on the K-matrix formalism and local frame transformations where all the higher angular momentum states are included. Applying this on higher partial wave scattering in harmonic waveguides we predict the effect of ℓ-wave CIRs and we analytically derive their resonance conditions. The analytical results are in excellent quantitative agreement with the corresponding numerical simulations.

In chapter 4 we extend the K-matrix approach by including not only the higher angular momentum states but also their in between couplings. This enables us to investigate systems where the two-body interactions are anisotropic. Hence, we consider dipolar collisions in the presence of a harmonic waveguide investigating in this manner the impact of the anisotropy of dipolar interaction on the CIR physics. We observe the effect of ℓ-wave dipolar CIRs and we analytically derived their resonance conditions. In contrast to the CIRs of non-dipolar collisions we observed that the positions of dipolar CIRs are sensitive to the strength of the dipolar interactions. This sensitivity arises due to an interplay of the anisotropy of the dipole-dipole interaction with the confinement. The analytical results of the K-matrix approach are compared with exact numerical simulations showing an excellent quantitative agreement.

In chapter 5 we provide the summary of the thesis and we discuss as well future research opportunities on more complicated systems, such as reactive polar molecules, non-polarized dipoles or atoms that interact with relativistic interactions (e.g. spin-spin or second order spin-orbit interactions). An interesting direction is also to extend the K-matrix approach for confining trapping potentials of different dimensionality.

Chapter 1

Quantum collisions in free space

In this chapter we will discuss and analyze the principles of the quantum scattering theory for two-body collisions in free space. With the term "free space" we declare that there are no further external fields acting on the colliding pair. This chapter mainly consists of a composition of Refs. [48, 49, 50, 51, 52, 53] and its main objective is to clarify and remind the reader of the various concepts of scattering theory that we will use in the rest of this thesis.

1.1 Hamiltonian of the two-body collisions

We consider the case of either two spinless alkali-atoms or alkali-atoms in the same spin state, with momentums, i.e. $\mathbf{p}_1$ and $\mathbf{p}_2$, assuming that they behave as free particles when they are far away each other, before and after the collision. However, when the two atoms are close enough, they interact via a spherically symmetric two-body interaction $V(\mathbf{r}_1 - \mathbf{r}_2)$, where $\mathbf{r}_1$ and $\mathbf{r}_2$ describe the position of each atom respectively. Hence, the corresponding Hamiltonian which fully describes the physical process of the two-body collisions is written as follows:

$$H_{\text{total}} = \frac{\mathbf{p}_1^2}{2m_1} + \frac{\mathbf{p}_2^2}{2m_2} + V(\mathbf{r}_1 - \mathbf{r}_2), \tag{1.1}$$

where m_1 and m_2 are the masses of the two atoms assuming $m_1 = m_2 = m$.

At first sight the two-body Hamiltonian in Eq. (1.1) is not very appealing since it is formulated in a rather complicated Hilbert space $\mathscr{H}_1 = \mathscr{L}^2(\mathbb{R}^6)$. Its form becomes simpler, by introducing the center-of-mass (COM) and relative frame of reference following the same procedure as in classical mechanics:

$$H_{\text{total}} = H_{\text{COM}} + H_{\text{relative}} = \frac{\mathbf{P}^2}{2M} + \frac{\mathbf{p}^2}{2\mu} + V(\mathbf{r}), \tag{1.2}$$

with $M = 2m$ being the total mass and $\mu = m/2$ being the reduced mass of the system of atoms. $\mathbf{R}$ ($\mathbf{r}$) is the COM coordinate (relative coordinate) and $\mathbf{P}$ ($\mathbf{p}$) is the

total momentum (relative momentum) and are related to each particle's momenta and positions according to the expressions:

$$\begin{aligned} \mathbf{R} &= \frac{\mathbf{r}_1+\mathbf{r}_2}{2}, \quad \mathbf{r}=\mathbf{r}_1-\mathbf{r}_2 \\ \mathbf{P} &= \mathbf{p}_1+\mathbf{p}_2, \quad \mathbf{p}=\frac{\mathbf{p}_1-\mathbf{p}_2}{2}, \end{aligned} \tag{1.3}$$

One immediately observes that in the Hamiltonian Eq. (1.2) the COM is fully decoupled from the relative motion. The latter simply means that the entire collisional process of the two atoms is described completely by the relative motion where the corresponding Hamiltonian $H \equiv H_{\text{relative}}$ belongs in the $\mathscr{H}_2 = \mathscr{L}^2(\mathbb{R}^3)$ Hilbert space. Thus, H corresponds to a fictitious particle with momentum $\mathbf{p}$ and mass μ being scattered off by a potential $V(\mathbf{r})$ placed at the origin, namely $\mathbf{r}=0$. In addition, due to Eq. (1.2) the two-body wave function of the scattering problem has the following form:

$$\Psi(\mathbf{r}_1,\mathbf{r}_2) = e^{i\mathbf{P}\cdot\mathbf{R}/\hbar}\psi(\mathbf{r}), \tag{1.4}$$

where $\psi(\mathbf{r})$ refers to the wave function of the relative motion. Having expressed the two-body Hamiltonian in the COM frame of reference we are interested now to formulate in more detail the Schrödinger equation and the corresponding boundary conditions that describe the scattering of a single particle by a central force potential. This is the main aim of the following section.

1.2 Stationary Schrödinger equation: Boundary conditions and scattering observables

The time-independent Schrödinger equation from Eqs. (1.2) and (1.4) reads:

$$\left[\frac{\mathbf{p}^2}{2\mu}+V(\mathbf{r})\right]\psi(\mathbf{r}) = E\psi(\mathbf{r}), \tag{1.5}$$

where we assume that $V(\mathbf{r})$ is a spherically symmetric potential, namely $V(\mathbf{r})=V(r)$.

In order to ensure that Eq. (1.5) indeed describes a scattering process one has to formulate the corresponding boundary conditions which the wave function $\psi(\mathbf{r})$ has to fulfill. These boundary conditions can be, intuitively, constructed from the properties of the spherically symmetric interatomic potential $V(r)$. Towards this direction it is essential to analyze the properties which the $V(r)$ potential satisfies. These are mainly determined by the fact that the two atoms should behave asymptotically ($\mathbf{r}\to\infty$) as free particles and for spherically symmetric potentials can be expressed and classified

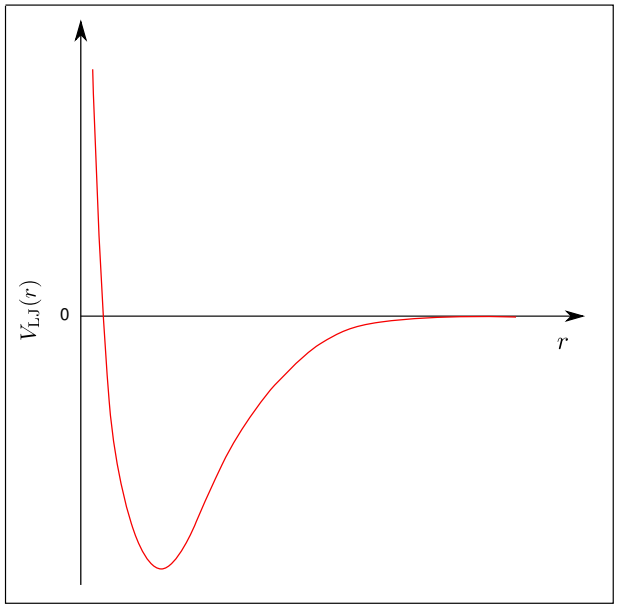

Figure 1.1: A schematic illustration of the Lennard-Jones 6-12 potential.

in a compact form by a set of three properties:

$$\begin{aligned} &\text{(i)} && V(r) = O(r^{-3-\epsilon}) \ \text{ as } \ r \to \infty \ \ (\epsilon > 0) \\ &\text{(ii)} && V(r) = O(r^{-2+\epsilon}) \ \text{ as } \ r \to 0 \ \ (\epsilon > 0) \\ &\text{(iii)} && V(r) \ \text{ is continuous for } \ 0 < r < \infty \end{aligned}$$

where the statements above stand for: (i) means that the two-body potential falling faster than r^{-3} at infinity; (ii) $V(r)$ being less singular than r^{-2} at the origin; and (iii) $V(r)$ being smooth in between. Thus, statement (i) excludes completely the Coulomb and the dipole-dipole potentials which we will regard them as *long-range* potentials. Repulsively singular potentials at the origin can be included in the scattering theory by means of Wentzel-Kramers-Brillouin theory as was shown in [48].

Specifying now the nature of the two-body interactions we assume that the collisions of the neutral atoms are described in good approximation by a Lennard-Jones potential 6-12 which reads:

$$V_{\rm LJ}(r) = \frac{C_{12}}{r^{12}} - \frac{C_6}{r^6}, \tag{1.6}$$

where, as it is illustrated in Fig.1.1, at small separation distances r the interaction is strongly repulsive due to the overlap of the electronic clouds of the two atoms, whereas at large distances Eq. (1.6) is dominated by a weakly attractive part that stands for the van der Waals interactions. The $1/r^6$ dependence of the attractive part of the

$V_{\rm LJ}$ potential arises from a second order perturbation theory on the electrostatic forces between charge distributions of the neutral alkali-atoms. The C_6 coefficient is called *dispersion coefficient* and controls the strength of the van der Waals forces depending on the species of the atoms. The range of the $V_{LJ}(r)$ is denoted as $l_{\rm vdW} = (2\mu C_6/\hbar^2)^{1/4}$. The $1/r^{12}$ dependence of the repulsive part of the V_{LJ} potential does not have a certain physical origin and serves as a smooth cut-off boundary in order to avoid the unphysical collapse of the wave function at the origin due to the attractive $-C_6/r^6$ term.

Having determined the properties and the form of the two-body interactions we can now proceed to the investigation of the boundary conditions which the wave function $\psi(\mathbf{r})$ in Eq. (1.5) must satisfy. The first boundary condition is related to the behavior of the wave function at the origin. Due to the repulsive barrier of the Lennard-Jones potential close to the origin the wave function exponentially tends to zero, namely $\sim e^{-\frac{\sqrt{2\mu}C_{12}}{5\hbar}r^{-5}}$[1] .

$$\text{(I)} \quad \psi(\mathbf{r}) = 0 \quad \text{at} \quad \mathrm{r} = 0. \tag{1.7}$$

The second boundary condition is defined at namely the asymptotic regime, $\mathbf{r} \to \infty$. There, the two-body interactions vanish ($V_{LJ}(r) \to 0$) and the two atoms behave as free particles. The wave function in this region should be a combination of plane and spherical waves.

$$\text{(II)} \quad \psi(\mathbf{r}) = e^{i\mathbf{k}'\cdot\mathbf{r}} + f(\mathbf{k},\ \mathbf{k}')\frac{e^{ikr}}{r} \quad \text{at} \quad |\mathbf{r}| \to \infty. \tag{1.8}$$

The first term describes the incoming wave function with momentum $\mathbf{k}'$ and its direction is given by the scalar product $\mathbf{k}' \cdot \mathbf{r}$. The second one describes the part of the wave function which is scattered by the $V_{LJ}(r)$ potential. More specifically, the term e^{ikr}/r refers to an outgoing wave which vanishes due to its spherical spreading to all the directions of the three dimensional space.

The coefficient $f(\mathbf{k},\ \mathbf{k}')$ is called *scattering amplitude* and represents a measure of the distortion of the unperturbed wave function by the presence of the potential V_{LJ}. Obviously, the scattering amplitude depends on the energy of relative motion and the orientation of the vectors $\mathbf{k}$ and $\mathbf{k}'$. Since we have considered spherically symmetric interactions the scattering amplitude depends only on the θ angle between $\mathbf{k}$ and $\mathbf{k}'$ vectors and thus it reduces to the expression $f(\mathbf{k},\ \mathbf{k}') = f(k, \theta)$. An additional aspect of the scattering amplitude $f(k, \theta)$ is its connection with other scattering observables, such as the *differential cross section* and the *total cross section* whose importance lies in the fact that they are the main measurable observables in scattering experiments.

In order now to define the connection between these two new quantities and the scattering amplitude we consider the two cases of distinguishable and indistinguishable atoms. For distinguishable atoms the deferential cross section and total cross section are directly related to $f(\mathbf{k},\ \mathbf{k}')$ according to the following relations:

$$\frac{\mathrm{d}\sigma}{\mathrm{d}\Omega} = |f(\mathbf{k},\ \mathbf{k}')|^2 \quad \text{and} \quad \sigma = \int |\mathrm{f}(\mathbf{k},\ \mathbf{k}')|^2 \mathrm{d}\Omega, \tag{1.9}$$

[1]For further details see Ref.[48]

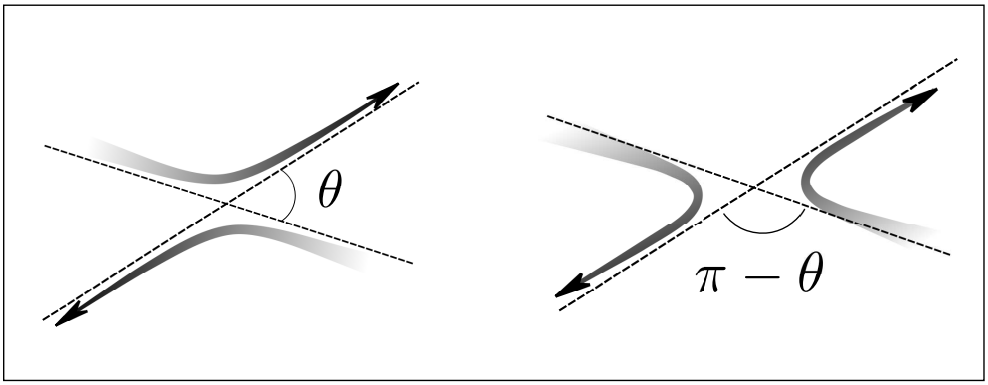

Figure 1.2: Scattering processes of identical particles yielding the same final state.

where $\mathrm{d}\Omega = \sin\theta\, \mathrm{d}\theta\, \mathrm{d}\phi$ is the solid angle element. Note that for a spherically symmetric potential the corresponding differential cross section and total cross section are obtained by substituting $f(\mathbf{k},\ \mathbf{k}')$ with $f(k,\theta)$ in Eq. (1.9). The physical interpretation of the total cross section is that it describes the percentage of the incident wave function which is scattered in all possible directions of the three dimensional space.

For indistinguishable, i.e. identical, atoms the two collision processes in Fig.1.2 correspond to the scattering amplitudes $f(k,\theta)$ and $f(k,\pi-\theta)$ respectively and cannot be distinguished since they yield the same final state. Consequently, in the evaluation of the differential and total cross section, one has to take the superposition of these two amplitudes, resulting in the following expressions:

$$\frac{\mathrm{d}\sigma}{\mathrm{d}\Omega} = |f(k,\theta) + \varepsilon f(k,\pi-\theta)|^2 \quad \text{and} \quad \sigma = \int |\mathrm{f(k},\theta) + \varepsilon \mathrm{f(k},\pi-\theta)|^2 \mathrm{d}\Omega, \tag{1.10}$$

with the constant $\varepsilon = \pm 1$ depending to whether we have bosonic or fermionic collisions leading to amplitudes with a positive or a negative overlap respectively. This difference arises from the fact that the two-body wave function $\Psi(\mathbf{r}_1,\mathbf{r}_2)$ in the case of bosons is symmetric under the exchange of the coordinates $\mathbf{r}_1$ and $\mathbf{r}_2$, namely $\Psi(\mathbf{r}_1,\mathbf{r}_2) = \Psi(\mathbf{r}_2,\mathbf{r}_1)$ whereas in the fermionic case it is antisymmetric, $\Psi(\mathbf{r}_1,\mathbf{r}_2) = -\Psi(\mathbf{r}_2,\mathbf{r}_1)$.

Finally, the total cross section can be expressed in terms of the imaginary part of the forward scattering amplitude irrespectively of the distinguishability of the atoms:

$$\sigma = \frac{4\pi}{k} \mathrm{Im\ f(k},\theta = 0), \tag{1.11}$$

where the term $1/k$ can be justified through a dimensional analysis since the total cross section has the units of a *length*^{2} and the scattering amplitude has the units of a *length*. Eq. (1.11) is the so-called *optical theorem* and its physical interpretation is based on the fact that the decreased amplitude of the incident wave function after the collision, represented by σ, emerges from the destructive interference of the incoming and outgoing wave function in the forward direction, described by the term $\mathrm{Im\ f(k},\theta = 0)$. The optical theorem represents therefore a direct result of the probability conservation.

1.3 Partial wave expansion

In order now to carry out a more detailed analysis of the two body scattering it is reasonable to exploit the spherical symmetry of the interatomic potential and expand the wave function of the relative motion on the angular momentum basis:

$$\psi(r) = \sum_{\ell=0}^{\infty} P_\ell(\cos\theta)\frac{u_{k,\ell}(r)}{r}, \tag{1.12}$$

where ℓ is the quantum number of the angular momentum, $P_\ell(\cos\theta)$ is the Legendre polynomial of ℓ-th order and k refers to the total colliding energy. Note that in the expansion of the wave function in Eq. (1.12) we have dropped the dependence on the azimuthial angle ϕ. This is permitted due to the specific symmetry of the potential. Substituting now Eq. (1.12) in the Schrödinger equation (see Eq. (1.5)) we obtain an effective one-dimensional Schrödinger equation for the radial wave functions $u_{k,\ell}(r)$:

$$\left[\frac{\mathrm{d}^2}{\mathrm{d}r^2} + k^2 - \frac{\ell(\ell+1)}{r^2} - \frac{2\mu}{\hbar^2}V_{LJ}(r)\right]u_{k,\ell}(r) = 0, \tag{1.13}$$

where $k = \sqrt{2\mu E/\hbar^2}$ refers to the total colliding energy and the term $\ell(\ell+1)/r^2$ is the *centrifugal barrier*. According to the boundary condition in Eq. (1.7) the radial wave function will be $u_{k,\ell}(0) = 0$ at $r = 0$ and therefore the term $\frac{u_{k,\ell}(r)}{r}$ is regular close to origin. In the asymptotic regime the boundary condition of Eq. (1.8) for the $u_{k,\ell}(r)$ wave function reads:

$$u_{k,\ell}(r) = \sqrt{\frac{2\mu k}{\pi\hbar^2}}r\Big[j_\ell(kr) - \tan\delta_\ell(k)\eta_\ell(kr)\Big], \tag{1.14}$$

where $j_\ell(kr)$ ($\eta_\ell(kr)$) are the spherical Bessel (von Neumann) functions and $\delta_\ell(k)$ is the *phase shift*. In an intuitive way, the phase shift represents the relative shift of the wave function due to the presence of the interatomic potential from the energetically corresponding free particle solution. In this manner all the relevant scattering information is embedded in the phase shifts. Note that the $u_{k,\ell}(r)$ fulfill the following orthogonality relation:

$$\int_0^\infty u^*_{k,\ell}(r)u_{k',\ell}(r)dr = \delta(E - E'), \tag{1.15}$$

meaning that radial wave functions $u_{k,\ell}(r)$ are *energy normalized*. The energy normalization provides us with a smooth behavior of the wave function close to the *threshold*, namely $E = 0$, where $u_{k,\ell}(r)$ might oscillate rapidly due to the presence of a weakly-bound state of the $V_{LJ}(r)$ potential.

Accordingly, the scattering amplitude in the angular momentum representation reads:

$$f(k,\theta) = \sum_{\ell=0}^{\infty}(2\ell+1)f_\ell(k)P_\ell(\cos\theta) = \frac{1}{2ik}\sum_{\ell=0}^{\infty}(2\ell+1)\big[S_\ell(k) - 1\big]P_\ell(\cos\theta), \tag{1.16}$$

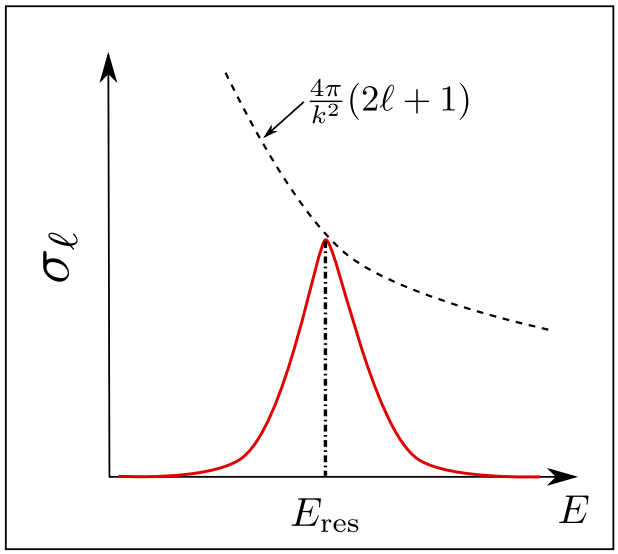

Figure 1.3: ℓ-wave cross section (solid red line) and unitarity limit (dashed line). The dashed-dotted line indicates the energy E_{res} where the partial cross section approaches the unitarity limit.

where $f_\ell(k)$ is the *partial wave scattering amplitude*, and $S_\ell(k) = e^{i2\delta_\ell(k)}$ is the *S-matrix* in the angular momentum representation, namely $S_\ell(k) =< E\ell m|S|E'\ell' m' >$. The *S*-matrix as we defined it above is a unitary matrix, $SS^\dagger = S^\dagger S = 1$. Hence, the *S*-matrix, actually, connects the incoming scattering states with the outgoing ones encapsulating in a simple manner the scattering properties of the interatomic potential through the phase shifts $\delta_\ell(k)$. Additionally, the S-matrix commutes with the unperturbed Hamiltonian, i.e. for $V_{LJ}(r) = 0$ and the total momentum $\mathbf{P}$ yielding the conservation of the energy and the momentum, respectively.

The total cross section in the angular momentum representation is expressed as follows:

$$\sigma = \sum_{\ell=0}^{\infty} \sigma_\ell = \frac{4\pi}{k^2} \sum_{\ell=0}^{\infty} (2\ell+1) \sin^2 \delta_\ell(k), \tag{1.17}$$

where σ_ℓ is the *partial wave cross sections*.

As Eq. (1.17) indicates, the maximum contribution of the partial wave cross section σ_ℓ for any angular momentum ℓ is bounded from above, namely $\sigma_\ell \leq \frac{4\pi}{k^2}(2\ell+1)$, where the equality is the so-called *unitarity limit*. The latter is a direct consequence of the S-matrix unitarity. Additionally, σ_ℓ tends to the unitarity limit if and only if the corresponding phase shift $\delta_\ell(k)$ is an odd multiple of $\pi/2$ and this is the case where *resonant scattering* occurs. This is illustrated in Fig.1.3 where schematically a particular σ_ℓ is indicated schematically by the red solid line as function of the colliding energy E. The unitarity limit is depicted by the dashed line and the dashed-dotted line refers to the energy $E_{\rm res}$ where the resonant scattering occurs. Note that in the case of

identical bosons or fermions Eq. (1.17) is multiplied by a factor 2 and the summation runs over even or odd ℓ partial waves respectively.

At this point we would like to discuss the behavior of the partial wave cross sections of any ℓ in high- or low-energies. First, we remark that at high-energies for $\ell \to \infty$, σ_ℓ goes to zero and $\delta_\ell(k)$ tends to a multiple of π. This could be intuitively understood by the fact that the kinetic energy dominates over the potential energy and consequently the atoms behave almost as free particles, namely $\sigma_\ell \to 0$. Now, we observe that for a given energy and $\ell \to \infty$ the partial wave cross section also tends to zero and $\delta_\ell \to n\pi$. In this case the repulsive centrifugal barrier becomes dominant enough and the wave function can not penetrate it in order to probe the actual interatomic potential. This conclusion leads us to the following estimation: for a given energy only a certain number of ℓ-wave states contributes significantly in the total cross section. The angular momentum states which are not contributing are given by the relation $\ell \gg k l_{\rm vdW}$ which we derive by setting the potential energy of the centrifugal barrier at distance $l_{\rm vdW}$ to be much larger than the colliding energy. One should note that this statement does not hold nearby resonances attributed to a certain ℓ-wave state. In such a case a particular partial wave cross section may contribute dominantly despite that $\ell \gg k l_{\rm vdW}$.

So far we have discussed and analyzed the behavior of the scattering process at high-energies. In the low-energy regime the colliding energy E approaches zero, which is the energy *threshold* ($E = 0$) for scattering processes, meaning that for energies below it the system is considered to be bound. Moreover, the bound states of the interatomic potential which lie nearby the threshold affect the collision properties of the atom-pair at low-energies. This intriguing threshold behavior of the atomic scattering constitutes the main subject of the following section.

1.4 The scattering properties of the low-energy regime

In the previous section we defined the phase shift $\delta_\ell(k)$ which obviously is a function of the total colliding energy. Thus in order to understand the properties of the collisions at low-energies $E = \hbar^2 k^2/2\mu$ it is essential to investigate how the phase shift of any ℓ depends on k. This dependence on the momentum as $k \to 0$ is called *Wigner threshold behavior*. Here we will consider for convenience the *Lippmann-Schwinger* equation for the radial wave function $u_{k,\ell}(r)$ for a general short-range potential $V(r)$[2] :

$$u_{k,\ell}(r) = \sqrt{\frac{2\mu k}{\pi\hbar^2}} r j_\ell(kr) + \int_0^\infty {\rm d}r' G_\ell(r', r) V(r') u_{k,\ell}(r'), \tag{1.18}$$

where $G_\ell(r', r)$ is the radial free particle Green's function, which reads:

$$G_\ell(r', r) = -\frac{2\mu k}{\hbar^2} \begin{cases} r j_\ell(kr) r' \eta_\ell(kr') & \text{for } r < r' \\ r' j_\ell(kr') r \eta_\ell(kr) & \text{for } r \geqslant r' \end{cases}$$

[2]Without loss of generality we assume initially that $V(r)$ falls off asymptotically faster than any power of r. Later we will define the threshold behavior of the colliding pair for $\sim 1/r^n$ potentials with $n > 3$.

The first term of Eq. (1.18) is the regular solution of the "homogeneous" Schrödinger equation ($V \equiv 0$). For $r \geqslant r'$, i.e. large separation distances, one can obtain an implicit equation for the phase shifts by inserting the corresponding expression of the free particle Green's function (Eq. (1.18)). Then the phase shifts are given according to the following expression:

$$\tan \delta_\ell(k) = -\sqrt{\frac{2\mu\pi k}{\hbar^2}} \int_0^\infty \mathrm{d}r' r' j_\ell(kr') V(r') u_{k,\ell}(r'). \tag{1.19}$$

Assuming that the potential $V(r)$ possesses no bound state, the wave function $u_{k,\ell}(r')$ close to the origin will not have a rapid oscillatory behavior. Thus, in a first order approximation the term $u_{k,\ell}(r')$ in Eq. (1.19) can be substituted by the regular solution $j_\ell(kr')$ yielding to the following relation:

$$\tan \delta_\ell(k) \approx -\frac{2\mu k}{\hbar^2} \int_0^\infty \mathrm{d}r' r'^2 j_\ell^2(kr') V(r'), \tag{1.20}$$

which constitutes the so-called *first-order Born approximation* and allows us to describe in an efficient way the properties of the phase shifts at low-energies. Moreover, Eq. (1.20) shows that for energies slightly above the threshold if the potential $V(r)$ is positive the phase shifts decreases and if $V(r) < 0$ the $\tan \delta_\ell(k)$ increases. The latter can be easily verified for a spherical well potential. However, we should mention at this point that this behavior of the phase shifts doesn't hold for potentials which are deep enough to support bound states.

Since $V(r)$ falls off asymptotically faster than any power of r we can extract the threshold behavior of the phase shifts. According to Eq. (1.20) for $kr \to 0$ the spherical Bessel $j_\ell(kr)$ is proportional of $(kr)^\ell$ and consequently the phase shifts $\delta_\ell(k)$ depend linearly on $k^{2\ell+1}$,

$$\delta_\ell(k) \xrightarrow[k\to 0]{} n\pi - a_\ell k^{2\ell+1}, \tag{1.21}$$

where the $k^{2\ell+1}$ energy dependence of the phase shifts is the Wigner threshold law, the term $n\pi$ emerges due to the modulo π ambiguity of the trigonometric functions and the term a_ℓ is some real constant, known as *scattering length*. Note that only for $\ell = 0$ this constant possesses the units of a length; nonetheless in the following we will use the same terminology for $\ell \neq 0$. As we will see below the scattering length is of exceptional importance since it permits us to retrieve information for the interatomic potential without knowing its specific details and thus characterizes the resonant phenomena of the collisional physics.

As we already mentioned above the general result of Eq. (1.21) is the first order Born approximation. A second order Born approximation results to additional energy corrections in Eq. (1.21). In total, the first and second order approximation yield the *effective range theory* [54, 55] with which one can describe more explicitly the near-threshold behavior of elastic collisions:

$$k^{2\ell+1} \cot \delta_\ell(k) = -\frac{1}{a_\ell} + \frac{1}{2} r_\ell k^2, \tag{1.22}$$

where r_ℓ is the *effective range parameter* and depends on the details of the potential $V(r)$.

At this point we should remark that Eqs. (1.21) and (1.22) do not hold for short range power law potentials, i.e. potentials that fall off as $\sim 1/r^n$ with $n > 3$. This can be understood by inserting the $V(r) \sim 1/r^n$ potential in Eq. (1.19). In this case even for small k the integral has contributions at large r leading to a divergence. Nevertheless, the Wigner threshold law can be generalized for inverse power potentials, where the threshold behavior of the phase shifts in Eq. (1.21) is still valid for $\ell < (n-3)/2$ whereas for $\ell > (n-3)/2$ we have that:

$$\tan \delta_\ell(k) \xrightarrow[k\to 0]{} O(k^{n-2}). \tag{1.23}$$

Eq. (1.23) manifests that the threshold behavior of the elastic scattering phase shifts is imposed only by the r-dependence of the tail of the interatomic potential.

Summarizing the results of the effective range theory for inverse power potentials leads us to the fact that the scattering length is only defined for $\ell < (n-3)/2$, where the integral in Eq. (1.20) converges. In a similar way, the convergence of the second order Born approximation, namely the condition $\ell < (n-5)/2$, ensures that the effective range parameter is well defined. However, Gao in Ref.[56] extends the effective range theory by means of the *quantum defect theory* permitting the definition of generalized scattering lengths and effective range parameters for any angular momentum ℓ.

Having understood so far the energy dependencies of the phase shifts at low-energy collisions it is instructive to calculate and study the s-wave scattering length and the corresponding wave function for the Lennard-Jones 6-12 potential. We focus only on the s-wave case since in the low-energy regime it is the only partial wave which contributes in the collisional process. Then the s-wave scattering length from Eq. (1.22) for $k \to 0$ reads:

$$a_s = -\lim_{k\to 0} \frac{\tan \delta_0(k)}{k} \tag{1.24}$$

By solving numerically the corresponding collision problem we calculate the phase shift related to the s-partial wave and from Eq. (1.24) for $k \to 0$ we obtain the scattering length.

Fig.1.4 illustrates the s-wave scattering length as function of the absolute value of the minimum of the Lennard-Jones potential, where the minimum is given by the expression, $V_{\min} = -C_6^2/4C_{12}$. We observe that as the potential minimum increases, i.e. becomes more attractive, the scattering length possesses divergences and abruptly changes its sign. These divergences are attributed to resonant phenomena which occur in low-energies and consequently are known as *zero-energy resonances*. The blue stars in Fig.1.4 indicate three cases for the s-wave scattering length (a) $a_s < 0$, (b) $a_s > 0$ and (c) $a_s = 0$. For these three cases the behavior of the wave function changes completely as Fig.1.5 depicts in panels (a)-(c).

In the case where the scattering length is negative we observe in Fig.1.5(a) that the scattering wave function (red solid line) possesses a phase shift less than $\pi/2$ from the free particle wave function (dashed line). This relation between the negative scattering

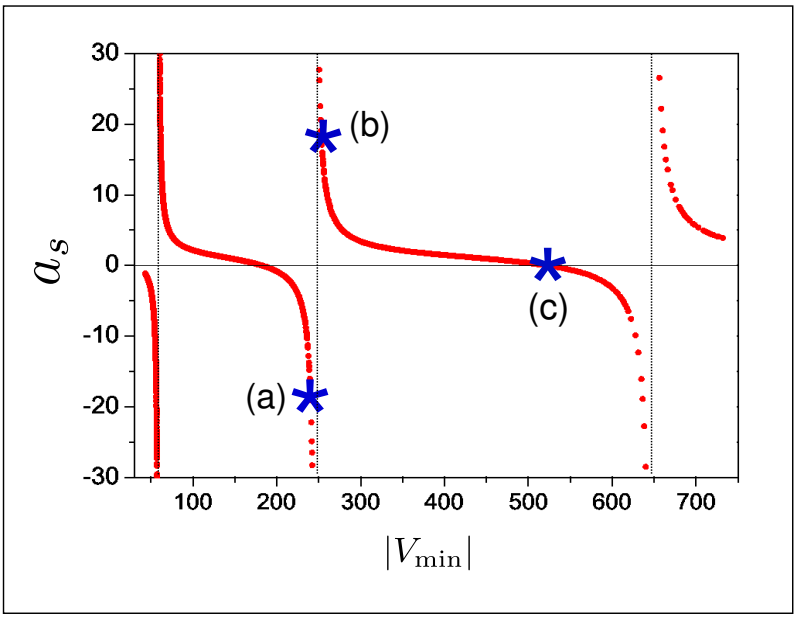

Figure 1.4: The scattering length a_s as a function of the minimum of the potential, $|V_{\min}|$. The dashed lines indicate the divergences of the scattering length and the blue asterisks refer to (a) $a_s < 0$, (b) $a_s > 0$ and (c) $a_s = 0$.

length and the corresponding phase shift can be understood in Fig.1.5(d) where we observe that for a phase shift less than $\pi/2$ the dotted line, which is the the asymptote of the scattering wave function, will intersect the horizontal axis at the negative values. This intersection point is the scattering length. Similarly, in Fig.1.5(b) the wave function is shifted more than $\pi/2$ from the free solution thus resulting in a positive scattering length. This occurs since the asymptote of the wave function illustrated in Fig.1.5(e) crosses the horizontal axis at its positive values yielding $a_s > 0$. In the case where $a_s = 0$ (see Fig.1.5(c)) we observe no phase lag between the scattering and free particle wave functions. Hence, the asymptote of the wave function crosses the horizontal axis at the origin (see Fig.1.5(f)).

Fig.1.6 provides us with intuitive pictures about the sign, the divergences and the zero crossings of the scattering length. More specific, Fig.1.6(a)-(c) depict the cases of $a_s < 0$, $a_s > 0$ and $a_s = 0$, where the solid green lines refer to the bound states of interatomic potential, the dashed green lines indicate the *virtual states*[3] and the blue fading area represents the *continuum*. In Fig.1.6(a) we observe that as the potential becomes attractive forms a virtual state just above the threshold which pulls the wave function towards to the origin resulting in a negative scattering length. By tuning the potential to be more attractive (see Fig.1.6(b)) the virtual state crosses the threshold

[3]With the term virtual states we refer to quasi-bound states.

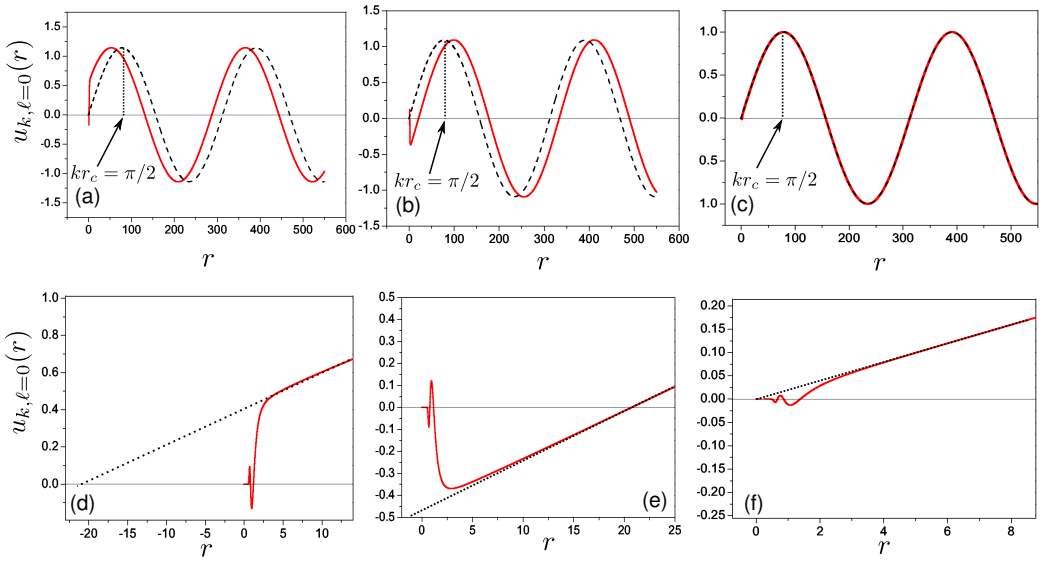

Figure 1.5: The radial wave function $u_{k,\ell=0}(r)$ versus the separation distance r. The panels (a)-(c) depict the wave function (red solid lines) being shifted from the free particle solution (dashed line) for the given scattering lengths (a)-(c) of Fig.1.4. The panels (d)-(f) consist zoom in plots close to the origin of panels (a)-(c), respectively. The dotted lines represent the asymptote of the wave function which intersects the horizontal axis to a point whose abscissa is the scattering length.

and becomes a true bound state slightly below the threshold, therefore the potential acts effectively as a repulsive one and pushes the wave function away from the origin yielding a positive scattering length. In Fig.1.6(c) the potential is more deep than the previous case and the corresponding bound state is away from the threshold whereas simultaneously the next virtual state approaches it. This leads to a destructive interference effect where the bound state repels the wave function from the origin and on the other hand the virtual state pulls the wave function close to it. The result of this interference is that the wave function behaves as if there is no potential yielding a zero scattering length. Note that this pattern of virtual state turning into bound repeats itself as the depth of the potential increases.

We have shown so far that the sign and the zero of the scattering length is related to the presence or not of a bound state nearby the threshold. Essentially, this means that the scattering length provides us with valuable and universal information for the spectrum of the interatomic potential around the threshold without addressing its details. Another aspect of a_s is its divergences which according to the intuitive pictures that we have discussed above emerge when the virtual state is right at the threshold. Consequently, this virtual state is transformed into a weakly bound state and the corresponding scattering length becomes singular. The resonances which are induced by

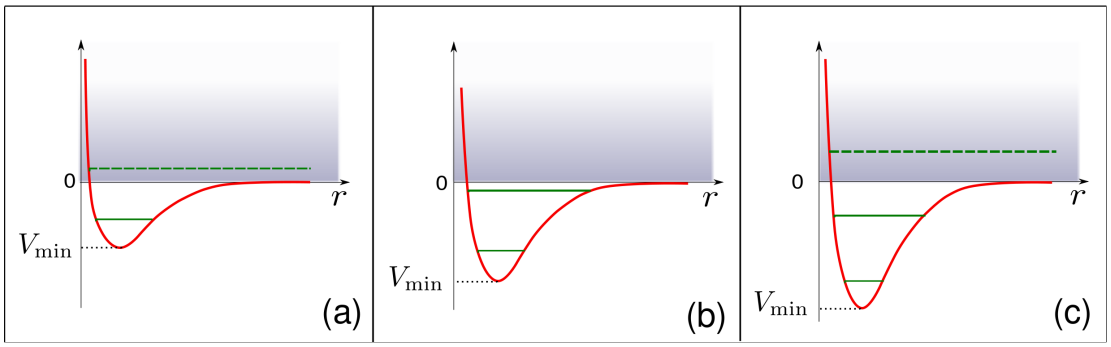

Figure 1.6: A schematic illustration of the $V_{LJ}(r)$ potential for the cases (a), (b) and (c) of Fig.1.4. The green solid (dashed) line refers to a bound (virtual) state and the fading blue area represents the continuum.

weakly bound states are referred to as zero-energy resonances. This remarkable relation between resonances and bound states turns out to be valid for any potential, and is known as the *Levinson's theorem*.

1.5 Resonances

An important feature of the resonant phenomena is that they provide us essentially with the ability to control the scattering length and therefore the interactions between the two atoms. In the previous section we investigated the two-body collisional properties in the low-energy regime. This insightful analysis resulted in the observation of the zero-energy resonances and lead us to an explicit determination of their physical origin. However, we should clarify that this is not the only resonant mechanism which appears in two-body collisions. The additional mechanisms on atom-atom scattering can be classified into two major categories: the *potential or shape resonances* and the *Fano-Feshbach resonances* [4]. The potential resonances appear in systems with one degree of freedom and from this perspective they do not differ much from the zero-energy resonances. On the contrary Fano-Feshbach resonances are manifested in systems which possess several degrees of freedom and their nature is intrinsically different from the case of the potential resonances.

1.5.1 Potential resonances

In this particular case the resonant phenomena occur due to a potential barrier which separates the configuration space into an inner and outer region which are located at small and large separation distances r, respectively.

As an instructive example of this situation we consider atomic collisions with angular momentum $\ell \neq 0$ where the two atoms interact via an effective potential emerging from

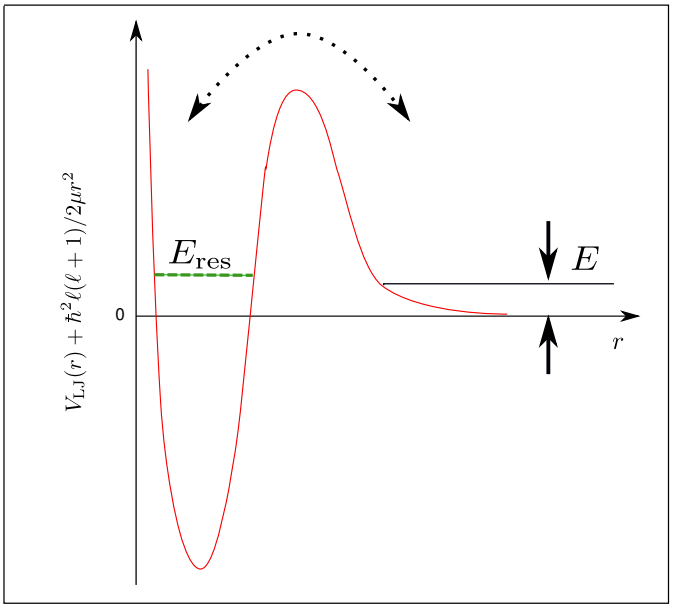

Figure 1.7: A schematic illustration of the effective potential, i.e. $V_{LJ}(r)$ with the centrifugal barrier for $\ell \neq 0$. The dashed green line indicates the quasi-bound state with energy $E_{\rm res}$, the solid black line refers to the energy E of the incoming wave function and the dotted double arrow depicts the coupling between the inner and outer region of the effective potential.

the repulsive centrifugal forces and the two-body interaction $V_{LJ}(r)$.

$$V_{\rm eff}(r) = V_{LJ}(r) + \frac{\hbar^2\ell(\ell+1)}{2\mu r^2}, \tag{1.25}$$

The potential of Eq. (1.25) is illustrated in Fig.1.7 indicated by the red line, where the repulsive barrier can be interpreted as a coupling (dotted double arrow) of the inner and outer regions. In the inner region the interplay of the centrifugal and the Lennard-Jones interactions results into a potential curve which supports bound and quasi-bound (green dashed line) states whose energy is negative or positive, respectively. The potential resonances which occur in such a set up are related to these quasi-bound states. More specific, the resonant mechanism is based on the fact that the energy of these states is very close to the energy E of the incoming two-body wave function. Thus, as the wave function approaches the repulsive barrier from the outer region, it penetrates it and becomes resonant with the corresponding quasi-bound state yielding a divergence in the scattering length or an enhanced peak in the cross section. The weakly bound states of the potential of Eq. (1.25) do not participate in any resonant mechanism. This can be understood from the fact that the weakly bound states energetically are placed below the threshold thus at these energies the $\sim 1/r^2$ tail of the potential in Eq. (1.25) shields completely the inner region and the wave function cannot probe it.

1.5.2 Fano-Feshbach resonances

Another important resonant mechanism is the Fano-Feshbach resonance. This particular type of resonances appears commonly in atomic and nuclear physics, and it has been extensively studied by physicists like Ugo Fano [57, 58, 59] and Herman Feshbach [60, 61]. In contrast to the zero- and potential resonances that we have discussed so far the Fano-Feshbach effect has a completely different origin. Specifically, the above mentioned resonant phenomena are considered in the framework of single channel scattering theory meaning that the two atoms do not possess any internal structure. The Fano-Feshbach effect occurs in systems where the colliding atoms have internal structure, namely spin degrees of freedom, and are better treated in the framework of the multichannel scattering theory.

In order to exemplify this type of resonances, we consider a system of two atoms where each one has composite spin degrees of freedom and the atom collision is performed in the low energy regime such that only the s-partial wave contributes. Then the corresponding wave function reads:

$$\psi(\mathbf{r}) = \sum_{\alpha} \frac{u_{\alpha,k,\ell=0}(r)}{r} P_{\ell=0}(\cos\theta) \left|\chi_{\alpha}\right\rangle \tag{1.26}$$

where $|\chi_\alpha\rangle$ is the wave function that describes the spin degrees of freedom. Additionally, the corresponding Hamiltonian is written as:

$$H = \frac{\mathbf{p}^2}{2\mu} + V_{LJ}(\mathbf{r}) + H^s + V^s(\mathbf{r}), \tag{1.27}$$

where the term H^s is the operator which acts only on the spin wave function, namely $H^s \left|\chi_\alpha\right\rangle = E_\alpha \left|\chi_\alpha\right\rangle$. The term $V^s(\mathbf{r})$ is the potential which couples the corresponding spin states χ_α with the radial wave function $u_{\alpha,k,0}(r)$. Then, the corresponding Schrödinger equation yields the following coupled form:

$$\left[-\frac{\hbar^2}{2\mu}\frac{d^2}{dr^2} + V_{LJ}(r) + V^s_{\alpha,\alpha}(r) + E_\alpha\right] u_{\alpha,k,0}(r) + \sum_{\alpha\neq\alpha'} V^s_{\alpha,\alpha'}(r) u_{\alpha',k,0}(r) = E u_{\alpha,k,0}(r), \tag{1.28}$$

where $E_\alpha = \left\langle\chi_\alpha\right| H_s \left|\chi_\alpha\right\rangle$ are the energies of the state $|\chi_\alpha\rangle$ which for our convenience we assume that are non-degenerate. In Eq. (1.28) we observe that it becomes fully decoupled when the off-diagonal terms $V^s_{\alpha,\alpha'}(r)$ vanish for $r \to \infty$ resulting in the following effective potential:

$$V_\alpha(r) = V_{LJ}(r) + V^s_{\alpha,\alpha}(r) + E_\alpha, \tag{1.29}$$

where each potential curve $V_\alpha(r)$ approaches the corresponding eigenvalue E_α as $r \to \infty$, defining in this manner a *channel*.

Having clarified the terminology of channels we can now distinguish them into energetically *open* or *closed channels*. We assume that a channel is open when the total colliding energy E of the atom pair is larger than a particular E_α eigenvalue,

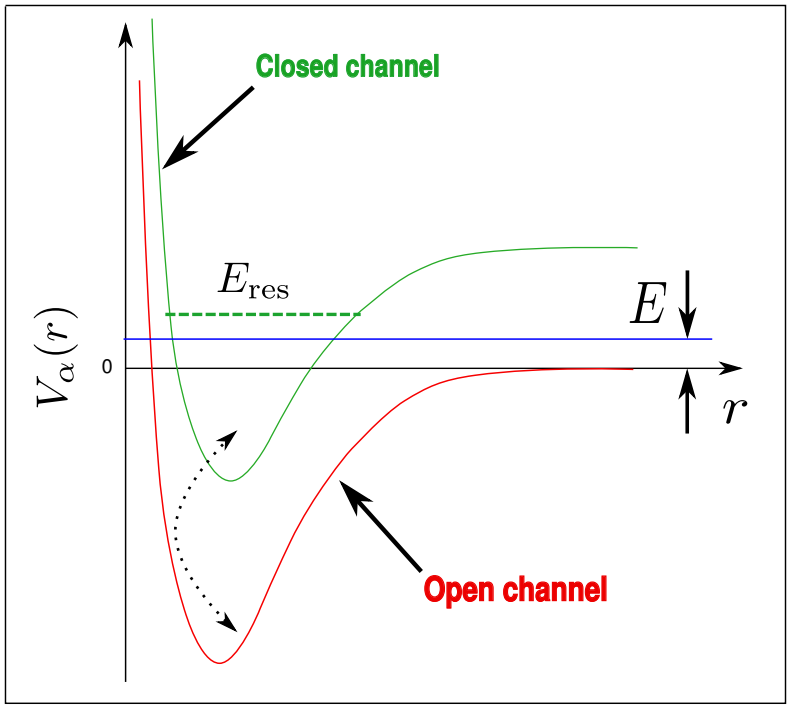

Figure 1.8: A schematic illustration of the Fano-Feshbach resonances for a two channel model: the open channel (red line) contains the total collisional energy E (blue line) of the incoming wave function and the closed channel (green line) whose threshold is energetically larger than E contains a bound state (green dashed line) which is very close to E. The dotted double arrow represents the coupling between the potential curves of the open and closed channel.

$E > E_\alpha$, whereas if $E < E_\alpha$ then we refer to the corresponding channel as a closed one. Consequently, the motion in the open channels is considered to be unbound, namely the radial wave function $u_{\alpha,k,0}(r)$ possesses an oscillatory behavior in the asymptotic regime, whereas in the case of closed channels the motion is bounded and the corresponding wave function vanishes as $r \to \infty$. From this perspective it becomes clear that the closed channels possess only bound states.

In the following, we restrict our discussion to the case of two channels, where one is considered to be open and the other one is closed. This two channel model is schematically represented in Fig.1.8, where the open (closed) channel is depicted by the red (green) potential curve. We observe that in the asymptotic regime there is an energy gap between the thresholds of the open and the closed channel, where the total colliding energy E (blue solid line) lies energetically just above the open channel. Additionally, the dotted double arrow represents the coupling namely it refers to the $V_{\alpha,\alpha'}$-terms in Eq. (1.28) among the red and green potential curves. The collision is performed in the open channel but due to the coupling terms a Fano-Feshbach resonance occurs

when the bound state of the closed channel (green dashed line) with energy $E_{\rm res}$ is energetically close enough to the total energy E of the open channel. Actually, in a nutshell we can say that the Fano-Feshbach scenario arises from the coupling of a discrete spectrum to a continuum. Obviously this scenario differs from the resonant mechanisms of the single-channel resonances, i.e. zero-energy and potential resonances which we have discussed in the previous sections. An additional difference between Fano-Feshbach and single-channel resonances consists in the corresponding line shape of their cross sections. The cross section for single-channel resonances possess a symmetric, Lorentzian-like line shape (see Fig.1.3 in section 1.3), whereas the line shape of the cross section for a Fano-Feshbach resonance is asymmetric. More specific, the cross section in this case possesses a peak and a minimum due to constructive and destructive interference, respectively, of the bound state with a continuum state.

The most fascinating feature of the Fano-Feshbach resonances is that they can be easily realized and probed in experiments, in contrast to the zero-energy and potential resonances. The controllability of this type of resonances permits us to control, by adjusting the s-wave scattering length, either the sign or the strength of the interactions of the atomic ensemble. The adjustment of the scattering length can be achieved either by tuning a magnetic or an optical Fano-Feshbach resonance [62, 63]. Apart from changing the two-body interactions, the Fano-Feshbach resonances can be used for the production of *ultracold molecules*, known as *Feshbach molecules* [64].

1.6 Pseudopotential theory

The pseudopotential approximation to the interatomic interaction is an ubiquitous tool for the theoretical description of ultracold gases. The atomic interactions are modeled in terms of a contact potential containing an additional operator known as the *regularization operator*. The basic idea of introducing delta potentials lies in the fact that the study of the macroscopic behavior of ultracold gases, for example, becomes complicated by using the real two-body potential. Thus in order to simplify the theoretical calculations we substitute the true interactions by structureless potentials, namely delta functions. These contact interactions are "normalized" in such a way that they mimic correctly the impact of the real potential on the wave function.

We will focus in the low-energy regime where the dominant s-wave interactions of the two-body collisions can be conveniently modeled by the following pseudopotential:

$$V_{\rm pseudo}(\mathbf{r}) = g\delta(\mathbf{r})\ \widehat{O}, \tag{1.30}$$

where g is the coupling constant and $\widehat{O}$ is the regularization operator, which acts on the wave function.

We would like to remark that the pseudopotential has this specific form for two reasons. The first of them lies in the fact that the "bare" delta function in three dimensions cannot lead to scattering. This can be conveniently understood by considering collisions with an impenetrable wall which has width R^*. Then the corresponding scattering length is equal to the width of the wall, namely $a_s = R^*$. Now in order to

recover the delta function we set the width of the impenetrable wall to go to zero ($R^* \to 0$). Consequently the scattering length goes to zero as well, meaning that no scattering can occur. Intuitively, we can think of the wave function going around the singularity of the delta function without being affected, since the configuration space is three dimensional.

On the other hand as we have mentioned above, Eq. (1.30) mimics by construction the behavior of a realistic potential. We recall that for the true interatomic potential the scattering wave function for s-partial waves is $\psi(r) = u_{k,0}(r)/r \sim 1 - a_s/r$. One can immediately observe that the action of the bare $\delta(\mathbf{r})$ on this wave function is meaningless, since it becomes singular as r tends to zero. Mainly, this "pathological" behavior arises from the fact that the delta function is zero everywhere except for $r = 0$. In this particular case the asymptotic regime is right after $r = 0$ where $\psi(r)$ diverges.[4] Hence, in order to recover such anomalies we introduce an operator $\widehat{O}$ which regularizes the wave function $\psi(r)$ of the real potential.

Having understood the importance of the operator $\widehat{O}$ we can now proceed and rigorously define it, together with the coupling constant g. As we have mentioned above the scattering wave function has the following form:

$$\psi(r) = \frac{u_{k,0}(r)}{r} \sim \frac{r - a_s}{r}, \tag{1.31}$$

where we observe that the reduced wave function $u_{k,0}(r)$ is regular at the origin.

It is obvious that $u_{k,0}(r)$ satisfies the Bethe-Peierls boundary condition [65] at the origin:

$$\left.\frac{u'_{k,0}(r)}{u_{k,0}(r)}\right|_{r=0} = -\frac{1}{a_s}, \tag{1.32}$$

The Schrödinger equation then reads:

$$-\frac{\hbar^2}{2\mu}\Delta\left(\frac{u_{k,0}(r)}{r}\right) + g\delta(\mathbf{r})\left(\widehat{O}\frac{u_{k,0}(r)}{r}\right) = E\frac{u_{k,0}(r)}{r} \tag{1.33}$$

Now we calculate the action of the Laplacian on $u_{k,0}(r)/r = u_{k,0}(0)/r + [u_{k,0}(r) - u_{k,0}(0)]/r$ which we modify according to Ref.[66], isolating in this manner the singular part of $u_{k,0}(r)/r$.

$$\Delta\left(\frac{u_{k,0}(0)}{r} + \frac{u_{k,0}(r) - u_{k,0}(0)}{r}\right) = -4\pi u_{k,0}(0)\delta(\mathbf{r}) + \frac{1}{r}u''_{k,0}(r) - \frac{1}{\hbar^2 r^2}\widehat{L}^2\left(\frac{u_{k,0}(r)}{r}\right), \tag{1.34}$$

where the Laplacian Δ is expressed in spherical coordinates. the second term in Eq. (1.34) refers to the centrifugal forces which in our case are zero since we have initially considered only s-partial wave contributions. Substituting Eq. (1.34) in Eq. (1.33) we get the following equation:

$$-\frac{\hbar^2}{2\mu}\frac{1}{r}u''_{k,0}(r) + \frac{2\pi\hbar^2}{\mu}u_{k,0}(0)\delta(\mathbf{r}) + g\delta(\mathbf{r})\left(\widehat{O}\frac{u_{k,0}(r)}{r}\right) = E\frac{u_{k,0}(r)}{r}. \tag{1.35}$$

[4] Note that in our previous discussions we did not face such difficulties since the interatomic potential possessed some structure and consequently $V(r) = 0$ at $r \to \infty$, where the wave function is well behaved.

By calculating the integral $\int_0^{\epsilon}(\ldots)4\pi r^2 dr$ of Eq. (1.35) and taking the limit of $\epsilon \to 0$ we obtain:

$$\frac{2\pi\hbar^2}{\mu}u_{k,0}(\epsilon \to 0) + g\left(\widehat{O}\frac{u_{k,0}(r)}{r}\right)\Big|_{r=0} = 0. \tag{1.36}$$

Now we substitute Eq. (1.32) in Eq. (1.36) and we get:

$$-\frac{2\pi\hbar^2}{\mu}a_s u'_{k,0}(\epsilon \to 0) + g\left(\widehat{O}\frac{u_{k,0}(r)}{r}\right)\Big|_{r=0} = 0 \tag{1.37}$$

or equivalently,

$$g\left(\widehat{O}\frac{u_{k,0}(r)}{r}\right)\Big|_{r=0} = \frac{2\pi\hbar^2 a_s}{\mu}\frac{d}{d\epsilon}\left(\epsilon \cdot \frac{u_{k,0}(\epsilon)}{\epsilon}\right)\Big|_{\epsilon=0} \equiv \frac{2\pi\hbar^2 a_s}{\mu}\frac{d}{dr}\left(r \cdot \frac{u_{k,0}(r)}{r}\right)\Big|_{r=0}, \tag{1.38}$$

from which we obtain the coupling constant $g = 2\pi\hbar^2 a_s/\mu$ and the expression for the regularization operator $\widehat{O} \equiv \frac{d}{dr}(r\cdot\quad)$. Hence, the pseudopotential of Eq. (1.30) can be rewritten as follows:

$$V_{\text{pseudo}}(r) = \frac{2\pi\hbar^2 a_s}{\mu}\delta(\mathbf{r})\frac{d}{dr}(r\cdot\quad), \tag{1.39}$$

which is known as the *Fermi-Huang's pseudopotential* [67, 68, 69].

1.7 Brief summary

In this chapter we have presented the main focus points of the non-relativistic quantum theory of two-body collisions. More specifically, we defined the corresponding scattering observables such as the scattering amplitude and the cross section and we have demonstrated the general aspects of the partial wave expansion. Additionally, we have studied the properties of the low-energy collisions yielding an insightful scattering parameter, the scattering length. We have clarified rigorously and with intuitive pictures the importance of the scattering length and its relation with the resonant scattering phenomena which in return result in the control of the two-body interactions. However, the discussion in this chapter has been restricted on two atom systems which interact in free space. Naturally one might wonder if the scattering process and the corresponding physics of such systems undergoes modifications in the presence of an external confinement. This is the point that we are going to address in detail in the following chapter.

Chapter 2

Ultracold collisions in quasi-one-dimensional geometries

Reduced dimensionality in degenerate ultracold atomic gases plays a key role for the experimental realization and theoretical investigation of exotic quantum phases such as the Tonks-Girardeau gas [8], which consists of a one-dimensional gas of impenetrable bosons repelling infinitely each other. The macroscopic properties of such many-body phases crucially depend on the collisional physics and the influence of the trapping potential. Hence, atomic collisions in quasi-one-dimensional waveguides constitute a fundamental system for studying the effects of the reduced dimensionality. Indeed, in two-body collisions, the confinement implies significant modifications on the scattering properties of the colliding pair. Existing theoretical studies on bosonic collisions show that resonant scattering can be induced by the confinement, yielding the so-called confinement-induced resonance (CIR) effect [70, 71]. A CIR emerges when the length scale of the confinement becomes comparable to the s-wave scattering length of the colliding bosons and it is interpreted as a Fano-Feshbach-like resonance. This remarkable effect paved the way for the experimental realization of the Tonks-Girardeau gas [11] and the Super-Tonks-Girardeau gas [12] in cigar-shaped traps. The latter is the equivalent of the Tonks-Girardeau gas with the interactions being infinitely attractive.

In this chapter we will discuss explicitly the effect of CIR clarifying its physical origin. In addition, we will briefly overview the confinement-induced processes in several systems providing a bird's eye on the current theoretical and experimental advances. In the last two subsections of this chapter we will focus on two-body collisions in the presence of a harmonic waveguide beyond the s-wave interactions including in this manner higher angular momentum contributions. This permits us to study the impact of the reduced dimensionality on the atomic pairs which interact with a certain angular momentum extending the scope of the CIR physics.

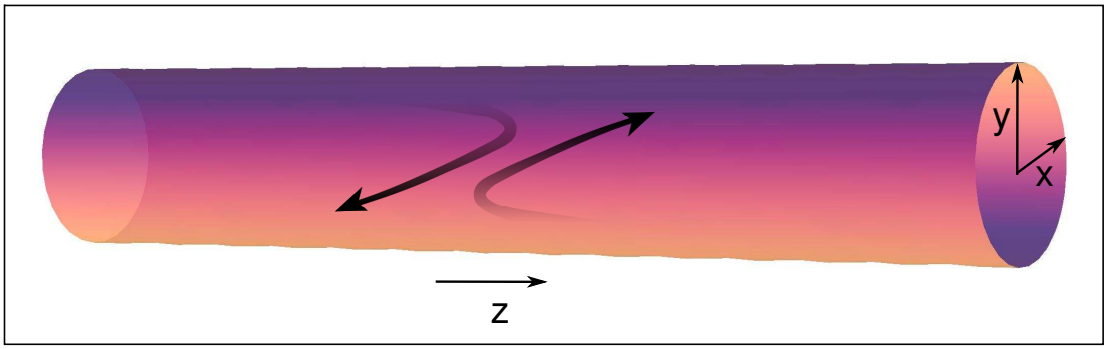

Figure 2.1: A schematic illustration of bosonic collisions in the presence of transversal harmonic waveguide.

2.1 s-wave interacting bosons in harmonic waveguides

In this section we will explicitly discuss the impact of the confinement on the scattering processes. As it was shown in the seminal work of Olshanii *et al.* [9], the resonant scattering in the presence of a confining potential yields a new type of resonances, namely CIR. Thus, in the following subsections we will mainly focus in studying the relevant physics and clarifying the physical origin of CIR.

2.1.1 Hamiltonian and scattering observables

We assume two-body collisions of identical bosons in a waveguide with their transversal degrees of freedom being confined by a harmonic oscillator potential. The harmonic confinement permits the separation of the center of mass and relative motion yielding a single-particle Hamiltonian with a scatterer fixed at the origin for the relative degree of freedom. The relative Hamiltonian expressed in cylindrical coordinates reads

$$H(z,\rho,\phi) = -\frac{\hbar^2}{2\mu}\left(\frac{\partial^2}{\partial z^2}+\frac{\partial^2}{\partial \rho^2}+\frac{1}{\rho}\frac{\partial}{\partial \rho}+\frac{1}{\rho^2}\frac{\partial^2}{\partial \phi^2}\right)+\frac{1}{2}\mu\omega_\perp^2\rho^2+V_{ps}(\mathbf{r}), \tag{2.1}$$

where $\mathbf{r}=\mathbf{r_1}-\mathbf{r_2}$ is the relative coordinate of the two bosons, and $V_{ps}(\mathbf{r})$ is the pseudopotential which models the s-wave interatomic interaction as we already discussed in the section 1.6 of chapter 1.

The symmetry of the transversal potential, $\frac{1}{2}\mu\omega_\perp^2\rho^2$, implies that the scattering solutions should be expanded in an axially symmetric basis. Such a basis set are the eigenstates of the two-dimensional (2D) harmonic oscillator which satisfy the following Schrödinger equation:

$$\left[-\frac{\hbar^2}{2\mu}\left(\frac{\partial^2}{\partial \rho^2}+\frac{1}{\rho}\frac{\partial}{\partial \rho}+\frac{1}{\rho^2}\frac{\partial^2}{\partial \phi^2}\right)+\frac{1}{2}\mu\omega_\perp^2\rho^2\right]\tilde{\Phi}_{n,m}(\rho,\phi)=E_{n,m}\tilde{\Phi}_{n,m}(\rho,\phi), \tag{2.2}$$

where $\tilde{\Phi}_{n,m}(\rho,\phi)$ are the eigenfunctions of the 2D harmonic oscillator, m is the azimuthal quantum number and $E_{n,m} = \hbar\omega_\perp(n+|m|+1)$ is the transversal energy spectrum of the 2D harmonic oscillator, with $n = 2n_\rho = 0, 2, 4, \ldots$ being the principal quantum number.

The spherical symmetry imprinted by the pseudopotential, $V_{ps}(\mathbf{r})$, leads to a separation of the azimuthal ϕ angle from the ρ coordinate in Eq.(2.2). The latter means that during the collision no virtual excitations will occur with respect to the m quantum number. However, virtual excitations will emerge with respect to the principal quantum number n, which will be taken into account in the calculation given below.

We focus on the single mode regime, where the collision takes place in the ground state of the transversal confinement with angular momentum $m = 0$ and represents the only "open channel". The latter means that the total energy of the pair collision is limited between the ground and the first excited axially symmetric transversal state

$$E_{n=0,m=0} \leqslant E < E_{n=2,m=0}. \tag{2.3}$$

Furthermore, the above-mentioned independence on the angle ϕ results in the following simplified Schrödinger equation of the corresponding Hamiltonian Eq. (2.1):

$$\left[-\frac{\hbar^2}{2\mu}\left(\frac{\partial^2}{\partial z^2}+\frac{\partial^2}{\partial\rho^2}+\frac{1}{\rho}\frac{\partial}{\partial\rho}\right)+\frac{1}{2}\mu\omega_\perp^2\rho^2+V_{ps}(\mathbf{r})\right]\Psi(z,\rho)=E\Psi(z,\rho), \tag{2.4}$$

where the colliding energy E asymptotically can be written as $E = E_\parallel + E_{n=0,m=0}$, which is defined as the sum of the longitudinal kinetic energy $E_\parallel = \dfrac{\hbar^2}{2\mu}k^2$ and the energy of the transverse ground state $E_{n=0,m=0} = \hbar\omega_\perp$. Hence, the eigenmode $n = 0$ of the transverse confinement will be considered as the energetically open channel, whereas the eigenmodes for $n \neq 0$ will be regarded as closed ones. Due to the constraint of Eq.(2.3) the momentum k is limited according to the relation $k < \sqrt{\dfrac{2\mu}{\hbar^2}\left(E_{n=2,m=0} - E_{n=0,m=0}\right)}$. Here, $\Psi(z,\rho)$ denotes the full 2D axially symmetric solution, which can be expanded in the $\tilde{\Phi}_{n,0}(\rho,\phi) \equiv \Phi_n(\rho)$ basis

$$\Psi(z,\rho) = \sum_{n=0}^{\infty} C_n(z)\Phi_n(\rho) \tag{2.5}$$

where we sum over all even n due to the bosonic symmetry.

Substituting Eq.(2.5) into Eq.(2.4), multiplying by $2\pi\rho\Phi_n^*(\rho)$, integrating and using Eq.(2.2) yields the following equation for the functions $C_n(z)$:

$$\left[-\frac{\hbar^2}{2\mu}\frac{\partial^2}{\partial z^2}+E_{n,m=0}-E\right]C_n(z) = -\int_0^\infty \Phi_n^*(\rho)V_{ps}(\mathbf{r})\ \Psi(z,\rho)\ 2\pi\rho d\rho. \tag{2.6}$$

By solving Eq.(2.6) for $n = 0$ we obtain the scattering wave function $C_0(z)$ in the open channel which has the following asymptotic form:

$$C_0(z) = \cos(kz) + f_{e,s}e^{ik|z|}, \quad \text{for } |z| \to \infty, \tag{2.7}$$

where $f_{e,s}$ is the one-dimensional scattering amplitude of the s-wave interaction which describes the even scattered waves.

For $n > 0$, Eq.(2.6) with $V_{ps}(\mathbf{r}) \equiv 0$ provides us with the solution for the virtual excitations associated with the closed channels, which decay exponentially according to the relation

$$C_n(z) = A_{n,s}e^{-\sqrt{\frac{n}{2}-\left(\frac{ka_\perp}{2}\right)^2}\frac{2|z|}{a_\perp}}, \tag{2.8}$$

where the coefficients $A_{n,s}$ refer to the s-wave interaction and denote the transition amplitudes from the transverse ground state to the n-th excited state.

In the case of the s-wave pseudopotential we substitute Eq.(2.7) into Eq.(2.6) for $n = 0$ and Eq.(2.8) into Eq.(2.6) for $n > 0$ and integrate over the z variable, respectively, in the interval $[-\epsilon, \epsilon]$ with $\epsilon \to 0$. Finally, we obtain the following relations for the one-dimensional scattering amplitude and the transition amplitudes:

$$f_{e,s} = -i\frac{2a_s(E)\sqrt{\pi}}{ka_\perp}\eta_s \; ; \quad A_{n,s} = -a_s(E)\sqrt{\pi}\eta_s \Big/ \sqrt{\frac{n}{2} - \left(\frac{ka_\perp}{2}\right)^2}, \tag{2.9}$$

where the $a_s(E)$ is the s-wave energy dependent scattering length as it is defined in Ref.[72] with E referring to the *total* colliding energy. η_s is the regularized part of the wave function Ψ in the limit $\mathbf{r} \to 0$, which is given by the expression:

$$\eta_s = \frac{d}{dz}[z\Psi(z, \rho = 0)]\Big|_{z\to 0^+}. \tag{2.10}$$

Then we substitute Eqs. (2.7), (2.8) and (2.9) in Eq. (2.5) yielding the following relation for the wave function:

$$\Psi(z,\rho) = \left[\cos(kz) - i\frac{2a_s(k)\sqrt{\pi}}{ka_\perp}\eta_s e^{ik|z|}\right]\Phi_0(\rho) - a_s\sqrt{\pi}\eta_s\Lambda(z,\rho), \tag{2.11}$$

where the function $\Lambda(z, \rho)$ is given by the expression

$$\Lambda(z,\rho) = \sum_{n=2}^{\infty} \frac{e^{-\sqrt{\frac{n}{2}-\left(\frac{ka_\perp}{2}\right)^2}\frac{2|z|}{a_\perp}}}{\sqrt{\frac{n}{2} - \left(\frac{ka_\perp}{2}\right)^2}}\,\Phi_n(\rho). \tag{2.12}$$

Since now we have the explicit form of the wave function we can substitute it in Eq. (2.10) and derive the explicit form of the η_s constant which reads:

$$n_s = \frac{1}{a_\perp\sqrt{\pi}}\frac{1}{1 + i\frac{2a_s(E)}{ka_\perp^2} + \frac{a_s(E)}{a_\perp}\frac{d}{dz}[z\Lambda(z,\rho=0)]|_{z\to 0^+}}. \tag{2.13}$$

However, we remark that the series $\Lambda(z,\rho=0)$ are not converging uniformly as z tends to zero. Thus, by regularizing[1] the divergent series $\Lambda(z,\rho=0)$ we obtain that :

$$\frac{d}{dz}[z\Lambda(z,\rho=0)]\bigg|_{z\to 0^+} = \zeta\left(1/2, 1-\left(\frac{ka_\perp}{2}\right)^2\right) = c_1(k), \tag{2.14}$$

where $\zeta(\cdot,\cdot)$ is the Hurwitz zeta function and for $ka_\perp \ll 1$ we have that $c_1 \approx -1.46035$. Consequently, using Eqs. (2.13) and (2.14) in Eq. (2.9) we obtain the explicit form for the scattering amplitude of s-wave interacting bosons in the presence of a harmonic trap:

$$f_{e,s} = -\frac{1}{1+ika_\perp\left(-\frac{a_\perp}{2a_s(E)}-\frac{c_1}{2}\right)}. \tag{2.15}$$

Unlike, to the free space case, the scattering amplitude of Eq. (2.15) can not be related to a cross section, since asymptotically, $\mathbf{r}\to\infty$, the corresponding Schrödinger equation (see Eq. (2.4)) becomes separable and is reduced to a one-dimensional equation of motion along the z degree of freedom. However, the equivalent of the cross section in one dimension is the transmission coefficient T and it is related to the scattering amplitude according to the relation[2] :

$$T = |1+f_{e,s}|^2 = \left|1-\frac{1}{1+ika_\perp\left(-\frac{a_\perp}{2a_s(E)}-\frac{c_1}{2}\right)}\right|^2. \tag{2.16}$$

In Eq. (2.16) we observe that for $a_s(E)/a_\perp \to -1/c_1$ the transmission coefficient T tends to zero. The latter means that for a particular value of the ratio $a_s(E)/a_\perp$ the two bosons inside the waveguide interact strongly which is manifested as total reflection. Somewhat counterintuitive in this particular system the interatomic interactions are enhanced not at $a_s(E)\to\infty$ as we already discuss in chapter 1 but at finite value of the scattering length. This remarkable resonant phenomenon is known as confinement-induced resonance (CIR) for s-wave interactions and the corresponding resonance condition reads:

$$\frac{a_s(E)}{a_\perp} = -1/c_1 = 0.68, \tag{2.17}$$

where Eq. (2.17) simply means that when the s-wave scattering length becomes nearly the half of the harmonic oscillator length then the collisions inside the waveguide are becoming resonant. Interestingly, Eq. (2.17) possesses universal characteristics since it does not depend on the specific form or the details of the interatomic interactions. An additional fascinating feature of the resonance condition in Eq. (2.17) is that it can be met either by tuning the s-wave scattering length, i.e. by means of a Fano-Feshbach resonance, or by adjusting the confinement frequency such that the ratio $a_s(E)/a_\perp$ obtains the particular value given by c_1.

[1] A detailed analysis on the regularization technique is provided in subsection 2.4

[2] For more details on the connection of the scattering amplitude and the transmission coefficient T see subsection 2.1.2

At this point we should remark that the constant c_1 arises from the virtual excitations of the two bosons over *all* the eigenmodes of the transversal potential. This means that the two atoms during the collision perform virtual transitions over the closed channels, since the interatomic potential couples all the spatial degrees of freedom as $\mathbf{r} \to 0$. Consequently, these transitions act collectively on the atom pair and after the collision result into the appearance of a resonance, namely the CIR, at a finite value of the s-wave scattering length.

2.1.2 The effective one-dimensional Hamiltonian

In the following we discuss the mapping of the Hamiltonian of Eq. (2.1) on to an effective one-dimensional Hamiltonian which encapsulates all the relevant scattering information. In order to achieve this goal we start from the expression of the asymptotic wave function of the full Hamiltonian. Hence, from Eqs. (2.5), (2.7) and (2.15) we obtain:

$$\Psi(z,\rho) = \Big(\cos(kz) + f_{e,s}e^{ik|z|}\Big)\Phi_0(\rho), \quad \text{for } |z| \to \infty, \tag{2.18}$$

with $f_{e,s} = -1/\big[1 + ika_\perp\left(-\frac{a_\perp}{2a_s(E)} - \frac{c_1}{2}\right)\big]$.

We observe that at $|z| \to \infty$ only the $n = 0$ term of the Eq. (2.5) survives since all the higher order terms for $n \neq 0$ vanish exponentially (see Eq. (2.8)). Additionally, it is evident that the wave function in the asymptotic regime is written as a product of wave functions that describe separately the z and ρ degree of motion since in this region the pseudopotential is zero. Interestingly, we observe that all the scattering information is embedded in the part of the wave function which refers to the z degree of freedom. Thus, we can substitute the pseudopotential with an effective potential which acts only on z component and provides us with a wave function equivalent to that of Eq. (2.18). We assume that the effective potential has the following simple form:

$$U_{1D}(z) = g_{1D}\delta(z), \tag{2.19}$$

where g_{1D} is the *coupling strength* and is regarded as the effective interaction among the two atoms. Then the corresponding Hamiltonian can be expressed as $H'(z,\rho,\phi) = H_{\text{eff}}(z) + H_\perp(\rho,\phi)$ which is fully separable and the terms $H_{\text{eff}}(z)$ and $H_\perp(\rho,\phi)$ are given by the relations:

$$H_{\text{eff}}(z) = -\frac{\hbar^2}{2\mu}\frac{\partial^2}{\partial z^2} + U_{1D}(z), \quad \text{and} \quad \mathrm{H}_\perp(\rho,\phi) = -\frac{\hbar^2}{2\mu}\Delta_\rho + \frac{1}{2}\mu\omega_\perp^2\rho^2, \tag{2.20}$$

where Δ_ρ is the Laplacian expressed in polar coordinates.

Hence, by integrating out the ρ component in the Schrödinger equation of the H' Hamiltonian we get the following reduced Schrödinger equation:

$$\Big(-\frac{\hbar^2}{2\mu}\frac{\partial^2}{\partial z^2} + U_{1D}(z)\Big)\psi_{1D}(z) = E_z\psi_{1D}(z), \tag{2.21}$$

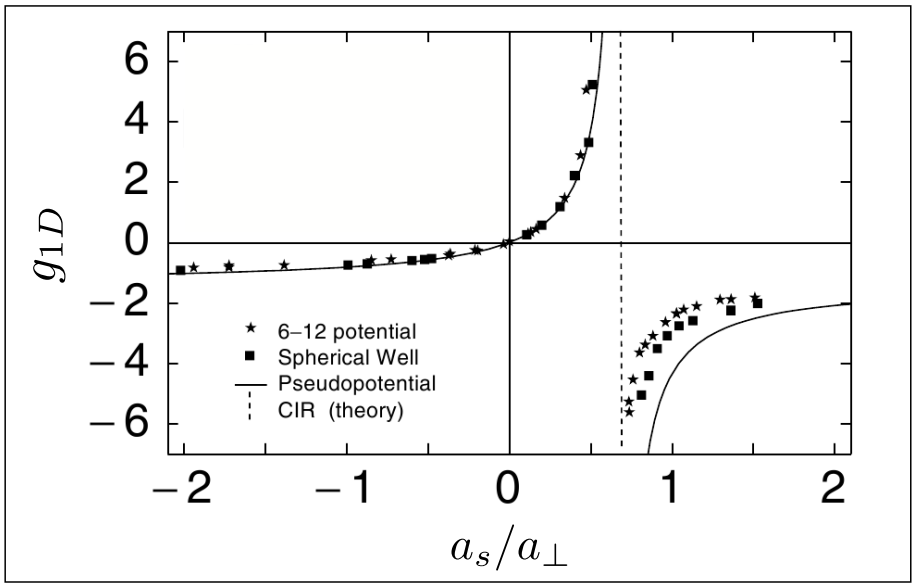

Figure 2.2: The coupling strength g_{1D} as a function of the ratio $a_s/a_\perp$. The solid line indicates Eq. (2.23) according to the pseudopotential theory. The analytical results are compared with exact numerical calculations for the interatomic potentials of a Lennard-Jones (stars) and a spherical well (squares). The dashed line depicts the position of s-wave CIR.

where the wave function $\psi_{1D}(z)$ fulfills due to the δ function the following boundary condition:

$$g_{1D} = \frac{\hbar^2}{2\mu} \frac{\psi'_{1D}(0^+) - \psi'_{1D}(0^-)}{\psi_{1D}(0)}. \tag{2.22}$$

As we have mentioned above the effective Hamiltonian H' must result into a wave function equal to the wave function of the true Hamiltonian H [see Eq. (2.1)]. Thus, by inserting the z component of Eq. (2.18) in Eq. (2.22), we obtain the corresponding coupling strength g_{1D} which reads:

$$g_{1D} = i\frac{\hbar^2 k}{\mu} \frac{f_{e,s}}{1 + f_{e,s}} = \frac{\hbar^2}{\mu a_\perp} \frac{2a_s(E)}{a_\perp + c_1 a_s(E)}, \tag{2.23}$$

where we observe that g_{1D} diverges, namely $g_{1D} \to \pm\infty$, as $a_s(E)/a_\perp \to -1/c_1$. Then the transmission coefficient T is defined with the help of the coupling strength and the corresponding relation reads:

$$T = \frac{1}{1 + (\mu g_{1D}/\hbar^2 k)^2} = |1 + f_{e,s}|^2 \tag{2.24}$$

In Fig.2.2 we show the coupling constant g_{1D} as a function of $a_s/a_\perp$. The analytical result (solid line) of Eq. (2.23) is compared with exact numerical calculations, where

the interatomic potential is modeled by a Lennard-Jones potential[3] 6-12 (stars) or by a spherical well (squares). We observe that the numerical and analytical calculations are in good agreement, since they both describe the singularity exactly at $a_s = 0.68a_\perp$. The latter illustrates in a straightforward manner that the CIR effect is system-independent, namely it does not depend on the details and the specific form of the interatomic interaction. We should remark that the deviations between numerical and analytical calculations in the negative branch of g_{1D} occur due to the breakdown of the zero-range pseudopotential theory.

Moreover, it is shown in Fig.2.2 that the effective two-body interactions change from strongly repulsive to strongly attractive when we sweep across the position of the resonance. Additionally, we observe that as $|a_s/a_\perp| \to \infty$ the coupling strength tends to a constant value, i.e. $g_{1D} \to \hbar^2/\mu c_1 a_\perp < 0$ ($c_1 < 0$) as expected, meaning that inside the waveguide the two particles are weakly attracted, despite the diverging a_s. We recall that in the case of free space collisions the divergence of the scattering length yields effective strong interatomic interactions. Interestingly, this intrinsic contradiction manifests the strong impact of the confinement on the two-body collisional properties which are significantly altered from the free space case. In the case of a_s tending to zero the coupling strength is zero as well, meaning that the two atoms do not interact with each other.

In Fig.2.3 we present the transmission coefficient T as a function of the ratio $a_s/a_\perp$. We compare the analytical results (solid line) of Eq. (2.24) with the corresponding numerical calculations (red circles) where the two-body interactions are modeled by the Lennard-Jones potential 6-12. We observe that the numerical simulations are in excellent agreement with the analytical results predicting accurate enough the position of the s-wave CIR indicated by the dashed line. At resonance the transmission is totally suppressed manifesting in this manner strong interactions between the two atoms inside the waveguide. In the limit of $a_s \to 0$ the transmission coefficient T tends to unit, since the atom pair does not interact yielding total transmission Moreover, the transmission coefficient T converges to a constant as the ratio $a_s/a_\perp$ tends to infinity, manifesting similar behavior as in Fig.2.2.

Surprisingly, we observe that T in Fig.2.3 illustrates a broad variation between unity and zero and does not exhibit a Lorentzian-like lineshape. Recalling our discussion for Fano-Feshbach resonances in chapter 1 we mentioned that an intrinsic characteristic of this type of resonances is their Fano asymmetric lineshape [58]. Hence, the asymmetric lineshape of the s-wave CIR constitutes a strong evidence that the CIR is a Fano-Feshbach type of resonance. This interpretation of CIR as a Fano-Feshbach resonance will be the main objective of the following subsection.

[3]In the case of the Lennard-Jones potential we consider collisions of ^{133}Cs atoms with dispersion coefficient $C_6 = 6890$ a.u.(a.u.$\equiv$ atomic units).

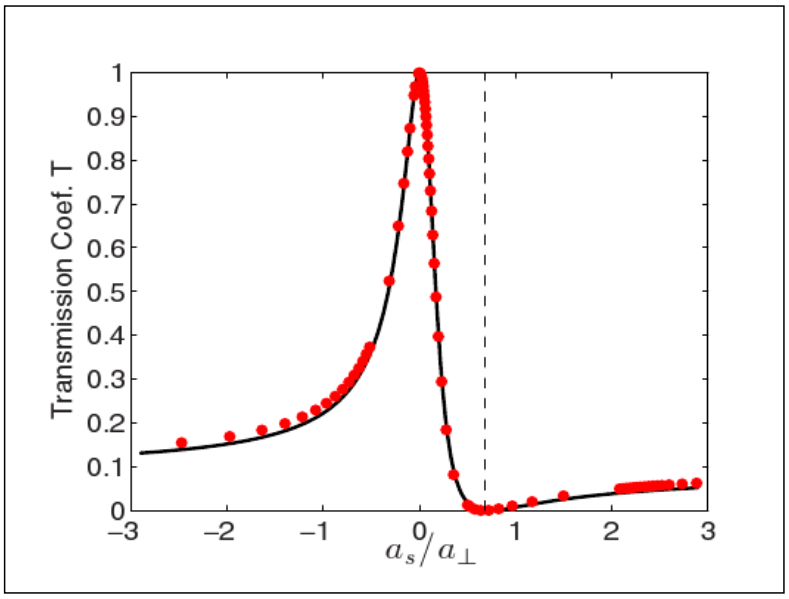

Figure 2.3: The transmission coefficient T as a function of the ratio $a_s/a_\perp$. The analytical results (solid line) are compared with the exact numerical calculations (red circles) for a Lennard-Jones potential. The dashed line denotes the position of the s-wave CIR at $T = 0$.

2.1.3 Confinement-induced resonances and their physical origin

In this subsection we will clarify the origin of the CIR effect as it was shown in Ref.[10]. As we pointed out at the end of the previous subsection the CIR resonance can be interpreted as a Fano-Feshbach resonance. Hence, we will base our analysis on the Fano-Feshbach scheme of a partitioning of the full Hamiltonian into ground and excited modes of the transverse harmonic confinement.

Towards this direction we consider the total Hamiltonian written in the form of operators $\widehat{H} = \widehat{H}_z + \widehat{H}_\perp + \widehat{V}_{\rm pseudo}$, where the $\widehat{V}_{\rm pseudo}$ is the Fermi-Huang pseudopotential. Additionally, we introduce the following projection operators for the ground and excited states:

$$\widehat{P}_g = |0\rangle\langle 0| \quad \text{and} \quad \widehat{P}_e = \sum_{n=1}^{\infty} |n\rangle\langle n| \,, \tag{2.25}$$

where $|n\rangle$ is the eigenstate of the transverse two-dimensional harmonic oscillator with a principal quantum number n. Note that the quantum number which refers to the axial angular momentum is chosen to be zero, namely $m = 0$.

Therefore acting with the projection operators on the total Hamiltonian we get $\widehat{H}_g = \widehat{P}_g \widehat{H} \widehat{P}_g$ and $\widehat{H}_e = \widehat{P}_e \widehat{H} \widehat{P}_e$ for the ground and excited state Hamiltonian, respectively. The coupling terms, which describe transitions from the ground to excited state and vice versa, are given by the relations $\widehat{V}_{ge} = \widehat{P}_g \widehat{V}_{\rm pseudo} \widehat{P}_e$ and $\widehat{V}_{eg} = \widehat{P}_e \widehat{V}_{\rm pseudo} \widehat{P}_g$ respectively.

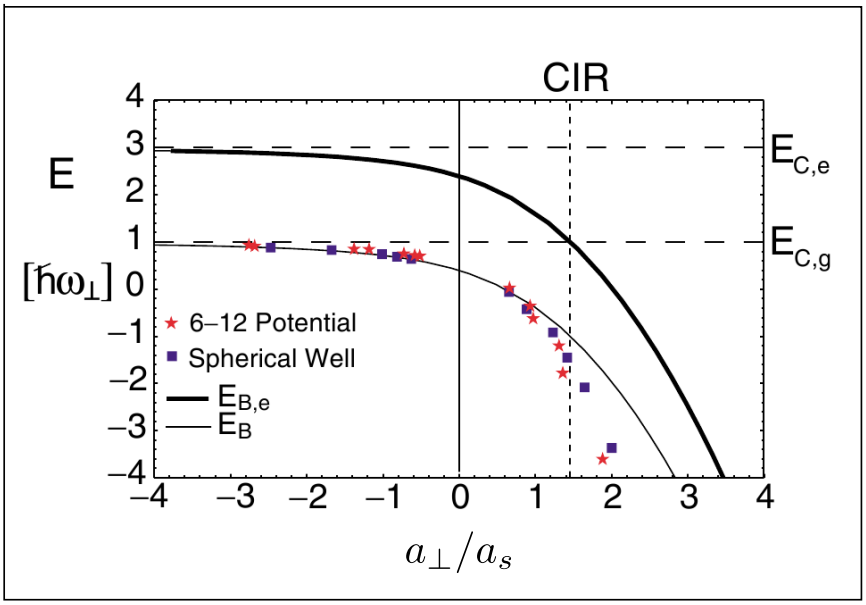

Figure 2.4: A schematic illustration of the of the Fano-Feshbach scenario. The stars and the squares represent the numerical calculations for the bound state energies and the solid lines depicts the analytical results of the pseudopotential theory.

Hence, the corresponding Schrödinger equation reads:

$$\begin{aligned} \widehat{H}_g \left|\psi_g\right\rangle + \widehat{V}_{ge} \left|\psi_e\right\rangle &= E \left|\psi_g\right\rangle \\ (\widehat{H}_e - E) \left|\psi_e\right\rangle &= -\widehat{V}_{eg} \left|\psi_g\right\rangle , \end{aligned} \tag{2.26}$$

where the first row refers to the ground state and the second to the excited states, which are however mutually coupled.

We remark that the Hamiltonians $\widehat{H}_g$ and $\widehat{H}_e$ possess a continuum threshold indicated as $E_{c,g}$ and $E_{c,e}$. Between these two thresholds there is an energy gap $\Delta = E_{c,e} - E_{c,g} = 2\hbar\omega_\perp > 0$. Additionally, the two atoms collide with a certain amount of energy which is larger than the threshold energy of the ground state and smaller than the threshold energy of the excited state, namely $E_{c,g} < E < E_{c,e}$. The latter indicates that the ground state serves as an open channel, whereas the excited are assumed to be the closed ones. Hence, in this manner the resonances will occur in the open channel when $(\widehat{H}_e - E)\left|\psi_e^B\right\rangle = 0$, where $\left|\psi_e^B\right\rangle$ describes a bound state of the closed channels with energy $E_{B,e}$ close to the total colliding E, namely $E_{B,e} = E$.

In order to find the bound state energy $E_{B,e}$ of $\widehat{H}_e$, as a first step we will calculate the bound state energy of the full Hamiltonian $\widehat{H}$. We recall that $\left|\psi_g\right\rangle$ is given in the configuration space by the wave function $\psi_0(z) = e^{ikz} + f_e e^{ik|z|}$, thus in the case of resonant scattering the wave function has to vanish meaning that $f_e \to -1$; hence from

Eq. (2.15) we find an implicit equation for the bound state energy E_B which reads:

$$\zeta[1/2, 1/2 - E_B/2\hbar\omega_\perp] = -a_\perp/a_s. \tag{2.27}$$

As a second step we observe that the full Hamiltonian and the Hamiltonian $\widehat{H}_e$ can be interchanged by a simple *shift* transformation. Namely, we have that $\widehat{H}_e = \widehat{A}^\dagger \widehat{H} \widehat{A}$ with the shift operator defined by the relation $\widehat{A}^\dagger = \sum_{n=0} |n+1\rangle \langle n|$. Then, according to this shift operation the bound state energy of $\widehat{H}_e$ is related with the bound state energy of the full Hamiltonian according to the expression $E_{B,e} = E_B + 2\hbar\omega_\perp$; hence Eq. (2.27) reads:

$$\zeta[1/2, 3/2 - E_{B,e}/2\hbar\omega_\perp] = -a_\perp/a_s. \tag{2.28}$$

In Fig.2.4 we schematically illustrate the Fano-Feshbach scenario, where the thick and the thin solid lines depict the analytical results for the excited bound state energy $E_{B,e}$ and the bound state energy E_B of Eqs. (2.28) and (2.27), respectively. The horizontal dashed lines indicate the continuum thresholds $E_{c,g}$ and $E_{c,e}$ of the ground and excited states. We observe that the analytical calculation of the bound state energy E_B is in a good agreement with the corresponding numerical calculations for two types of interatomic potentials: the Lennard-Jones (red stars) and the square well (blue squares). Additionally, we observe that the excited bound state energy $E_{B,e}$ crosses the threshold of the ground state exactly at $a_\perp/a_s = 1.46$ or $a_s/a_\perp = 0.68$ manifesting that the CIR is indeed a Fano-Feshbach resonance. Note that the latter justifies the observation of the Fano asymmetric lineshape of the transmission coefficient T in Fig.2.3. In addition, one should note in Fig. 2.4 on the right side of the vertical dashed line that the energy $E_{B,e}$ is calculated by analytically continuing Eq. (2.28). Therefore, the energy difference $E_{B,e} - E_B$ is not equal to $2\hbar\omega_\perp$ as it occurs in the left side of the vertical sashed line, namely for $a_\perp/a_s < 1.4603$.

At this point we would like to remark that the CIR effect can be interpreted in two ways as we have mentioned. The first one is the picture of virtual excitations and the second is the Fano-Feshbach scenario. Remarkably, these two interpretations of the same effect at first glance do not overlap, but as we will see in chapter 3 there is a systematic way where the two physical pictures merge together, providing a unified description of the CIR effect.

2.2 Confinement-induced resonant mechanisms: a brief overview

The very intriguing perspective of resonant collisions by adjusting the confinement of the trapping potential has triggered an immense theoretical interest in studying confinement-induced resonant mechanisms in various systems. Therefore in this section we will have the chance to briefly overview types of CIR which have been studied theoretically or realized experimentally.

So far we have considered atoms of bosonic symmetry in the presence of harmonic quasi-one-dimensional waveguide. In Ref. [13] Moore *et al.* presented a generalized

theory for bosonic collisions in waveguides, where the atoms before or after the collision were allowed to occupy the excited states of the transversal degrees of freedom. A more detailed analysis was carried out in Ref.[14] where Saeidian *et al.* analyzed the impact of the transversal excitations and de-excitations of the atoms on the CIR effect. It was shown that either for bosons or fermions as well as for distinguishable atoms there are a series of CIR type resonances, where the corresponding transmission coefficient possesses a non-zero minimum in all open channels illustrating that resonant scattering can be induced by the confinement even in the multi-mode regime. Moreover, in Ref.[15] Saeidian *et al.* developed a theoretical model incorporating broad and narrow free space Fano-Feshbach resonances in order to describe the shifts and widths of CIRs. Additionally, in the case of anisotropic waveguides it was shown in Ref.[16] that the atomic collisions in the multi-mode regime can lead to a splitting of the confinement-induced resonances.

In all the above-mentioned cases the center of mass and relative motion could be described separately due to the specific symmetry of the considered confining geometry. However, in Ref.[17] Peano *et al.* studied s-wave collisions in an arbitrary trapping potential, which couples the center of mass and relative degrees of freedom yielding a resonant structure with more than one CIRs. Based on the same mechanism in Refs.[18, 19] a similar effect has been observed for anharmonic traps yielding *inelastic (or anharmonic) confinement-induced resonances*. The intrinsic property of the non-separable center of mass and relative coordinates is the one that yields the coupling of the continuum of the relative motion directly to the excited molecular states of the center of mass, permitting in this manner the formation of confinement-induced molecules as it is presented in [20]. Furthermore, in Ref.[21] a theoretical model was developed within the Green's function formalism for arbitrary trapping potentials incorporating in addition contributions for higher-partial wave interactions.

Apart from single sited traps or waveguide geometries the CIR effect has been studied for the case of lattices. Specifically, in Ref.[22] Fedichev *et al.* developed a tight-binding model for atomic collisions in an isotropic three-dimensional lattice, and it was shown that near the corresponding CIR emerges a weakly-bound Wannier-Mott molecule being extended in several lattice sites. In addition, Cui *et al.* in Ref.[23] presented a detailed study on atomic collisions in lattices which do not lead to the separation of center of mass and relative coordinates. Using a renormalization group approach, an effective potential is constructed which includes higher-bands effects and multiple scattering processes in the lowest band. At a particular lattice depth, a CIR appears for an arbitrary negative s-wave scattering length. This new type of CIR can be driven either by intraband or both intra- and interband effects depending on the magnitude of the scattering length. Moreover, the domination of the interband effects leads to molecular formation.

The concept of confinement-induced processes has been extended also to many-body collisions. Mora *et al.* in Refs. [24, 25, 26] studied three- and four-body collisions in the presence of a transverse harmonic potential. Specifically, in Ref.[24] the fermionic case is analyzed, and it is shown that close to the dimer limit there is an effective zero-range

potential where the atom-dimer interact repulsively, whereas near the zero crossing of the two-body s-wave scattering length the effective potential has a long range character. In this case the three-body scattering problem is universal and characterized by two scattering lengths related to the atom-dimer pair. On the contrary, this universality does not occur for three-body collisions of bosonic symmetry as it is presented in Ref.[25]. However, a remarkable result of such a system is the existence of a single confinement-induced three-body state. In Ref.[26] dimer-dimer collisions are considered for a two-species Fermi gas confined in a quasi-one-dimensional parabolic trap and it is shown that the dimer-dimer scattering length determines completely the many-body solution related to the Bose-Einstein-condensate-Bardeen-Cooper-Schrieffer (BEC-BCS) crossover.

Liberating the CIR physics from the quasi-one dimensional perspective Petrov *et al.* in Ref.[27] considered bosonic collisions in a quasi-two-dimensional waveguides, where they observed the two-dimensional counterpart of CIR. The corresponding resonance occurs when the two-body potential does not possess any bound state near threshold, namely when $a_s < 0$. Similar resonances have been observed for fermionic collisions [28], as well. Assuming now that different particles live in different spatial dimensions Nishida *et al.* predicted in Ref.[29] the appearance of p-wave confinement-induced resonances. This resonant phenomenon occurs from the combination of pure s-wave interactions and the fact that the two-body collisions take place in mixed-dimensions yielding a series of molecular states induced by the confinement. Zhang *et al.* in Ref.[30] developed a theory based on the idea of local frame transformations for arbitrary confining potentials yielding the prediction of generalized confinement-induced resonances.

In the following we will discuss about collisional processes beyond the s-wave interactions, which is the main focus of this thesis. A fascinating example of higher-partial wave interactions was presented in Ref.[31] where the collisions of distinguishable atoms unraveled a novel resonant mechanism induced by the confinement, the so-called *dual* CIR. In contrast to the CIR effect, dual CIR results in a total transmission due to destructive interference effects between the s- and p-partial waves. In Ref.[32] a more detailed analysis was carried out on the dual CIR effect, investigating the quantum dynamics of such scattering processes. On the other hand, Granger *et al.* in Ref.[33] employed a K-matrix formalism for spin-polarized fermions in a harmonic waveguide. In such a system the s-wave interactions are intrinsically forbidden due to the fermionic symmetry and the p-wave scattering becomes dominant yielding thus a p-wave CIR. Similarly, in Refs.[34, 35] it is shown for the bosonic collisions at low energies that the transmission spectrum possesses a richer resonant structure yielding s- and d-wave CIRs. The interference between s- and d-partial waves results into a strongly asymmetric Fano-lineshape in the transmission spectrum near d-wave resonances. Moreover, in ref.[36] a generalized theoretical framework of the K-matrix formalism was developed for atomic collisions in quasi-one-dimensional geometries which takes into account all the higher-partial wave interactions either for bosons or for fermions. Evidently, this new framework avoids all the complications of the pseudopotential theory, providing

new insights on confinement-induced processes. Additionally, as it was shown in Ref.[37] that the K-matrix formalism can be extended, incorporating anisotropic interactions, in order to describe collisions of systems such as dipoles, where different ℓ-wave dominated dipolar confinement-induced resonances yield new properties from the non-dipolar ones. s-wave dipolar confinement-induced resonances have been so far numerically studied in quasi-one- and quasi-two-dimensional trapping geometries [38, 39].

From an experimental point of view the pioneering novelties in quantum technologies paved the way to explore the corresponding physics of CIRs. As we mentioned at the beginning of this chapter by means of the CIR effect Kinoshita *et al.* as well as Paredes *et al.* observed the Tonks-Girardeau many-body phase in an effectively one-dimensional ultracold gas[11]. Moreover, Haller *et al.* in Ref.[12] utilizing CIR explored an excited many-body state yielding the creation of the super Tonks-Girardeau gas. The latter was achieved by abruptly sweeping the magnetic field across the confinement-induced resonance changing thus the effective interactions of the atoms from strongly repulsive to strongly attractive. In addition, in Ref.[40] Haller *et al.* investigated the transition from cigar-shaped to pancake traps and its impact on the CIR effect. This transition from quasi-one- to quasi-two-dimensional geometries yielded additional resonances which were attributed on the lift of the degeneracies of the eigenspectrum of the isotropic harmonic confinement in the cigar-shaped traps. Furthermore, in the effectively two-dimensional limit they observed a resonance for positive s-wave scattering length contradicting with the corresponding theory [27]. However, the theoretical predictions were finally verified in the experiment by Fröhlich *et al.* [42], where they realized a strongly interacting two-component Fermi gas in two dimensions observing the corresponding CIR. Moreover, a detailed experimental investigation was provided showing that the splitting of CIRs is attributed to the coupling of center of mass and relative degrees of freedom due to the weak anharmonicity of the confining potential [41]. Additionally, by means of radio-frequency spectroscopy they achieved to form confinement-induced molecules. On the other hand, Günter *et al.* in Ref.[43] realized a strongly interacting atomic gas of spin-polarized fermions in cigar-shaped and pancake trap probing the p-wave CIR. In the case of the cigar-shaped traps the location of the resonance was found to depend on the orientation of the longitudinal axis of the trap respective to that of the polarisation axis. Concerning the case of the pancake trap, two confinement-induced resonances were observed, a fact that was attributed to the multiplet structure of the p-wave Fano-Feshbach resonance [73] which was employed in order to tune the interatomic interactions. Lamporesi *et al.* in Ref.[44] explored the scattering processes in mixed dimensions. Specifically, they created an atomic gas of two species, i.e. ^{41}K and ^{87}Rb, where the ^{41}K atoms were confined in one dimension and scattered off the unconfined ^{87}Rb atoms. This fascinating set up yielded a series of confinement-induced resonances, where it was observed that the corresponding resonant features vanish at the limit of equally confined species.

Overviewing the theoretical and experimental advances in confinement-induced processes the importance of the reduced dimensionality in scattering processes becomes evident. In the following subsections we will focus on atomic collisions with higher-partial

wave interactions.

2.3 Confinement-induced processes beyond s-wave interactions

In the following we will study in more detail confinement-induced processes beyond s-wave interactions as it has been presented in Ref.[34]. This extension of the resonant scattering physics of low-dimensional systems into higher partial wave interactions, constitutes an intriguing perspective since the it is expected to provide new many-body phenomena. A promising example is the possibility that the higher partial wave interactions are responsible for high-temperature superconductivity and superfluidity [74, 75, 76].

Hereafter, we will provide a numerical study on the impact of the reduced dimensionality on the two-body collisions with higher partial wave interactions. In the following subsection we will study the corresponding resonant phenomena induced by the confinement within the framework of pseudopotential theory, providing the physical picture of their origin.

2.3.1 Hamiltonian, methodology and set-up

We consider bosonic collisions in the presence of a quasi-one-dimensional harmonic waveguide with a transverse potential $\frac{1}{2}\mu\omega_\perp^2\rho^2$ ($\rho = r\sin\theta$). The colliding pair can interact with s- and $d-$wave interactions. This is achieved by making the two-body interaction potential deep enough such that it could support s-wave weakly bound states and d-wave quasi-bound states. The transverse harmonic potential permits a separation of the center of mass and relative motion yielding the following Hamiltonian for the relative motion:

$$H(r,\theta,\phi) = -\frac{\hbar^2}{2\mu}\frac{\partial^2}{\partial r^2} + \frac{\hbar^2}{2\mu}\frac{L^2(\theta,\phi)}{r^2} + \frac{1}{2}\mu\omega_\perp^2\rho^2 + V_{LJ}(r), \tag{2.29}$$

where $V_{LJ}(r) = C_{12}/r^{12} - C_6/r^6$ is the interatomic potential modeled by a Lennard-Jones potential 6-12, r is the relative radial coordinate and $\mu = m/2$ is the reduced mass of the two bosons. The boundary conditions for quasi-1D scattering in the waveguide read, for $z = r\cos\theta \to \pm\infty$,

$$\psi(r,\theta) \to \left[\cos(kr\cos\theta) + f_0 e^{ikr|\cos\theta|}\right]\Phi_{0,0}(r\sin\theta) \tag{2.30}$$

where f_0 is the elastic scattering amplitude of the ground transversal channel, $\Phi_{0,0}(r\sin\theta)$ is the ground-state wave-function of the 2D harmonic oscillator with transversal energy $\varepsilon_\perp = \hbar\omega_\perp$ and $k = \sqrt{2\mu(\varepsilon - \hbar\omega_\perp)}$ is the relative momentum of the colliding pair in the longitudinal direction. For $z \to \pm\infty$ the total colliding energy can be written as $\varepsilon = \varepsilon_\parallel + \varepsilon_\perp$, where $\varepsilon_\parallel$ is the longitudinal energy and $\varepsilon_\perp$ is the transversal energy. We focus on the single mode regime for which the energy lies below the first excited transversal energy level, $\hbar\omega_\perp \leq \varepsilon < 3\hbar\omega_\perp$. Obviously, the scattering state (2.30) is parity ($\mathbf{r} \to -\mathbf{r}$) symmetric, corresponding to the case of two colliding identical bosons.

The Hamiltonian allows for a separation of the azimuthal motion, corresponding to the conservation of the projection of the angular momentum onto the symmetry axis of the waveguide. Consequently, we obtain a 2D scattering problem [Eqs. (2.29) and(2.30)] in spherical coordinates, which is solved by employing the discrete-variable method suggested in Ref. [131], with the radial part of the Schrödinger equation discretized using a B-spline basis [78, 79][4] . We hereafter employ the units $m_{\rm Cs}/2 = \hbar = \omega_0 = 1$, where $m_{\rm Cs}$ is the mass of the Cs atom and $\omega_0 = 2\pi \times 10$ MHz in SI units. The following investigations are performed for the dispersion coefficients C_6 defining the long-range part of the interatomic potential for three different atomic species, Cs, Rb and Sr [80, 81]. The longitudinal energy is set to $\varepsilon_{\|} = 2 \times 10^{-6}$ and the transversal energy is varied within the interval $2 \times 10^{-4} \leq \varepsilon_{\perp} \leq 2 \times 10^{-2}$, corresponding to a range 4π KHz $\leq \omega_{\perp} \leq 400\pi$ KHz (SI) for the waveguide confinement frequency. We thereby focus on the low energy regime, characterized by $ka_{\perp} \ll 1$.

Important quantities of our analysis are the scattering amplitude f_0 and the transmission coefficient

$$T = |1 + f_0|^2, \tag{2.31}$$

which we analyze in the limit of very small longitudinal collision energies for which the s-wave CIR was initially defined [9].

2.3.2 Results, analysis and discussion

Let us first briefly address free space Cs-Cs collisions ($C_6 = 28.82$ [80, 81]) in the energy range for which s-wave scattering dominates the elastic scattering process. By varying C_{12} (which changes the short range part of the interatomic interaction) we observe s- and d-wave resonances in the corresponding partial cross sections, $\sigma_{\ell=0}$ and $\sigma_{\ell=2}$, respectively [see Fig. 2.5(a)]. As expected, the width of the d-wave resonance is by orders of magnitude smaller than that of the s-wave resonance. This difference in the widths arises due to the centrifugal barrier in the case of d-wave resonance, where the the two-atoms have to tunnel through in order to become resonant. In the presence of the waveguide [see Fig. 2.5(b)] the free near resonant s-wave scattering turns into a s-wave CIR, which appears as a broad dip in the transmission coefficient with a zero-valued minimum at $C_{12} \cong 1.65$, coinciding with a divergence of the interaction strength $g_{1D} = \lim_{\varepsilon_{\|} \to 0}(k{\rm Re}f_0/{\rm Im}f_0)$. In order to compare the numerically calculated position of the s-wave CIR with the analytical result [9] we map the C_{12} parameter onto the s-wave scattering length a_s in free space and obtain the ratio $a_s(C_{12} \cong 1.65)/a_{\perp} \cong 0.65$ which is in good agreement with the analytical prediction $a_s/a_{\perp} \cong 0.68$.

The d-wave resonance persists also in the waveguide, where it appears as a strongly varying transmission coefficient between the limiting values 0 and 1 on top of the s-wave scattering background [Fig. 2.5(b)]. This strongly asymmetric lineshape indicates that the d-wave resonance in the confined case fulfills a Fano-Feshbach scenario. In addition, as in the case of the s-wave CIR, we observe a divergence of g_{1D} at the resonant value

[4] In the appendix A we discuss in detail the numerical methods which we employ in order to treat two-body collisions in the presence of harmonic waveguides

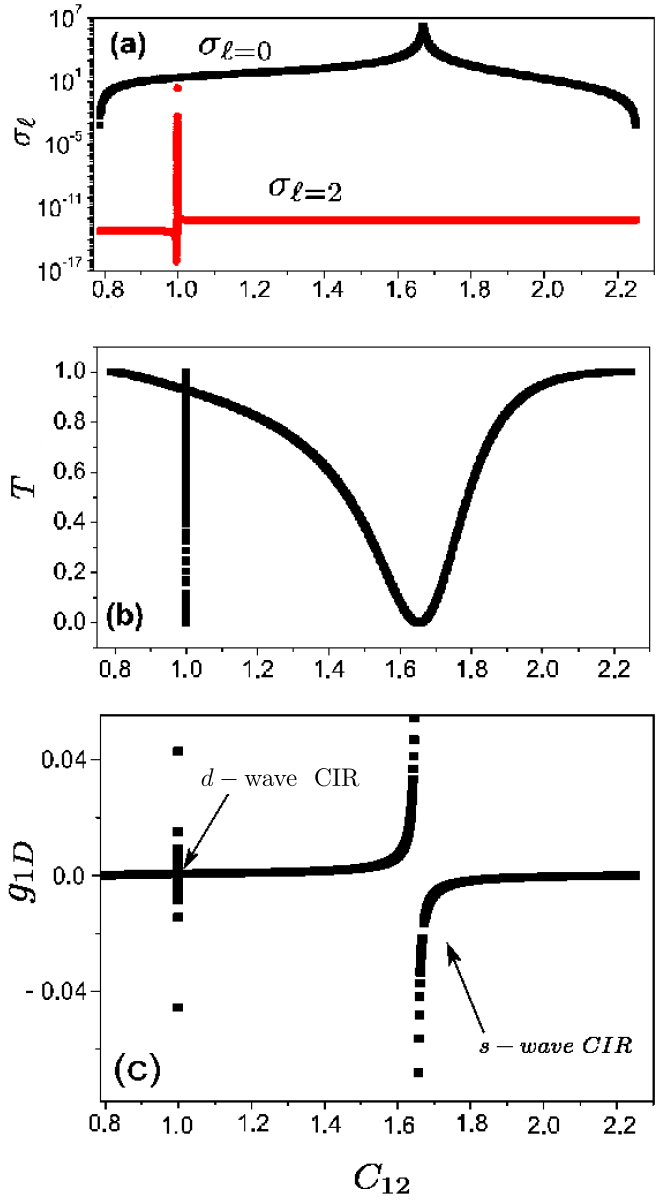

Figure 2.5: (a) Partial cross sections for s- and d-wave scattering in free space, (b) transmission coefficient T in the waveguide and (c) interaction strength g_{1D} as a function of the parameter C_{12} ($C_6 = 28.82$ for Cs).

$C_{12} = 0.9988731$ [Fig. 2.5(c)] meaning that the effective two-body interaction close to a d-wave resonance can be strongly repulsive or attractive yielding in general similar characteristics as in the case of the s-wave CIR.

The transversal confinement leads to a shift of the d-wave resonance when passing from free space to confined scattering, as is clearly seen in the high resolution graph

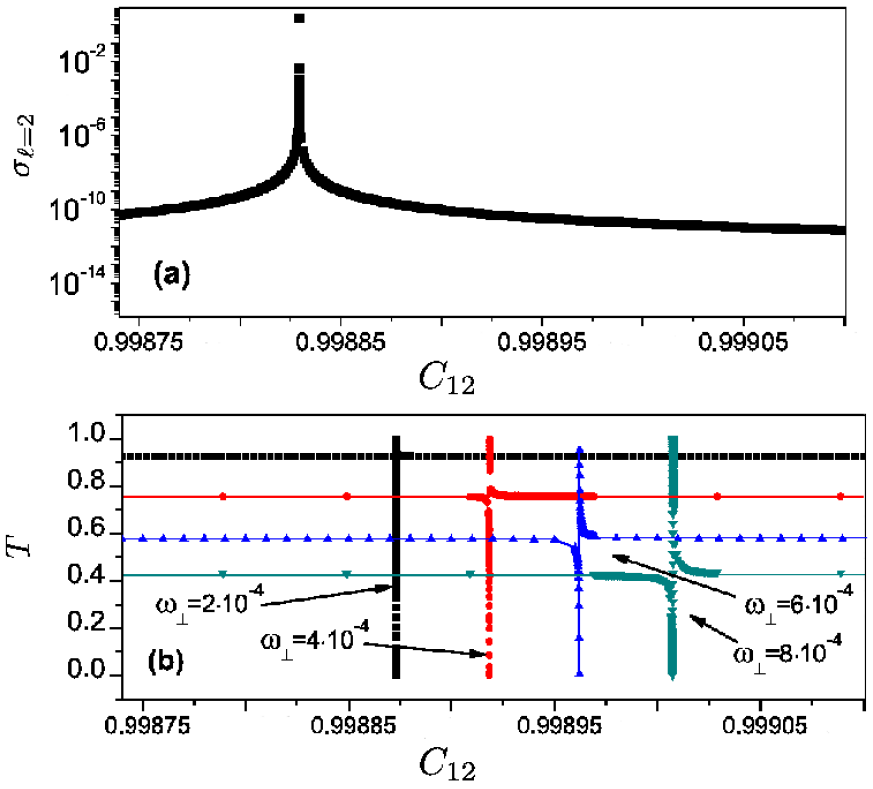

Figure 2.6: (a) Partial cross section $\sigma_{\ell=2}$ for d-wave scattering in free space and (b) transmission coefficient for several values of the confinement frequency $\omega_\perp$, as a function of the parameter C_{12} around the d-wave resonance.

of Fig. 2.6. This shift, as well as the corresponding width, increase with the trap frequency $\omega_\perp$ [see Fig. 2.6(b)]. We also observe a strong suppression of the s-wave background with increasing $\omega_\perp$. The above behavior of the transmission coefficient $T(\omega_\perp,C_{12})$ under the action of the confining potential can be interpreted in terms of a strong coupling of s- and d-waves in harmonic traps, since the trap potential can be represented as a sum of the Legendre polynomials:

$$\frac{1}{2}\mu\omega_\perp^2\rho^2 = \frac{1}{6}\mu\omega_\perp^2 r^2[2P_0(\cos\theta) - P_2(\cos\theta)] \tag{2.32}$$

Consequently, the confining potential induces a coupling between partial waves ℓ and $\ell+2$ in the course of the atomic collisions in the trap. This coupling can be tuned by changing the trap frequency.

Let us now inspect the probability density $|\Psi(r,\theta)|^2$ for different regimes of Cs-Cs collisions, plotted in Fig. 2.7. The non-resonant case [Fig. 2.7(a)] leads to a probability density which is substantial only far from the origin $r=0$. Fig. 2.7(b) and (c) refer to the s-wave CIR and d-wave CIR in the waveguide, respectively. For the s-wave CIR we

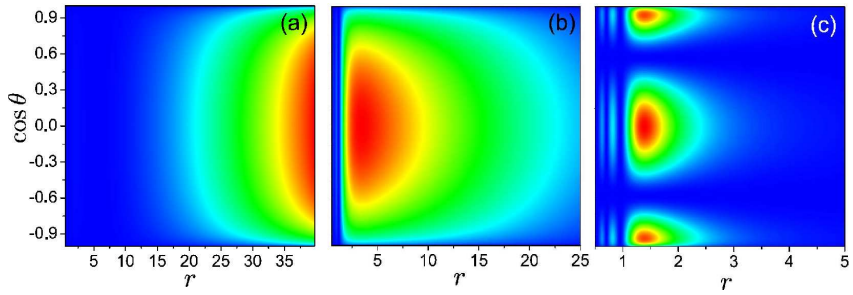

Figure 2.7: Probability density $|\Psi(r,\theta)|^2$ for Cs-Cs collisions (a) for the off-resonant case, (b) at the s-wave CIR and (c) at the d-wave CIR, for $\omega_\perp = 2 \times 10^{-4}$.

observe a localization of the probability density near the origin, while the angular distribution does not possess any nodes. In contrast, the d-wave CIR exhibits, as expected, two nodes in the θ coordinate. This provides further evidence that the sharp variation of the transmission coefficient T in Fig. 2.5 is caused due to a d-wave quasi-bound state. In addition, Fig. 2.7 (b)-(c) show that the bound state of the closed channels possesses s- or d-wave symmetry in the case of s- or d-wave CIR respectively. This can be understood from the fact that at interparticle distances close to the origin the two-body interaction overwhelms the external confining potential imposing its symmetry. The latter is imprinted in the corresponding wave function close to the origin.

Fig. 2.8 together with Fig. 2.9 illustrate how the d-wave interactions in harmonic waveguides can be controlled by altering the trap width. Varying $\omega_\perp$ ($a_\perp$) changes the transmission coefficient T near the d-wave CIR accordingly and so the strength of the d-wave interaction between the bosons can be tuned. In order to further illustrate this we show in Fig. 2.9(a)-(c) the probability density distributions for the resonant value of $\omega_\perp$ as well as far from the resonant region. A weak anisotropy is observed far from resonance whereas strong anisotropy characterizes the density profile close to resonance [Fig. 2.9(b)]. We emphasize the principal difference in the resonant behavior of the transmission coefficient near the s-wave CIR and d-wave CIR [see Figs. 2.5(b) and 2.8]. Near the s-wave CIR the contribution of d-wave scattering is negligible with respect to the total 1D scattering amplitude. However, near the d-wave CIR the d- and s-wave scattering states are strongly coupled and their interference leads to a sharp variation of the transmission coefficient between unity and zero, characterized by the Fano asymmetric lineshape [58]. Changing the confinement length $a_\perp$ one can therefore completely alter the nature of the bosonic interactions from s- to d-wave character and vice versa, since the s- and d-wave scattering coexist in the transmission coefficient. From Fig. 2.9 one can conclude that the region of significant d-wave scattering is rather broad with respect to the variation of $\omega_\perp$ and exceeds the width of the d-wave resonance in Fig. 2.8.

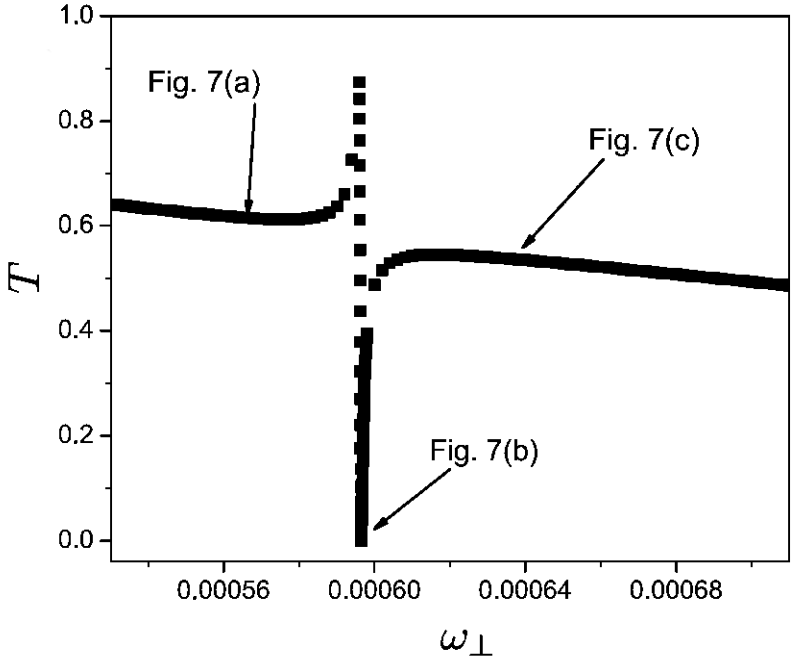

Figure 2.8: Transmission coefficient for $C_{12} = 0.9989621$ as a function of the confinement frequency $\omega_\perp$ near the d-wave CIR.

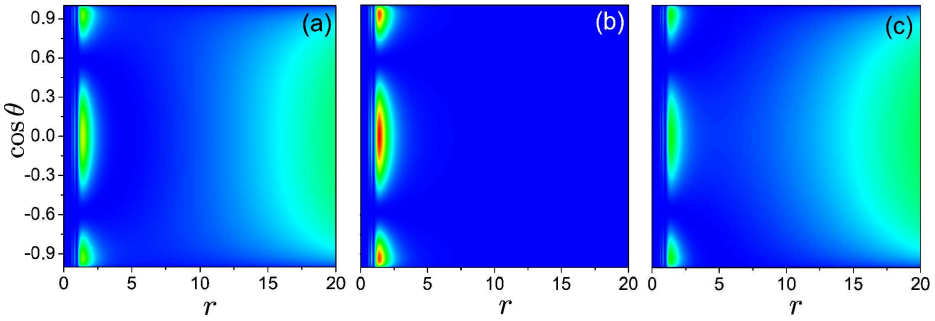

Figure 2.9: Probability density $|\Psi(r,\theta)|^2$ for Cs-Cs collisions (a) $\omega = 5.7 \times 10^{-4}$ ('left side' of the d-wave CIR), (b) $\omega = 5.96 \times 10^{-4}$ (position of the d-wave CIR) and (c) $\omega = 6.36 \times 10^{-4}$('right side' of the d-wave CIR).

2.3.3 Universal scaling law of the d-wave confinement-induced resonances

We now analyze more precisely the condition for the occurrence of the d-wave CIR. The experimental determination of the d-wave scattering length and in particular of the position of the corresponding resonance is a difficult task. However, in the following

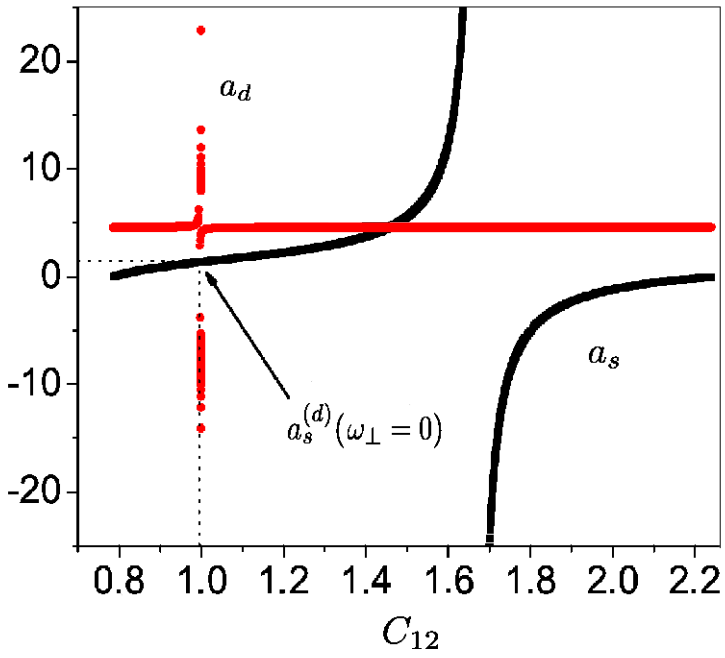

Figure 2.10: s- and d-wave scattering lengths a_s and a_d in free space as a function of the C_{12} parameter, where a_d is defined through $a_\ell^{2\ell+1} = -\tan\delta_\ell / k^{2\ell+1}$ [82] for $\ell = 2$. $a_s^{(d)}(\omega_\perp = 0) \equiv a_{s,0}^{(d)}$ is the value of the s-wave scattering length at the point of divergence of the d-wave scattering length a_d.

we will show the existence of a very useful scaling relation for the position of the d-wave CIR that provides us with an accurate estimate of its position.

Let us firstly introduce the quantity $a_s^{(d)}$, which is the free space s-wave scattering length a_s at the position of the free space d-wave shape resonance. This is well defined since a_s in general varies smoothly in the vicinity of the d-wave resonance (see Fig. 2.10). Similarly in [83] the crucial role of a_s for the analysis of the ultracold scattering near the shape resonances in free space was shown. We denote its value $a_s^{(d)}(\omega_\perp = 0)$ in free space by $a_{s,0}^{(d)}$. The next step is to determine the shift $\Delta a_s^{(d)} = a_s^{(d)} - a_{s,0}^{(d)}$ of the position of the d-wave CIR in the waveguide $a_s^{(d)} = a_s^{(d)}(\omega_\perp \neq 0)$ with respect to the resonance position in free space, in the limit $\varepsilon_\parallel \to 0$. Note that a_s is altered here by varying the C_{12} parameter, while experimentally it may be achieved by employing e.g. magnetic Feshbach resonances [12, 4]. In Fig. 2.11(a) we show the dependence of the quotient $p = \Delta a_s^{(d)}/C_6$ on $1/a_\perp^2$ for the three different atomic species Cs, Rb and Sr with corresponding C_6 coefficients [80, 81]. By fitting the numerical data we find this

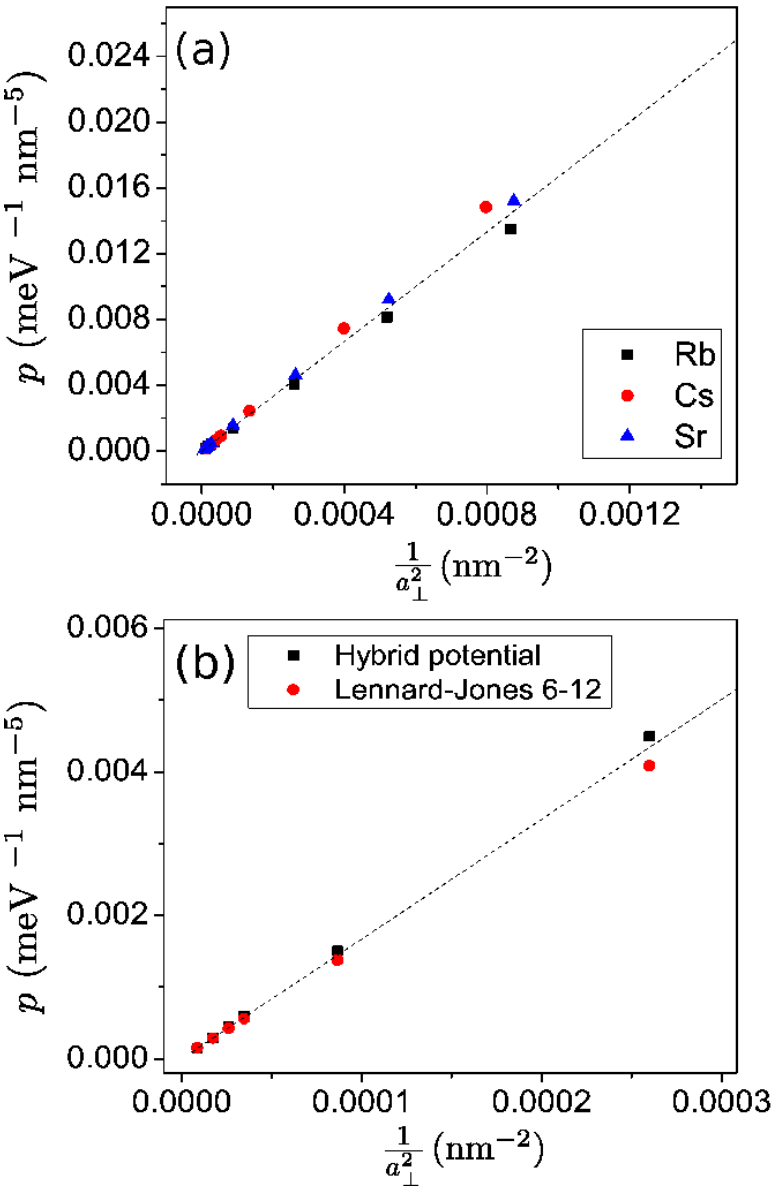

Figure 2.11: Quotient $p = \Delta a_s^{(d)}/C_6$ as a function of $1/a_\perp^2$ (a) for different values of C_6 corresponding to the atomic species Cs, Rb and Sr and (b) for Rb atoms with different interatomic potentials (see text), for confinement frequencies $4\pi\text{KHz} \leq \omega_\perp \leq 400\pi\text{KHz}$. Dashed lines correspond to the resonance condition given in Eq. (2.33).

dependence to be rather accurately described by the linear relation

$$p \;=\; \frac{\Delta a_s^{(d)}}{C_6} \;=\; 16.7\,\frac{1}{a_\perp^2}\;(\text{meV}^{-1}\text{nm}^{-5}) \tag{2.33}$$

for a comparatively broad range of values of $\omega_\perp$ for all considered C_6 coefficients. This shows that the quotient p changes with the confinement strength independently of the type of colliding atomic species. In contrast to the s-wave CIR, whose position depends exclusively on the ratio $a_s/a_\perp$, the shift $\Delta a_s^{(d)}$ of the d-wave CIR depends on $a_\perp^{-2} = \mu\omega_\perp/\hbar$ and additionally on the dispersion coefficient C_6. This is because the Van-der-Waals potential tail determines the width of the centrifugal barrier (absent in s-wave scattering), which in turn strongly influences the d-wave CIR state. Note that p possesses the correct asymptotic value $p(a_\perp \to \infty) = 0$ in the limiting case of scattering in free space. Additionally, a fitting of experimental data with the Eq. (2.33) can provide an alternative way for measuring the dispersion coefficient C_6.

In order to assure that Eq. (2.33) is not specific to the model used for the interatomic interaction, we have further studied a hybrid potential which possesses a short-range part different from the Lennard-Jones 6-12 potential, reading:

$$V_h(r) = Ae^{-qr^2} - f_c(r)\frac{C_6}{r^6} \tag{2.34}$$

where A and q are constants and $f_c(r)$ is a cut-off function [84].

$$f_c(r) = \theta(r - r_c) + \theta(r_c - r)\exp\left[-\left(\frac{r_c - r}{r}\right)^2\right] \tag{2.35}$$

with $\theta(x)$ being the Heaviside step function and r_c the cut-off radius. We choose $A = 5000$, $r_c = 1.2$ and vary the parameter q. Fig.2.11(b) shows p for Rb-Rb collisions as a function of $1/a_\perp^2$ for the Lennard-Jones and the hybrid potential. The values for $p(1/a_\perp^2)$ are for both potentials in very good agreement with the scaling relation Eq. (2.33).

Concluding, we observe that there is a universal scaling law that describes the positions of d-wave CIRs, which is independent from the short-range physics, namely the repulsive part of the Lennard-Jones potential as Fig.2.11 (b) indicates. However, this scaling law possesses an intrinsic dependence on the tail of the two-body interactions indicated by the dispersion coefficient C_6 in contrast to the s-wave CIR whose position does not depend on the details of the interactions. In the case of d-wave CIR this dependence can be understood by the fact that the attractive part of $V_{LJ}(r)$ and the centrifugal barrier $1/r^2$ form a repulsive barrier of finite width. This repulsive barrier permits the formation of d-wave quasi-bound states, which participate in the resonant mechanism of d-wave CIRs.

2.3.4 Concluding remarks

In this section we have demonstrated how strong d-wave interactions can be developed in a harmonic waveguide and analyzed their properties in detail. The d-wave CIR observed is controllable by adjusting the frequency of the trap. The confinement plays here a two-fold role: It can control the strength of the interactions among the bosons,

as well as alter the nature of the interactions from s- to d-wave character. The d-wave CIR effect can be analyzed and exploited in experiments analogous to [40] with the help of the scaling relation (2.33). We have discussed and studied the universal aspects of the positions of d-wave CIRs, which intrinsically depend on the long-range tail of the two-body interactions. The observation and application of it in anisotropic waveguides constitutes an intriguing perspective, since in the limit of the quasi-2D regime the anisotropic profile of the d-wave interactions can be exploited to introduce novel properties into quantum gases, or more specifically, strongly correlated bosonic systems, paving the way to study unconventional superfluidity and superconductivity in the presence of higher partial wave interactions.

So far, Fig. 2.5 (b) hints that the d-wave CIRs may fulfill a Fano-Feshbach scenario due to the apparent asymmetric Fano profile in the transmission spectrum. Nevertheless, a more rigorous analysis is needed in order to clarify the physical origin of the d-wave CIR. Such an analysis will provide more insights into the physics involved in understanding why in the presence of the confinement, the *Breit-Wigner* resonances originating from the free space collisions are mapped into Fano-Feshbach resonances. In the following section we will discuss the effect of d-wave CIR within the framework of pseudopotential theory in an attempt to deepen our understanding of the collisions with higher partial wave interactions under the action of the external confinement.

2.4 Pseudopotential approximation for d-wave collisions in harmonic waveguides

Over the last decade, pseudopotential theory has become an essential theoretical tool in particular for analytical studies of ultracold systems, e.g., see Busch *et al.* [85] concerning two atoms in harmonic traps or atomic collisions in cylindrical waveguides as we already discussed in section 2.1. In the following we provide a brief overview of the higher partial wave pseudopotential theory [68, 69, 28, 82, 86, 87, 88, 89, 90, 91, 92] which we will employ in order to treat bosonic collisions in a harmonic waveguide beyond mere s-wave scattering. The main goal of this section is to present an analytical model for the d-wave CIR effect in a harmonic waveguide. Our starting-point is to assume that the transversal confinement frequency is weak enough in order to avoid a strong interference between the free space d-wave resonance and the s-wave scattering. The corresponding interatomic potential is modeled through a zero-range higher partial wave pseudopotential, which allow us to study the relevant collisional physics including the virtual excitations over the eigenmodes of the transversal confinement. In order to verify the validity of the approximative analytical results we compare them with corresponding numerical calculations where the interatomic interaction is modeled by a Lennard-Jones 6-12 potential.

2.4.1 Higher partial wave pseudopotential theory

The pseudopotential approximation to the interatomic interaction is an ubiquitous tool for the theoretical description of ultracold gases: the atomic interactions are modeled in terms of a contact potential. Huang and Yang [68, 69] derived a generalized pseudopotential for all partial waves, which represents a multipolar expansion over delta function contributions. The Huang-Yang approach (HY) was revised by Derevianko [86], who corrected an algebraic error for $\ell > 0$. However, other derivations have been developed for higher partial wave pseudopotentials, which differ from the HY-approach, by using a more rigorous treatment of the derivatives of the delta-functions in the framework of distribution theory [28, 87] yielding the following representation:

$$V_{ps}(\mathbf{r})\Psi(\mathbf{r}) = \sum_{\ell=0}^{\infty} \frac{(-1)^{\ell}\left[(2\ell+1)!!\right]^2}{4\pi(2\ell)!\ell!} g_{\ell} \frac{\delta^{(\ell)}(r)}{r^2} \left[\frac{\partial^{2\ell+1}}{\partial r'^{2\ell+1}} r'^{\ell+1} \int d\mathbf{\Omega}' P_{\ell}(\hat{\mathbf{r}}\cdot\hat{\mathbf{r}}')\Psi(\mathbf{r}')\right]_{\mathbf{r}'=0}, \tag{2.36}$$

where $g_{\ell} = \hbar^2 a_{\ell}^{2\ell+1}(k)/(2\mu)$, with $a_{\ell}^{2\ell+1}(k) = -\tan\delta_{\ell}(k)/k^{2\ell+1}$ defined as the ℓ-th energy-dependent scattering length [82, 93, 94]. Here, $\delta^{(\ell)}(r)$ is the ℓ-th derivative of the delta function and the integral over the solid angle $\mathbf{\Omega}'$ acts as a projection operator of the total wave function on each $\ell-$state. For $\ell = 0$ one obtains from Eq.(2.36) the Huang-Fermi pseudopotential. However, the Eq.(2.36) for $\ell > 0$ differs by a factor $(2\ell+1)/(\ell+1)$ from Huang and Yang's result [69], whereas if we substitute in Eq.(2.36) the relations $\delta(\mathbf{r}) = \delta(r)/(4\pi r^2)$ and $\delta^{(\ell)}(r) = (-1)^{\ell}\ell!\delta(r)/r^{\ell}$ we obtain the pseudopotential of Derevianko [86].

Additionally, Stampfer and Wagner [88] introduce the following pseudopotential for higher partial waves:

$$\widetilde{V}_{ps}(\mathbf{r})\Psi(\mathbf{r}) = \sum_{\ell=0}^{\infty}\sum_{m=-\ell}^{\ell}\frac{4\pi(-1)^{\ell}}{(2\ell)!!}g_{\ell}Y_{\ell m}(\partial)\delta(\mathbf{r})\left[\frac{\partial^{2\ell+1}}{\partial r'^{2\ell+1}}r'^{\ell+1}\int d\mathbf{\Omega}' Y^{*}_{\ell m}(\hat{\mathbf{r}}')\Psi(\mathbf{r}')\right]_{\mathbf{r}'=0}, \tag{2.37}$$

where the operator $Y_{\ell m}(\partial)$, introduced by Maxwell [95], is obtained from the spherical harmonic polynomial $r^{\ell}Y_{\ell m}(\hat{\mathbf{r}})$, by replacing the Cartesian coordinates x_k with the partial derivatives ∂_{x_k}. Note that Eq.(2.37) is equal to Eq.(2.36) as it was proven in [87] by using the relation

$$\frac{\delta^{(\ell)}(r)}{r^2}Y_{\ell m}(\hat{\mathbf{r}}) = \frac{4\pi\ell!}{(2\ell+1)!!}Y_{\ell m}(\partial)\delta(\mathbf{r}). \tag{2.38}$$

The above-mentioned pseudopotentials can be simplified [87] in order to describe interactions of a single partial wave character. This simplification is based on the fact that in general the atomic interaction is dominated by the ℓ-partial wave scattering in the vicinity of the corresponding ℓ-partial wave resonance. Thus, one can focus on a single partial wave, which yields the following pseudopotential:

$$V_{ps,\ell}(\mathbf{r})\Psi(\mathbf{r}) = \sum_{m=-\ell}^{\ell}\frac{16\pi^2(-1)^{\ell}}{(2\ell+1)!}g_{\ell}Y_{\ell m}(\partial)\delta(\mathbf{r})\left[\frac{\partial^{2\ell+1}}{\partial r'^{2\ell+1}}r'^{2\ell+1}Y^{*}_{\ell m}(\partial')\Psi(\mathbf{r}')\right]_{\mathbf{r}'=0}. \tag{2.39}$$

Furthermore, the sum with respect to m can be simplified with the help of the following summation formula:

$$\frac{4\pi}{2\ell+1}\sum_{m=-\ell}^{m=\ell}Y_{\ell m}(\partial)Y^{*}_{\ell m}(\partial') = \sum_{k=0}^{[\ell/2]}c_k\left(\boldsymbol{\nabla}\cdot\boldsymbol{\nabla}'\right)^{\ell-2k}\nabla^{2k}(\nabla')^{2k}, \tag{2.40}$$

where $[\ell/2]$ is the largest, smaller or equal integer of $\ell/2$ and c_k are the coefficients of the Legendre polynomials $P_{\ell}(x) = \sum_{k=0}^{[\ell/2]}c_k x^{\ell-2k}$ given by the expression $c_k = \frac{(-1)^{\ell}(2\ell+1)!}{2^{\ell}k!(\ell-k)!(\ell-2k)!}$.

Eqs.(2.39) and (2.40) constitute pseudopotentials for any ℓ-partial wave. These pseudopotentials are expressed in terms of differential operators which are more convenient in analytical derivations than the ones in terms of the projection operator (see Eqs.(2.36) and (2.37)).

2.4.2 Quasi-one-dimensional scattering with s- and d-wave interactions

s- and d-wave pseudopotentials

In the following we consider ultracold collisions of identical bosons in the presence of an external harmonic confinement. The scattering process is taking place in the low

energy regime, $ka_\perp \ll 1$, where k is the relative momentum in the unconfined degree of freedom and $a_\perp = \sqrt{\frac{\mu\omega_\perp}{\hbar}}$ is the oscillator length defined via the trap frequency $\omega_\perp$ and the reduced mass μ of the colliding bosonic pair. Furthermore, in order to go beyond s-wave physics we assume that the momentum k is very small but not equal to zero. Consequently, as already discussed in section 2.3 except for the well known s-wave CIR, an additional resonance emerges in this system, the so-called d-wave CIR, which is based on the interference of a free space d-wave shape resonance with s-wave scattering. The coexistence of s- and d-wave resonances implies interactions between the bosons of s- and d-wave symmetries.

However, the modeling of s- and d-wave interactions with pseudopotentials in systems of non-spherical symmetry, as the above-mentioned one, is not a trivial task. As the symmetry of the system is cylindrical the angular momentum is not conserved and consequently, the application of pseudopotentials, Eqs. (2.36) and (2.37), leads to an explicit integration over all ℓ-partial waves.

Nevertheless, as it was proposed in [87] one can avoid such difficulties by considering a single ℓ-partial wave in the vicinity of the ℓ-wave resonance, where contributions from other partial waves are sufficiently suppressed. The latter means that in the vicinity of the s-wave resonance, we assume that the interaction can be modeled with the help of Eqs. (2.39) and (2.40) by the following pseudopotential:

$$V_{ps,s}(\mathbf{r}) = \frac{2\pi\hbar^2 a_s(k)}{\mu}\delta(\mathbf{r})\frac{\partial}{\partial r}[r\cdot\,], \tag{2.41}$$

which is the Fermi-Huang pseudopotential[5] , with the s-wave scattering length $a_s(k)$ being energy dependent. Note that Eq.(2.41) coincides with the pseudopotential proposed in [94].

Equivalently, in the vicinity of the d-wave resonance, we assume that the interaction can be modeled by the following pseudopotential [28, 87]:

$$V_{ps,d}(\mathbf{r}) = \frac{\pi\hbar^2 a_d^5(k)}{8\mu}\sum_{i,j,k,l} D_{ijkl}\,{}^{\leftarrow}(\partial^2_{x_i x_j})\delta(\mathbf{r})\frac{\partial^5}{\partial r^5}r^5(\partial^2_{x_k x_l})^{\rightarrow}, \tag{2.42}$$

where $D_{ijkl} = \delta_{ik}\delta_{jl} - \frac{1}{3}\delta_{ij}\delta_{kl}$ with the indices $i,j,k,l = 1,\ldots,3$ and $a_d^5(k) = -\tan\delta_{\ell=2}(k)/k^5$ is the energy dependent d-wave scattering length. The operator, ${}^{\leftarrow}(\partial^2_{x_i x_j})$ $\left((\partial^2_{x_k x_l})^{\rightarrow}\right)$ denotes the differential operator in Cartesian coordinates, that acts to the left (right) of the pseudopotential $V_{ps,d}(\mathbf{r})$.

We emphasize that application of the expressions (2.41) and (2.42) simultaneously is inconsistent and incompatible since the pseudopotentials $V_{ps,s}(\mathbf{r})$ and $V_{ps,d}(\mathbf{r})$ are valid for the cases where the wave function exhibits only $1/r$- or $1/r^3$- singularities for small r, respectively.

[5] We recall that in section 1.6 in chapter 1 one can find more details on its derivation

Hamiltonian, scattering states and virtual excitations

We assume two-body collisions of identical bosons in a harmonic waveguide. Due to the specific confining potential the center of mass and relative degrees of freedom decouple. Hence, the relevant collisional physics is encapsulated in the following Hamiltonian of the relative motion:

$$H(z,\rho,\phi) = -\frac{\hbar^2}{2\mu}\left(\frac{\partial^2}{\partial z^2} + \frac{\partial^2}{\partial \rho^2} + \frac{1}{\rho}\frac{\partial}{\partial \rho} + \frac{1}{\rho^2}\frac{\partial^2}{\partial \phi^2}\right) + \frac{1}{2}\mu\omega_\perp^2\rho^2 + V_{ps,\ell}(\mathbf{r}), \tag{2.43}$$

where $\mathbf{r} = \mathbf{r_1} - \mathbf{r_2}$ is the relative coordinate of the two bosons, and $V_{ps,\ell}(\mathbf{r})$ is the pseudopotential which models the arbitrary ℓ-wave inter-atomic interaction.

We expand the scattering solutions in an axially symmetric basis being imposed by the symmetry of the transversal trapping potential, $\frac{1}{2}\mu\omega_\perp^2\rho^2$. Such a basis set are the eigenstates of the two-dimensional (2D) harmonic oscillator which satisfy the Schrödinger equation

$$\left[-\frac{\hbar^2}{2\mu}\left(\frac{\partial^2}{\partial \rho^2} + \frac{1}{\rho}\frac{\partial}{\partial \rho} + \frac{1}{\rho^2}\frac{\partial^2}{\partial \phi^2}\right) + \frac{1}{2}\mu\omega_\perp^2\rho^2\right]\tilde{\Phi}_{n,m_z}(\rho,\phi) = E_{n,m_z}\tilde{\Phi}_{n,m_z}(\rho,\phi), \tag{2.44}$$

where $\tilde{\Phi}_{n,m_z}(\rho,\phi)$ are the eigenfunctions of the 2D harmonic oscillator, m_z is the azimuthal quantum number and $E_{n,m_z} = \hbar\omega_\perp(n + |m_z| + 1)$ is the transversal energy spectrum of the 2D harmonic oscillator, with $n = 2n_\rho = 0, 2, 4, \ldots$ being the principal quantum number.

The spherical symmetry imprinted by the pseudopotential, $V_{ps,\ell}(\mathbf{r})$, and the cylindrical symmetry of the external confining potential implies that the azimuthal symmetry is preserved throughout all the configuration space. Hence, the azimuthal ϕ angle can be eliminated for the Hamiltonian in Eq. (2.43). The latter means that during the collision no virtual excitations will occur with respect to the m_z quantum number. However, virtual excitations will emerge with respect to the principal quantum number n, which will be taken into account in the calculation given below.

We assume that the collision takes place in the single mode regime of the transversal confinement. This means that excitations to higher modes of the harmonic oscillator will not occur. Hence, the ground state of the transversal confinement with azimuthal angular momentum $m_z = 0$ will be regarded as the only "open channel". Therefore, the total energy of the pair collision is limited between the ground and the first excited axially symmetric transversal state

$$E_{n=0,m_z=0} \leqslant E < E_{n=2,m_z=0}. \tag{2.45}$$

Furthermore, the above-mentioned independence of the angle ϕ results in the following simplified Schrödinger equation:

$$\left[-\frac{\hbar^2}{2\mu}\left(\frac{\partial^2}{\partial z^2} + \frac{\partial^2}{\partial \rho^2} + \frac{1}{\rho}\frac{\partial}{\partial \rho}\right) + \frac{1}{2}\mu\omega_\perp^2\rho^2 + V_{ps,\ell}(\mathbf{r})\right]\Psi(z,\rho) = E\Psi(z,\rho), \tag{2.46}$$

where $E = E_{\parallel} + E_{n=0,m_z=0}$ is the total colliding energy, which is defined as the sum of the longitudinal kinetic energy $E_{\parallel} = \frac{\hbar^2}{2\mu}k^2$ and the energy of the transverse ground state $E_{n=0,m_z=0} = \hbar\omega_{\perp}$. Due to the constraint of Eq.(2.45) the momentum k is limited according to the relation $k < \sqrt{\frac{2\mu}{\hbar^2}\left(E_{n=2,m_z=0} - E_{n=0,m_z=0}\right)}$. Here, $\Psi(z,\rho)$ denotes the full 2D axially symmetric solution, which can be expanded in the $\tilde{\Phi}_{n,0}(\rho,\phi) \equiv \Phi_n(\rho)$ basis

$$\Psi(z,\rho) = \sum_{n=0}^{\infty} C_n(z)\Phi_n(\rho) \tag{2.47}$$

where we sum over all even n due to the bosonic symmetry.

Substituting Eq.(2.47) into Eq.(2.46), multiplying by $2\pi\rho\Phi_n^*(\rho)$, integrating and using Eq.(2.2) yields the following equation for the functions $C_n(z)$:

$$\left[-\frac{\hbar^2}{2\mu}\frac{\partial^2}{\partial z^2} + E_{n,m_z=0} - E\right] C_n(z) = -\int_0^{\infty} \Phi_n^*(\rho) V_{ps,\ell}(\mathbf{r})\ \Psi(z,\rho)\ 2\pi\rho d\rho. \tag{2.48}$$

By solving Eq.(2.48) for $n = 0$ we obtain the scattering wave function $C_0(z)$ in the open channel which has the following asymptotic form:

$$C_0(z) = \cos(kz) + f_{e,\ell}e^{ik|z|}, \quad \text{for } |z| \to \infty, \tag{2.49}$$

where $f_{e,\ell}$ is the one-dimensional scattering amplitude of the ℓ-wave interaction which describe the even scattered waves.

For $n > 0$, Eq.(2.48) provides us with the solution for the virtual excitations associated with the closed channels, which decay exponentially according to the relation

$$C_n(z) = A_{n,\ell}e^{-\sqrt{\frac{n}{2}-\left(\frac{ka_{\perp}}{2}\right)^2}\frac{2|z|}{a_{\perp}}}, \tag{2.50}$$

where the coefficients $A_{n,\ell}$ refer to the ℓ-wave interaction and denote the transition amplitudes from the transverse ground state to the n-th excited state.

In the case of the d-wave pseudopotential we substitute Eq.(2.49) into Eq.(2.48) for $n = 0$ and Eq.(2.50) into Eq.(2.48) for $n > 0$ and integrate over the z variable , respectively, in the interval $[-\epsilon,\epsilon]$ with $\epsilon \to 0$. Finally, we obtain the following relations for the d-wave scattering and transition amplitudes:

$$f_{e,d} = i\frac{a_d^5(k)\sqrt{\pi}}{24ka_{\perp}^3}\eta_d\ ; \quad A_{n,d} = \frac{a_d^5(k)\sqrt{\pi}}{48a_{\perp}^3}\eta_d\frac{2n+1}{\sqrt{\frac{n}{2}-\left(\frac{ka_{\perp}}{2}\right)^2}}, \tag{2.51}$$

where η_d is the regularized part of the wave function Ψ in the limit $\mathbf{r} \to 0$,

$$\eta_d = \frac{\partial^5}{\partial z^5}\left\{ z^5 \left[(\partial_x^2 + \partial_y^2)\Psi(z,\rho)\Big|_{\substack{x\to 0\\ y\to 0}} - 2\partial_z^2 \Psi(z,\rho)\Big|_{\substack{x\to 0\\ y\to 0}} \right] \right\}\Bigg|_{z\to 0^+}, \tag{2.52}$$

with ρ given by the relation $\rho = \sqrt{x^2+y^2}$.

Then the expression for the wave function reads

$$\Psi(z,\rho) = \left[\cos(kz) + i\frac{a_d^5(k)\sqrt{\pi}}{24ka_\perp^3}\eta_d e^{ik|z|}\right]\Phi_0(\rho) + \frac{a_d^5(k)\sqrt{\pi}}{48a_\perp^2}\eta_d\Lambda_1(z,\rho), \tag{2.53}$$

where $\Lambda_1(z,\rho)$ is defined as follows:

$$\Lambda_1(z,\rho) = \sum_{n=2}^{\infty} \frac{2n+1}{\sqrt{\frac{n}{2} - \left(\frac{ka_\perp}{2}\right)^2}}\; e^{-\sqrt{\frac{n}{2}-\left(\frac{ka_\perp}{2}\right)^2}\frac{2|z|}{a_\perp}}\Phi_n(\rho). \tag{2.54}$$

Let us now to proceed with the explicit definition of the regular part η_d of the wave function, being a solution of Eq.(2.52). The action of the operator $\left(\partial_x^2+\partial_y^2\right)$ on $\Psi(\mathbf{r})$ for $x, y \to 0$ results in the following relation:

$$\left(\partial_x^2+\partial_y^2\right)\Psi(z,\rho)\Big|_{\substack{x\to 0\\ y\to 0}} = -\frac{2}{a_\perp^3\sqrt{\pi}}\left[\cos(kz) + i\frac{a_d^5(k)\sqrt{\pi}}{24ka_\perp^3}\eta_d e^{ik|z|}\right] - \frac{a_d^5(k)}{24a_\perp^5}\eta_d\Lambda_2(z,\rho=0), \tag{2.55}$$

where $\Lambda_2(z,\rho=0)$ reads:

$$\Lambda_2(z,\rho=0) = \sum_{n=2}^{\infty} \frac{(2n+1)^2}{\sqrt{\frac{n}{2} - \left(\frac{ka_\perp}{2}\right)^2}}\; e^{-\sqrt{\frac{n}{2}-\left(\frac{ka_\perp}{2}\right)^2}\frac{2|z|}{a_\perp}}. \tag{2.56}$$

Here, we should note that the Λ-series at $\rho = 0$ are not converging uniformly as $z \to 0$. The latter means that the partial derivative with respect to z-coordinate cannot be interchanged with the sum over all even n. Thus, firstly one has to perform the summation and then differentiate with respect to the z coordinate. However, with the help of Euler's summation formula [96] one can express the Λ-series as an expansion with respect to the z variable, where the singular part of the Λ-series will be written in closed form yielding the following expressions:

$$\Lambda_1(z,\rho=0) = \frac{2a_\perp^3}{|z|^3} + \frac{a_\perp}{|z|} + q_1 + q_2\frac{2|z|}{a_\perp} + q_3\left(\frac{2|z|}{a_\perp}\right)^2 + \cdots, \tag{2.57}$$

$$\Lambda_2(z,\rho=0) = \frac{24a_\perp^5}{|z|^5} + \frac{4a_\perp^3}{|z|^3} + \frac{a_\perp}{|z|} + b_1 + \cdots, \tag{2.58}$$

where $q_1 \approx -2.29225$, $q_2 = 0.83333$, $q_3 \approx -0.154912$ and $b_1 \approx -3.5336$ are constants calculated via Euler's summation formula.

Consequently, by substituting Eqs.(2.53)-(2.58) into Eq.(2.52) we obtain η_d, which is now free of divergences. This in turn yields the following expression for the one-dimensional scattering amplitude:

$$f_{e,d} = -\frac{1}{1 + ika_\perp \left(-\frac{a_\perp^5}{10a_d^5(k)} + b_2\right)}, \tag{2.59}$$

where the constant $b_2 \approx 2.386445$ is defined by the relation $b_2 = -\frac{b_1}{2} - 4q_3$. The resonance condition for $f_{e,d}$ then reads

$$\frac{a_\perp}{a_d(k)} = \sqrt[5]{10b_2}. \tag{2.60}$$

Eq.(2.59) shows that the d-wave scattering in the presence of the waveguide becomes resonant at an off-resonant value of the free space $a_d(k)$ scattering length, due to the significant contributions of the virtual excitations. The latter holds equally for the case of the s-wave CIR. Therefore, one can conclude that in general the appearance of resonances in systems with transversal confinement is generated by the virtual excitations in the transverse modes.

2.4.3 Results and discussion

In this section we compare the analytical results of the previous subsection for the s- and d-wave pseudopotentials with the corresponding numerical simulations. First we evaluate the d- and s-wave energy dependent scattering lengths by solving numerically a model of Cs atoms in free space interacting via a Lennard-Jones potential, $V(r) = \frac{C_{12}}{r^{12}} - \frac{C_6}{r^6}$. Note that Cs atoms are ideal candidate for studying scattering phenomena, since they provide a rich spectrum of resonances [97, 98].

The dispersion coefficient C_6 has been taken from [80, 81] and C_{12} is a free parameter, which controls the values for the s- and d-wave scattering lengths. This yields a parametrization of the one-dimensional s- and d-wave scattering amplitudes, Eqs.(2.15) and (2.59), respectively, in terms of C_{12}.

In order to numerically solve the Cs-Cs collisions in the harmonic waveguide we employ the units $m_{\rm Cs}/2 = \hbar = \omega_0 = 1$, where $m_{\rm Cs}$ is the mass of the Cs atom and $\omega_0 = 2\pi \times 10$ MHz. The longitudinal energy is set to $\varepsilon_\parallel = 2 \times 10^{-6}$ and the transversal energy is varied within the interval $10^{-5} \leq \varepsilon_\perp \leq 8 \times 10^{-4}$, corresponding to a range 0.2π kHz $\leq \omega_\perp \leq 16\pi$ kHz for the waveguide confinement frequency. We thereby focus on the low energy regime, characterized by $ka_\perp \ll 1$. In the following we calculate the transmission coefficient given by:

$$T_\ell = |1 + f_{e,\ell}|^2, \tag{2.61}$$

where $f_{e,\ell}$ is the one-dimensional scattering amplitude for the ℓ-wave.

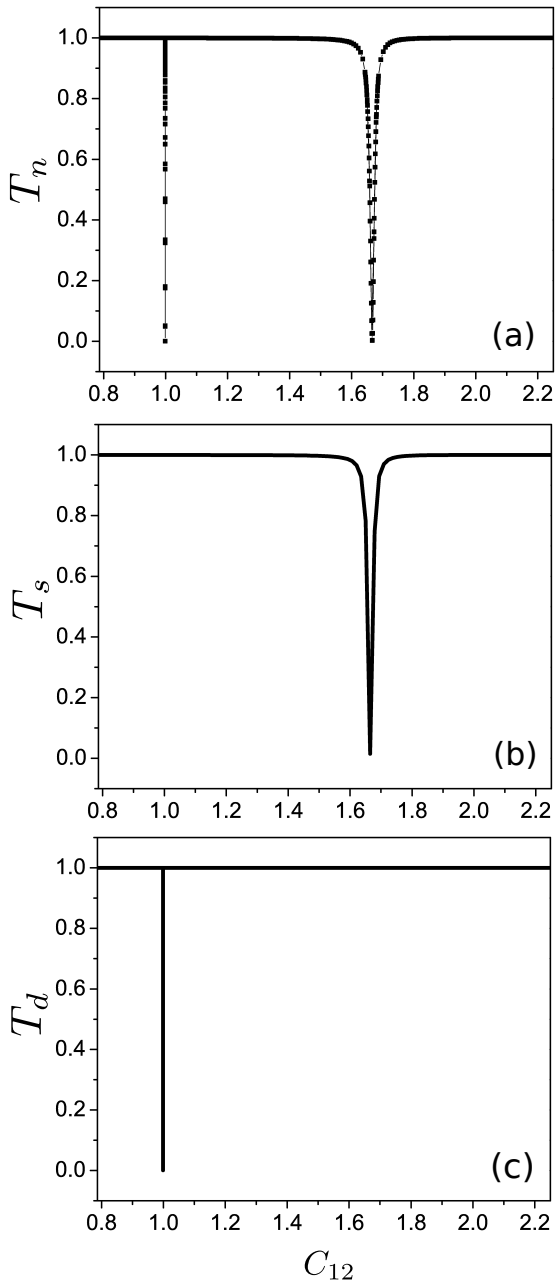

Figure 2.12: (a) Numerically calculated transmission coefficient T_n,which shows the d-wave CIR on the l.h.s and the s-wave CIR on the right hand side. The analytically calculated (b) s-wave transmission coefficient, T_s, and (c) d-wave transmission coefficient, T_d. The transversal confinement frequency is $\omega_\perp = 10^{-5}$.

In Fig. 2.12 we present the transmission coefficient as a function of C_{12} at a transversal frequency $\omega_\perp = 10^{-5}$. T_n in Fig. 2.12(a) denotes the numerically calculated trans-

mission coefficient, as it was shown in [34, 131].[6] We observe the appearance of two minima ($T_n = 0$) due to resonances. The minimum on the right hand side of Fig. 2.12(a) refers to the s-wave CIR and the minimum on the left hand side to the d-wave CIR. Due to the centrifugal barrier the width of the d-wave CIR is much narrower than that of the s-wave CIR. Additionally, we observe that both resonances yield a Lorentzian-like lineshape in the transmission spectrum. This occurs due to the fact that the weak confinement suppresses the interference effects between the s-wave and d-wave interactions.

In Fig. 2.12(b) the analytically calculated transmission coefficient T_s, as given by Eqs.(2.15) and (2.61), is shown which refers to s-wave interactions only. T_s describes very accurately the s-wave CIR (see Fig. 2.12(a)-(b)), whereas there is no trace of the d-wave CIR, since contributions from higher partial waves are not included in Eq.(2.15). In Fig. 2.12(c) the analytic expression of the transmission coefficient T_d is depicted according to Eqs.(2.59) and (2.61). We observe that the d-wave CIR is described qualitatively accurate enough (see also insets of Figs.2.13(a)-(b)), despite the fact that in the analytical calculations we have neglected the contributions of s-wave scattering, since the transversal confinement is very weak. We note that the results shown in Figs. 2.12(b) and 2.12(c) being obtained analytically for the pure s- and d-wave scattering cases lead to an accurate description of the scattering processes in the presence of a weak external harmonic potential.

Let us now determine the regime of validity of the approximative analytical results for the d-wave pseudopotential scattering by comparing it with the corresponding numerical simulations. In Fig. 2.13 we show the transmission coefficient T calculated numerically (Fig. 2.13(a)) and analytically (Fig. 2.13(b)) for several transversal confinement frequencies $\omega_\perp$. In Fig. 2.13(a) for a strong confinement, e.g. $\omega_\perp = 8 \times 10^{-4}$, we first observe that the numerically calculated position of the resonance deviates substantially from the analytical one. However, as $\omega_\perp$ decreases the numerical results for the position of the d-wave CIR converges to the corresponding analytical one. The origin of this behavior is the fact that we considered only d-wave interactions in the analytical calculations and neglected contributions from the s-wave interactions. This approximation is eligible in the regime of a weak confinement, e.g. $\omega_\perp \leqslant 4 \times 10^{-5}$, where the s- and d-wave free space resonances are weakly coupled, and in the vicinity of the d-wave CIR the d-wave interactions are dominant over the s-wave. In the regime of strong confinement the transmission spectrum T, in the vicinity of the d-wave CIR, exhibits a strong asymmetric Fano-lineshape, with T_n changing abruptly from zero to one. The latter is an interference effect of the strong s- and d-wave interactions in the confinement and cannot be described by this analytical pure d-wave model. However, this asymmetric profile gets suppressed with decreasing $\omega_\perp$ yielding a Lorentzian-like lineshape.

The right panels of Fig. 2.13 show a high-resolution graph of the d-wave CIR calculated analytically and numerically for $\omega_\perp = 10^{-5}$, where the dashed vertical line in both plots indicates the position of the minimum of the numerically calculated transmission

[6] For more details on the numerical techniques which we employ see appendix A.

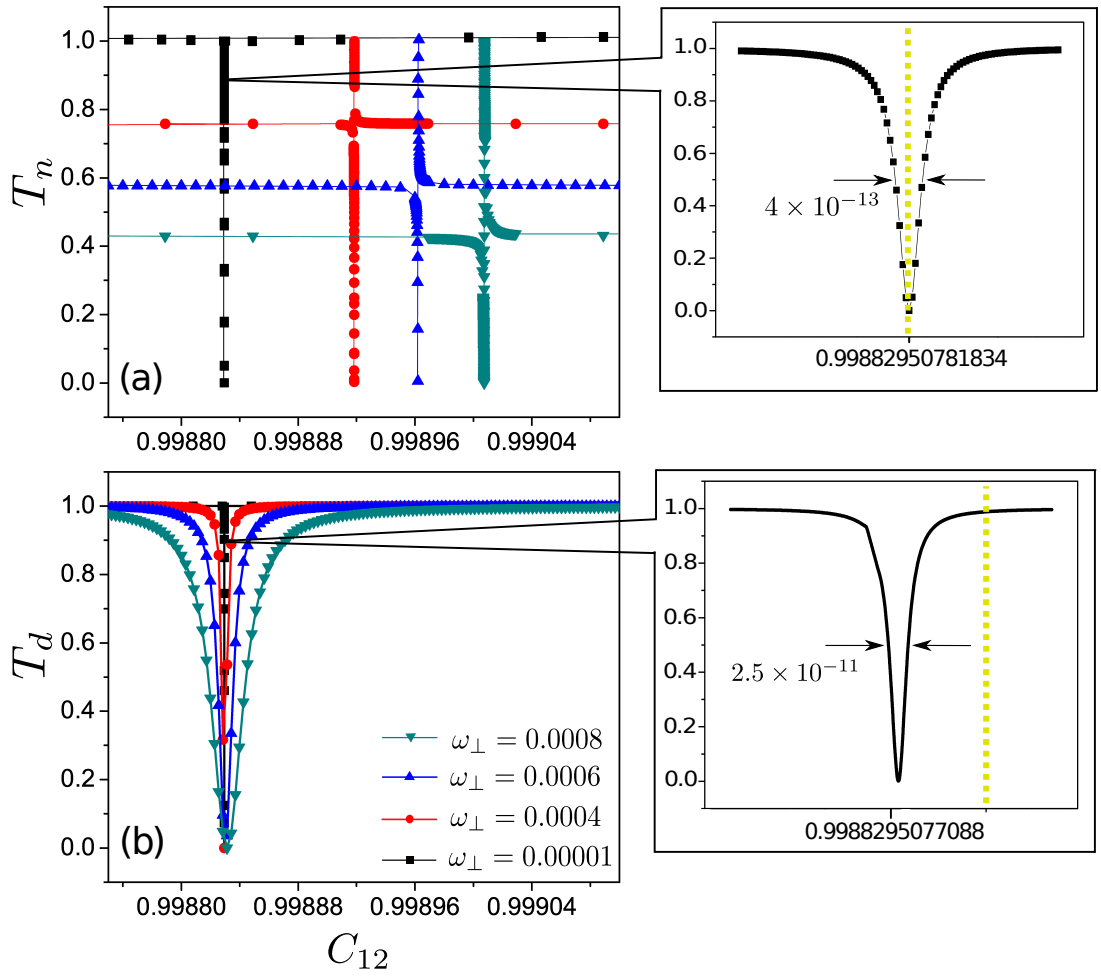

Figure 2.13: (a)(left panel) The numerically calculated transmission coefficient T_n versus C_{12} parameter for several confinement frequencies $\omega_\perp$, (right panel) high-resolution figure of the d-wave CIR for $\omega_\perp = 10^{-5}$ where the inwards-pointing arrows denote the width of the resonance. (b)(left panel) The analytically calculated transmission coefficient T_d as a function of the C_{12} parameter calculated with the d-wave pseudopotential for the corresponding values of $\omega_\perp$, (right panel) high-resolution graph of the d-wave CIR for $\omega_\perp = 10^{-5}$. The yellow dashed line in the right panels indicates the minimum of the numerical calculated transmission coefficient ($T_n = 0$) in comparison with the corresponding analytical result.

coefficient T_n. We observe that the d-wave pseudopotential approximation qualitatively describes the numerical simulations in the regime of weak confinement. However, in this small scale of the C_{12} values the analytical results show that the width of the d-wave CIR is by two orders wider than the numerical predictions, as well as there is a slight difference in the position of the d-wave CIR. These quantitative deviations again occur

due to s-wave interactions, which act as corrections in the transmission coefficient T_n despite the weak coupling of the s-wave and d-wave interactions.

2.4.4 Concluding remarks

We have derived and analyzed analytical expressions for resonant d-wave scattering in a harmonic waveguide in the framework of pseudopotential theory. The interatomic interaction has been modeled by a pure d-wave pseudopotential introduced in [28, 87], which enable us to analytically derive the resonance condition for the d-wave CIRs. Despite its simplicity, we observe that the analytical pseudopotential approach provides results which are in qualitative agreement with the corresponding numerical results in the regime of weak confinement, due to the very small interference effects of s- and d-wave interactions. The appearance of the d-wave CIR in a waveguide is strongly affected by the virtual excitations over all the closed excited modes of the transversal confinement, which occur during the collision process. However, for a strong transversal confinement the analytically and numerically calculated lineshapes of the transmission coefficient T, as well as the respective positions of the d-wave CIR, deviate from each other. This is attributed to the strong interference effect of the s- and d- partial waves in the confinement, which yields an asymmetric Fano profile. Such an interference effect can not be predicted within the single partial wave model which we employed. Nevertheless, our analytical result given by Eq.(2.59) can be used for weak confinement for the analysis of resonant scattering processes in confined geometries beyond s-wave physics.

Finally, we remark that our work clearly demonstrates the necessity of a scattering theory describing systems which possess mixed symmetries, capturing interference effects between different partial waves. One can note that the system which we have examined in this subsection has two specific symmetries imposed by the interatomic and confining potentials. In particular, the interatomic potential possesses a spherical symmetry, whereas the external harmonic confining potential has a cylindrical one. This mixing of symmetries leads to two regimes in the configuration space where only one symmetry prevails and consequently the good quantum numbers can differ from one region to the other. On the other hand, the pseudopotentials that exist so far in the literature are constructed in such a way that they only capture the spherical symmetry of the two-body interactions and the corresponding good quantum numbers. Hence, the need for extended pseudopotential theories encapsulating mixed symmetries is apparent.

2.5 Brief summary

In this chapter we have examined the modifications which the two-body scattering undergoes in the low-dimensional gases. In particular, we have shown that the s-wave collisions of an atomic pair in the presence of a harmonic waveguide demonstrate a new class of resonant phenomena: the so-called confinement-induced resonances. We have shown that the CIR effect fulfills a Fano-Feshbach scenario or it can be thought as the result of the virtual excitations spanned over all the energetically closed channels of the transversal confinement. These two interpretations at first glance do not complement each other, though as we will see in chapter 3 they can be unified providing a more insightful physical picture.

From an experimental point of view the CIR effect permits to control the interactions of the atomic ensembles in the low-dimensional systems introducing extra handling parameters such as the confinement frequency. In the direction of strongly correlated gases the utility of the CIR effect played a pivotal role providing the necessary means for the experimental realization of the effectively one-dimensional bosonic gases interacting either strongly repulsive or attractive, the so-called Tonks-Girardeau and super-Tonks-Girardeau phases, respectively. These successes of the CIR effect have triggered the interest of the scientific community, leading to a deeper theoretical and experimental investigation of other types of confinement-induced processes which emerge in various low-dimensional systems.

In particular, we have focused in this chapter on confinement-induced processes beyond the s-wave physics, investigating the impact of the confinement on the atomic ensembles which collide with higher partial wave interactions. Such systems possibly provide the means to study high-temperature superconductivity and superfluidity with higher partial wave interactions. Investigating a system of s- and d-wave interacting bosonic atoms in a harmonic waveguide we have observed an additional structure in the resonant spectrum yielding d-wave CIRs. The positions of the d-wave CIRs possess some universal characteristics since they do not depend on the short-range physics. Contrary to the s-wave CIRs, we have observed that the positions of d-wave CIRs depend on the long-range tail of the interatomic potential. Analyzing further the d-wave CIRs within the pseudopotential framework we analytically derived their resonance condition and showed that this effect arises from the virtual excitations over all the closed eigenmodes of the transversal confinement. Although this analysis is valid in the regime of weak confinement and provides a good qualitative agreement with the exact numerical calculations, in the limit of strong confining trapping frequencies our model did not capture the interference effects of s- and d-partial waves.

Concluding, a thorough theoretical treatment is still needed, extending the CIR physics in quasi-one-dimensional geometries beyond s-wave interactions. Therefore, in chapter 3 we will present the development of a nonperturbative theoretical framework for multichannel scattering based on first principles in order to highlight the underlying collisional physics of these systems. Moreover, in chapter 4 we will show that the robustness of this theoretical treatment plays a crucial role in systems which do not

conserve the angular momentum, i.e. dipoles or quandrupoles, providing deeper insights on the corresponding collisional physics. The theoretical understanding of the physics of the corresponding scattering properties will help us to manipulate or design new many-body phases of ultracold gases which interact with anisotropic forces.

Chapter 3

K-matrix theory for atomic collisions in harmonic waveguides

In the previous chapter we already presented the theoretical limitations of the pseudopotential theory to tackle systems where different higher partial wave interactions yield strong interfering phenomena in two-body collisional events.

In order to deepen our understanding on the collisional properties of such systems the necessity of a multichannel scattering treatment is apparent. Thereby, in this chapter we will present a nonperturbative theoretical framework to treat atom-atom collisions within a harmonic waveguide, where all the higher partial waves are properly taken into account either for bosons or fermions [36]. This method is based on the K-matrix theory generalising the ideas which were presented in [33]. Furthermore, converting the "physical" quasi-one-dimensional K-matrix into a Dyson-like form of equations allows us to classify, in terms of specific transition diagrams, all possible processes which the two atoms undergo during the collision. This detailed analysis permits us to illustrate the connection of the transitions in the manifold of the closed channels of the transverse confinement with the Fano-Feshbach scenario for resonant scattering.

In contrast to free-space scattering, collisions in waveguides never approach the zero-energy limit since the total colliding energy of the atoms is bounded from below. This bound from below is equal to the energy of the transversal ground state of the confining potential, which is definitely nonzero. As a result the atoms perform collisions with a finite nonzero energy and therefore it is logical to assume that in such scattering process more than one partial waves either in the case of bosons or fermions may get involved. Hence, the inclusion of all higher partial waves during the collision processes in the presence of a confining potential yield non-trivial corrections to the position of the s- or p-wave CIRs in the case of bosons or fermions, respectively. Even further, the higher partial waves yield a rich resonant structure of mutually coupled ℓ-wave confinement-induced resonances where their positions can be described analytically. Another aspect of this method is that it captures fully the strong interference effects among different partial waves and the corresponding asymmetric Fano lineshapes in

the transmission spectra.

The ℓ-wave CIRs may play a crucial role in strongly correlated many-body systems rendering new properties. For example in the bosonic case being close to a particular ℓ-wave CIR means that in the atomic ensemble the corresponding ℓ-wave interactions are enhanced. Thus, the intrinsically different nature of these interactions are expected to alter the phase diagram of the transition from a non-interacting gas to the fermionization limit, namely the Tonks-Girardeau gas phase. Similar changes in the phase diagrams are expected also in the case of the super-Tonks-Girardeau phase.

3.1 An introduction to K-matrix representation

In general the K-matrix representation constitutes an essential mathematical technique for the theoretical study of scattering processes. As we have already mentioned in chapter 1 the scattering processes can be well described by the S-matrix which is a unitary matrix.

The K-matrix is defined as a Cayley transformation of the S-matrix given by the following relation [49]:

$$S = \frac{1 + iK}{1 - iK}. \tag{3.1}$$

where the simplicity of the K-matrix, according to Eq. (3.1), is based on the fact that one has only to ensure its hermiticity and immediately the unitarity of the S-matrix is fulfilled. From a mathematical point of view the construction of a hermitian matrix is not that elaborate as the case of unitary matrices.

One important feature of the K-matrix formalism is that it constitutes a meromorphic function yielding a simple pole structure, and its analyticity is a crucial key allowing for the theoretical investigation in a wide range of the parametric space, especially in cases where the poles overlap. The latter is permitted due to the fact that unitarity is fulfilled automatically [99].

Assuming free space collisions, where the atoms interact via a short-range potential $V_{sh}(\mathbf{r})$, we already now from chapter 1 that the S-matrix in the angular-momentum representation is diagonal with dimensions $\ell \times \ell$, where ℓ refers to the angular momentum quantum number. For the S-matrix we then have the following relation:

$$\underline{S} = \begin{pmatrix} \ddots & & 0 \\ & e^{2i\delta_\ell} & \\ 0 & & \ddots \end{pmatrix}, \tag{3.2}$$

where δ_ℓ denotes the phase shift of a particular ℓ-wave.

Hence, with the help of Eqs. (3.1) and (3.3) one finds that the K-matrix is also a

diagonal matrix of dimensions $\ell \times \ell$ and has the following form:

$$\underline{K} = \begin{pmatrix} \ddots & & 0 \\ & \tan\delta_\ell & \\ 0 & & \ddots \end{pmatrix}, \tag{3.3}$$

where one might note that the K-matrix is not only hermitian but is also symmetric, and hence real. This holds in the case of two spinless atoms where the S-matrix is symmetric, provided that the corresponding interactions are invariant under rotations. Note that the K-matrix can be intuitively understood as a measure of the deformation of the wave function from the form it has when the scattering potential $V_{sh}(\mathbf{r})$ is zero [53].

In addition, the K-matrix can be related also to other scattering observables such as the scattering amplitude, with the matrix elements given by the following expression [49]:

$$f_{\ell\ell'} = \frac{1}{k}\frac{K_{\ell\ell'}}{1 - iK_{\ell\ell'}}. \tag{3.4}$$

3.2 K-matrix approach for quasi-one dimensional systems

3.2.1 Hamiltonian and symmetries

Hamiltonian

We consider collisions of two atoms in the presence of an external potential, which confines the transversal degrees of freedoms. The transversal confinement is induced by a harmonic potential, which permits a separation of center of mass and relative degrees of freedom. Thus the two-body scattering problem can be reduced to a problem of a single particle (relative particle) scattered by a potential (interatomic potential) placed at the origin. The Hamiltonian of the relative degrees of freedom contains all the relevant physics and, expressed in cylindrical coordinates, reads:

$$H = -\frac{\hbar^2}{2\mu}\nabla^2 + \frac{1}{2}\mu\omega_\perp^2\rho^2 + V_{sh}(\mathbf{r}), \tag{3.5}$$

where μ is the reduced mass of the two colliding atoms, $\omega_\perp$ is the transversal confinement frequency and $V_{sh}(\mathbf{r})$ is a short-range interatomic potential. We assume that the interatomic and the transversal confinement potential do not depend on the azimuthal angle ϕ. Consequently, the corresponding quantum number m is conserved and throughout this chapter we will focus on $m = 0$. We remark that the Hamiltonian in Eq. (3.5) describes either bosons or fermions.

Symmetries

We observe that the relative Hamiltonian possesses two characteristic length scales, which are defined by the corresponding potential terms. Hence, we have one length

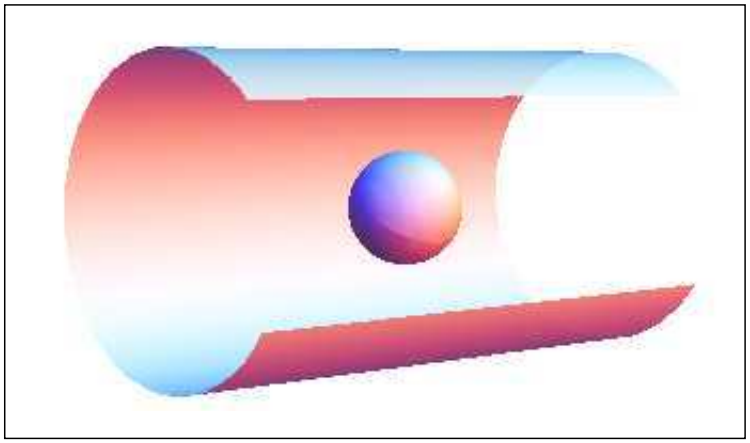

Figure 3.1: A schematic illustration of the symmetries of the potential terms in Hamiltonian Eq. (3.5). The cylindrical symmetry refers to the waveguide geometry and the spherical symmetry is imposed by the two-body interaction potential.

scale which is the range r_0 of the interatomic interactions $V_{sh}(\mathbf{r})$ while the second length scale refers the length of the transversal confinement, namely $a_\perp = \sqrt{\mu/\hbar\omega_\perp}$. Consequently, in an experimental environment the range of the two-body interactions is orders of magnitude smaller than the experimental achievable confining trapping frequencies, $r_0 \ll a_\perp$. Therefore, the length scale separation imposes that the relative Hamiltonian possesses two approximate symmetries in different regions of the configuration space as it is illustrated in Fig. 3.1: the spherical symmetry of the two-body interaction potential and the cylindrical symmetry of the harmonic waveguide potential. This remarkable property allows us to partition the configuration space into three regions and approximate the corresponding wave functions which encapsulate the relevant scattering information avoiding to calculate the total wave function in the whole configuration space.

More specifically, we observe that near the origin, $r < r_0$, the interatomic potential $V_{sh}(\mathbf{r})$ of range r_0 dominates and therefore the collision process obeys spherical symmetry. Thus in this regime, for $r \approx r_0$, the relative particle experiences a free-space collision off the interatomic potential with the total colliding energy $E = \hbar^2 k^2/2\mu$. This process can be described by the following wave function:

$$\Psi_{\ell'}(\mathbf{r}) = \sum_{\ell} F_\ell(r,\theta)\delta_{\ell\ell'} - G_\ell(r,\theta)K^{3D}_{\ell\ell'}, \tag{3.6}$$

where ℓ' labels the linearly independent solutions, $F_\ell(r,\theta)$ ($G_\ell(r,\theta)$) is the regular (irregular) solution, i.e. spherical Bessel $j_\ell(r)$ (spherical von Neumann $n_\ell(r)$) functions multiplied by the Legendre polynomials $P_\ell(\theta)$. The summation runs over all the even (odd) ℓ for the case of bosons (fermions). $K^{3D}_{\ell\ell'}$ are the elements of the K-matrix $\underline{K}^{3D}$ in three-dimensions encapsulating all the scattering information related to the interatomic potential $V_{sh}(\mathbf{r})$. Due to the short-range character of the interatomic interactions $\underline{K}^{3D}$

is diagonal and its elements are equal to $\tan\delta_\ell$, with δ_ℓ being the phase shift of the ℓ-th partial wave [see Eq.3.3)].

Additionally, in the asymptotic limit, $|\mathbf{r}| \to \infty$, the transversal confinement term in Eq. (3.5) dominates implying its cylindrical symmetry. The total colliding energy E can be written as a sum of the transversal energy being determined by the harmonic confinement and the longitudinal energy, which involves the z-component of the momentum of the relative particle, according to the relation $E = \hbar^2 k^2/2\mu = \hbar\omega_\perp(2n+1) + \hbar^2 q_n^2/2\mu$. In this region the wave functions are axially symmetric and can be written as:

$$\Psi_{n'}(\mathbf{r}) = \sum_n f_n(z,\rho)\delta_{nn'} - g_n(z,\rho)K^{1D}_{nn'}, \tag{3.7}$$

where n' labels the linearly independent solutions, $K^{1D}_{nn'}$ are the elements of the K-matrix $\underline{K}^{1D}$ in quasi-one dimension and $f_n(z,\rho)$ ($g_n(z,\rho)$) is the regular (irregular) solution in the presence of the trap with no interactions. The specific form of the regular and irregular solutions are as follows:

$$\begin{pmatrix} f_n(z,\rho) \\ g_n(z,\rho) \end{pmatrix} = \Phi_n(\rho) \begin{cases} \begin{pmatrix} \cos q_n|z| \\ \sin q_n|z| \end{pmatrix} & \text{for bosons} \\ \frac{z}{|z|}\begin{pmatrix} \sin q_n|z| \\ -\cos q_n|z| \end{pmatrix} & \text{for fermions} \end{cases} \tag{3.8}$$

where $\Phi_n(\rho)$ are the eigenfunctions of the two-dimensional harmonic oscillator for $m = 0$ and the functions in the curly bracket refer to the longitudinal degree of freedom including the symmetrization (antisymmetrization) for the case of bosons (fermions).

So far it is clear that the scattering process of atomic collisions in the presence of a harmonic waveguide is characterized by two distinct regions in the configuration space which possess different symmetries. Thus, the key idea is to perform a frame transformation which will permit the matching of Eqs. (3.6) and (3.7) yielding an expression of $\underline{K}^{1D}$ in terms of $\underline{K}^{3D}$, allowing in this manner the information of the collision events which occurred close to the origin to be "propagated" outwards to the asymptotic regime. Obviously, a unitary frame transformation in this case does not exist since Eqs. (3.6) and (3.7) do not fulfill the same Schrödinger equation in complete configuration space. However, since the length scales of the interatomic potential r_0 and the harmonic oscillator $a_\perp$ are well separated we have that between the two distinct regions of spherical and cylindrical symmetry there is an intermediate region where $V_{sh}(\mathbf{r}) \approx \frac{1}{2}\mu\omega_\perp^2\rho^2 \approx 0$. Consequently, for this configuration subspace Eqs. (3.6) and (3.7) fulfill approximately the same Schrödinger equation which is simplified to a Helmholtz equation. Therefore, in this region one can perform a local and non-orthogonal frame transformation. The idea of local frame transformations was introduced by Harmin and Fano [100, 101, 102] and extended later on by Greene [103].

3.2.2 Local frame transformation

As it was shown in [103] a frame transformation can not be derived by projecting directly Eq. (3.6) onto Eq. (3.7) and vice versa, since these two sets of solutions refer

to two different Schrödinger equations. Hence, a different approach is needed.

Initially, we consider the Hamiltonian Eq. (3.5) with no external trapping potential. At interparticle distances larger than the range of the two-body interactions the corresponding Schödinger equation trivially becomes a Helmholtz equation. Therefore, one can interrelate the scattering solutions expressed in spherical representation to those which are expressed in cylindrical coordinates. This interrelation renders an orthogonal frame transformation matrix, which can be derived by projecting the energy normalized regular spherical solutions onto the regular cylindrical ones.

The regular energy normalized scattering solutions in spherical representation are given by

$$F_{\ell m}(\mathbf{r}) = \sqrt{\frac{(2\ell+1)(l-m)!}{4\pi(l+m)!}} e^{im\phi} P_\ell^m(\cos\theta)(2k/\pi)^{1/2} j_\ell(kr), \tag{3.9}$$

where $P_\ell^m(\cos\theta)$ are the associated Legendre polynomials and $j_\ell(kr)$ are the spherical Bessel functions with the wave vector k being defined by the total colliding energy $E = \hbar^2 k^2/\mu$.

In addition, the energy normalized regular scattering solution in cylindrical coordinates is given by

$$f_{qm}(\mathbf{r}) = (2\pi)^{-1/2} e^{im\phi} J_m(\sqrt{k^2-q^2}\rho)(\pi q)^{-1/2} \begin{cases} \cos q|z| & \text{for bosons} \\ \frac{z}{|z|}\sin q|z| & \text{for fermions} \end{cases} \tag{3.10}$$

where the wave vector q refers to the z-component of the wave function F_{qm} ranging from 0 to k and $J_m(\sqrt{k^2-q^2}\rho)$ are the Bessel functions and the functions in curly bracket refer to different particle symmetries.

The two solutions are matched according to the following relation:

$$f_{qm}(\mathbf{r}) = \sum_\ell F_{\ell m}(\mathbf{r}) \tilde{U}_{\ell q}(m), \tag{3.11}$$

where the summation runs over all the even (odd) ℓ for particles of bosonic (fermionic) symmetry. The quantity $\tilde{U}_{\ell q}(m)$ refers to the elements of the frame transformation matrix. These matrix elements can be derived analytically (see Ref.[104]) by projecting Eq. (3.9) onto Eq. (3.10), yielding

$$\tilde{U}_{\ell q}(m) = \sqrt{\frac{(2\ell+1)(\ell-m)!}{kq(\ell+m)!}} (-1)^{[\frac{\ell-m-1}{2}]} P_\ell^m(q/k), \tag{3.12}$$

where in the quantity $(-1)^{[\frac{\ell-m-1}{2}]}$, the term $[\frac{\ell-m-1}{2}]$ denotes the smallest integer greater than or equal to $\frac{\ell-m-1}{2}$. The frame transformation $\underline{\tilde{U}}$ is orthogonal within an energy shell defined by the total colliding energy E. Namely, we have that

$$F_{\ell m}(\mathbf{r}) = \int_0^{k^2/2} d(\frac{q^2}{2}) \tilde{U}_{\ell q}(m) f_{qm}(\mathbf{r}). \tag{3.13}$$

Note that the integration arises from the fact that the wave vector q is a continuous variable. Consequently, the frame transformation obeys the following relations:

$$\int_0^{k^2/2} d(\frac{q^2}{2})\tilde{U}_{\ell' q}(m)\tilde{U}_{q\ell}(m) = \delta_{\ell'\ell} \quad \text{and} \tag{3.14}$$

$$\sum_{\ell} \tilde{U}_{q'\ell}(m)\tilde{U}_{\ell q}(m) = \delta(q' - q). \tag{3.15}$$

As it was proposed in Ref.[103] this frame transformation can be generalized for the case of Hamiltonian Eq. (3.5) including the external harmonic potential. The exact regular cylindrical solutions in the presence of a harmonic potential at large separation distances are given by

$$f_{nm}(\mathbf{r}) = N_{nm} e^{im\phi} e^{-\frac{\rho^2}{2a_\perp^2}} (\frac{\rho}{a_\perp})^{|m|} L_n^{|m|}(\frac{\rho^2}{a_\perp^2})(\pi q_n)^{-1/2} \begin{cases} \cos q_n|z| & \text{for bosons} \\ \frac{z}{|z|}\sin q_n|z| & \text{for fermions} \end{cases} \tag{3.16}$$

where $N_{nm} = \sqrt{\frac{n!}{\pi a_\perp^2 (n+|m|)!}}$ is the normalization constant and $L_n^{|m|}(\cdot)$ are the associated Laguerre polynomials. The momentum q_n refers to the z-component of the wave function and it is quantized according to the following energy relation:

$$\frac{k^2}{2} = (1/a_\perp)(2n + |m| + 1) + \frac{q_n^2}{2}, \tag{3.17}$$

where the term $(1/a_\perp)(2n + |m| + 1)$ refers to the discretized energy levels of the 2D harmonic oscillator.

The crucial observation here is that, at distances $\mathbf{r}$ smaller than the characteristic length scale $a_\perp$ and simultaneously larger than the range of interatomic potential, namely $r_0 < r < a_\perp$, the potential terms in Eq. (3.5) are negligible and the solutions in Eq. (3.16) become proportional to those of Eq. (3.10). Hence, multiplying Eq. (3.10) by this proportionality factor and converting the integral of Eq. (3.13) into sums over n with $\int -d(q^2/2) \to (2/a_\perp)\sum_n$, we obtain

$$F_{\ell m}(\mathbf{r}) = \sum_{n=0}^{n_{\max}} U_{\ell n}(m) f_{nm}(\mathbf{r}) \tag{3.18}$$

where $U_{\ell n}(m) = (2/a_\perp)^{1/2}\sqrt{\frac{n!}{(n+|m|)!}}[(2n + |m| + 1)/2]^{1/2}\tilde{U}_{\ell q_n}(m)$ are the coefficients of the transformation U.

We remark that we are interested in the case of $m = 0$, for which the transformation U becomes $U_{\ell n} \equiv U_{\ell n}(0) = (2/a_\perp)^{1/2}\tilde{U}_{\ell q_n}(0)$. Then, by using the identity $U^T U = I$ in Eq. (3.18) the corresponding solutions $f_n(\mathbf{r})$ with $F_\ell(\mathbf{r})$ are connected according to the relation

$$f_n(\mathbf{r}) = \sum_{\ell} F_\ell(\mathbf{r}) U_{\ell n}. \tag{3.19}$$

A key point is that the transformation U is not orthogonal as $\tilde{U}$, since $f_n(\mathbf{r})$ and $F_\ell(\mathbf{r})$ do not fulfill the same Schrödinger equation everywhere in the configuration space. However, this set of solutions fulfills the same Schrödinger equation at a particular subregion of the configuration space where the external harmonic and interatomic potential are assumed to be approximately zero. Therefore, the frame transformation U is valid only in this *local* part of the configuration space, where one can interrelate $f_n(\mathbf{r})$ and $F_\ell(\mathbf{r})$.

So far we have managed to match only the regular parts of Eqs. (3.6) and (3.7). The irregular parts of Eqs. (3.6) and (3.7) can be connected by the same local frame transformation U. As Fano pointed out in Ref.[102] at $r > r_0$ we can construct the Green function, $G_s(\mathbf{r}, \mathbf{r}')$, from the solutions of Eq. (3.6) to a good approximation. In addition, from the solutions in Eq. (3.7) we can compose the corresponding Green function $G_c(\mathbf{r}, \mathbf{r}')$ which refers to distances $r > a_\perp$. Hence, at distances $r_0 < r < a_\perp$ the two Green functions become equal, since the corresponding Schrödinger equation is turned into a Helmholtz equation. Then for $r_0 < r, r' < a_\perp$ we have that

$$G_s(r, r') = G_c(r, r') \Rightarrow \pi \sum_\ell G_\ell(\mathbf{r}) F_\ell(\mathbf{r}') = \pi \sum_n g_n(\mathbf{r}) f_n(\mathbf{r}'). \tag{3.20}$$

Multiplying with $F^*_\ell(\mathbf{r}')$ and integrating over $d^3\mathbf{r}'$ Eq. (3.20) takes the following form:

$$G_\ell(\mathbf{r}) = \sum_n^{n_{\max}} g_n(\mathbf{r}) U_{n\ell}. \tag{3.21}$$

With the help of Eqs. (3.19) and (3.21) we can now express the $\underline{K}^{1D}$ matrix in Eq. (3.7) in terms of the $\underline{K}^{3D}$ of Eq. (3.6). Namely, we have that:

$$\begin{aligned}
\sum_{\ell'} \Psi_{\ell'}(\mathbf{r}) U_{\ell' n'} &= \sum_{\ell'} F_{\ell'}(\mathbf{r}) U_{\ell' n'} - \sum_{\ell, \ell'} G_\ell(\mathbf{r}) K^{3D}_{\ell\ell'} U_{\ell' n'} \\
&= f_{n'}(\mathbf{r}) - \sum_{\ell, \ell', n} g_n(\mathbf{r}) U_{n\ell} K^{3D}_{\ell\ell'} U_{\ell' n'} \Rightarrow \\
\Psi_{n'}(\mathbf{r}) &= f_{n'}(\mathbf{r}) - \sum_n g_n(\mathbf{r}) \underbrace{\left(\sum_{\ell, \ell'} U_{n\ell} K^{3D}_{\ell\ell'} U_{\ell' n'} \right)}_{K^{1D}_{nn'}}
\end{aligned} \tag{3.22}$$

Hence, the $\underline{K}^{1D}$ has the following compact matrix form:

$$\underline{K}^{1D} = \underline{U}^T \underline{K}^{3D} \underline{U}, \tag{3.23}$$

where we recall that the matrix elements of the local frame transformation U have the following explicit form:

$$U_{\ell n} = \frac{\sqrt{2}(-1)^{d_0}}{a_\perp} \sqrt{\frac{2\ell + 1}{k q_n}} P_\ell\left(\frac{q_n}{k} \right). \tag{3.24}$$

In Eq. (3.24), $P_\ell(\frac{q_n}{k})$ is the ℓ-th Legendre polynomial and the term d_0 is $\ell/2$ or $(\ell-1)/2$ for the case of bosons or fermions, respectively. Note that the local transformation U connects the partial waves ℓ with the modes n of the transversal confining potential.

In Eq. (3.23) the matrix $\underline{K}^{1D}$ thus involves an admixture of all partial waves of the interatomic potential with all energetically *open* channels of the transversal confinement for all energies. However, as was shown in Ref.[33], one can perform an analytic continuation in Eq. (3.24) by setting $q_n \to iq_n$. Then, in this case one can include in the local frame transformation U also the energetically *closed* channels of the transversal confinement. We remark that the corresponding $\underline{K}^{1D}$ has the same structure as in Eq. (3.23). Though, the drawback of this analytic continuation is that the $\underline{K}^{1D}$ is not anymore a *physical* one, in the sense that it corresponds to a wave function which asymptotically, at $|\mathbf{r}| \to \infty$, does not possess the physically accepted behavior. This can be understood from Eq. (3.7) where for the energetically open channels the wave function shows the correct oscillatory behavior. Now, in order to describe the closed channels we substitute q_n with iq_n, therefore the wave function contains exponentially growing subterms as $|\mathbf{r}| \to \infty$ instead of decaying. The latter is the correct boundary behavior of the wave function in the closed channels. In the following subsection we will discuss how such discrepancies can be removed with the help of *multichannel quantum defect theory* (MQDT)[105] yielding a *physical* $\underline{K}^{1D}$ matrix which will correspond to a wave function with the correct asymptotic behavior.

3.2.3 Boundary conditions and physical one-dimensional K-matrix

In our study we focus on the single-mode regime, where the collision takes place in the ground state of the transversal confinement. Thus, the total colliding energy is $E = \hbar^2 k^2/2\mu = \hbar\omega_\perp + \hbar^2 q_0^2/2\mu$ yielding one energetically open channel ($n = 0$) and n energetically closed channels, where $E < \hbar\omega_\perp(2n+1)$ for $n \neq 0$. Note that the total amount of the open and the closed channels is N and it is related to the principal quantum number according to the relation $N = n + 1$ ($N \to \infty$). However, the above-mentioned consideration results in an unphysical asymptotic wave function $\Psi_{n'}(z,\rho)$. Equation (3.7) is given in terms of $f_n(z,\rho)$ and $g_n(z,\rho)$, where the motion in the z-direction is described by $\cos q_n|z|$ and $\sin q_n|z|$ (see Eq. (3.8)). Now, the quantity $q_n|z|$ becomes imaginary for $n \neq 0$ (closed channels), and consequently the z-dependent terms in Eq. (3.8) contain exponentially diverging subterms for $z \to \infty$. In order to restore the correct boundary conditions of the asymptotic wave function one has to "renormalize" these divergences. This can be done within the framework of MQDT by partitioning the wave function in open and closed channel subspaces [105, 53]. In general the wave function can be written as follows:

$$\begin{pmatrix} \underline{\Psi}_{oo} & \underline{\Psi}_{oc} \\ \underline{\Psi}_{co} & \underline{\Psi}_{cc} \end{pmatrix} \begin{pmatrix} \underline{Y}_{oo} \\ \underline{Y}_{co} \end{pmatrix} = \left[\begin{pmatrix} \underline{f}_o & 0 \\ 0 & \underline{f}_c \end{pmatrix} - \begin{pmatrix} \underline{g}_o & 0 \\ 0 & \underline{g}_c \end{pmatrix} \begin{pmatrix} \underline{K}^{1D}_{oo} & \underline{K}^{1D}_{oc} \\ \underline{K}^{1D}_{co} & \underline{K}^{1D}_{cc} \end{pmatrix} \right] \begin{pmatrix} \underline{Y}_{oo} \\ \underline{Y}_{co} \end{pmatrix}, \qquad (3.25)$$

where "o" ("c") indicates the open (closed) subspace referring to $n = 0$ ($n \neq 0$), respectively and $\underline{\Psi}$, $\underline{Y}$, $\underline{f}$, $\underline{g}$, $\underline{K}$ are partitioned submatrices dictated by the channel

decomposition of the considered problem. We choose a linear combination of Eq. (3.25) in order to eliminate the diverging terms in the closed channels[1] . Hence, by setting the coefficients $\underline{Y}_{oo} = \mathbb{I}$ then the coefficients $\underline{Y}_{co}$ are determined by the following relation:

$$\underline{\Psi}_{co}\underline{Y}_{oo} + \underline{\Psi}_{cc}\underline{Y}_{co} = 0 \Rightarrow \underline{Y}_{co} = \left(\frac{\underline{f}_c}{\underline{g}_c} - \underline{K}_{cc}^{1D}\right)^{-1} \underline{K}_{co}^{1D}, \tag{3.25}$$

where the term $\underline{f}_c/\underline{g}_c \xrightarrow{|z|\to\infty} -iI$.

Then Eq. (3.25) takes the form:

$$\begin{aligned} \underline{\Psi}^{phys} &\equiv \underline{\Psi}_{oo}\underline{Y}_{oo} + \underline{\Psi}_{oc}(-\underline{K}_{cc}^{1D} - i\mathbb{I})^{-1}\underline{K}_{co}^{1D} \\ &= \underline{f}_o - \underline{g}_o[\underline{K}_{oo}^{1D} + i\underline{K}_{oc}^{1D}(\mathbb{I} - i\underline{K}_{cc}^{1D})^{-1}\underline{K}_{co}^{1D}], \end{aligned} \tag{3.26}$$

where $\underline{\Psi}^{phys}$ is the *physical* wave function, which involves only the open channels since the diverging parts of the closed channels, namely $\underline{f}_c$ and $\underline{g}_c$, are removed. Moreover, the contribution of the closed channels during the collision process is imprinted in the corresponding *physical* K-matrix, which has the following form:

$$\underline{K}_{oo}^{1D,\ phys} \equiv \underline{K}_{oo}^{1D} + i\underline{K}_{oc}^{1D}(\mathbb{I} - i\underline{K}_{cc}^{1D})^{-1}\underline{K}_{co}^{1D}. \tag{3.27}$$

We remark that the resonances appear as poles of the $\underline{K}_{oo}^{1D,\ phys}$ matrix. This is achieved when the matrix $(\mathbb{I} - i\underline{K}_{cc}^{1D})$ becomes singular or otherwise when its determinant becomes zero. Namely, we have that:

$$det(\mathbb{I} - i\underline{K}_{cc}^{1D}) = 0 \tag{3.28}$$

Hence, the roots of Eq. (3.28) provide the location of the bound states of the closed channels in the parameter space, which energetically lie in the continuum of the open channel or in other words, the condition given in Eq. (3.28) describes resonances which fulfill a Fano-Feshbach scenario.

We remark that the physical K-matrix is not restricted only to the single mode regime which we examine in this chapter. Due to its general form it can be easily expended in to the multi-mode regime, namely more than one open channels, permitting thus the study of multichannel effects and their impact on scattering processes in the presence of external potentials.

3.3 Results and discussion

3.3.1 Dyson form of physical K-matrix for multiple partial waves

Physical K^{1D} matrix for a single partial wave

As it was shown in [33], for collisions which involve a single partial wave, the matrix elements of the $\underline{K}^{1D} \equiv \underline{K}_\ell^{1D}$ are given by the simple relation $\{\underline{K}_\ell^{1D}\}_{nn'} = (U^T)_{n\ell}\tan\delta_\ell U_{\ell n'}$,

[1]The terms $\underline{f}_c$ and $\underline{g}_c$ contain the $\cos q_n|z|$ and $\sin q_n|z|$ [see Eq. (3.8)]. In the closed channels ($n \neq 0$) the quantity q_n becomes imaginary [see Eq. (3.17)]. Hence the cosine and sine functions become exponential functions which diverge for $|z| \to \infty$.

where after the diagonalization and the inversion of $(\mathbb{I}-i\underline{K}^{1D}_{cc,\ell})$ one can obtain $\underline{K}^{1D,\ phys}_{oo,\ell}$ in closed form. However, one should note that $\underline{K}^{1D}_{\ell}$ in this case is a rank one matrix. Interestingly, one can rewrite $\underline{K}^{1D,\ phys}_{oo,\ell}$ in a much simpler form by exploiting this property with the help of an identity for matrix inversions, which involve rank one matrices [106]. More specifically, if the matrices $I - i\underline{K}^{1D}_{cc}$ and I are nonsingular with $-i\underline{K}^{1D}_{cc}$ being a rank one matrix then the $I - i\underline{K}^{1D}_{cc}$ can be inverted according to the following relation:

$$(I - i\underline{K}^{1D}_{cc})^{-1} = \mathbb{I} + \frac{i}{1 - i\gamma}\underline{K}^{1D}_{cc,\ell}, \tag{3.29}$$

where $\gamma = Tr(\underline{K}^{1D}_{cc,\ell})$. Then $\underline{K}^{1D,\ phys}_{oo,\ell}$ reads

$$\underline{K}^{1D,\ phys}_{oo,\ell} = \underline{K}^{1D}_{oo,\ell} + i\underline{K}^{1D}_{oc,\ell}\big(\mathbb{I} + \frac{i}{1 - i\gamma}\underline{K}^{1D}_{cc,\ell}\big)\underline{K}^{1D}_{co,\ell}. \tag{3.30}$$

Transition diagrams: virtual excitations and Fano-Feshbach resonances

A remarkable feature of Eq. (3.30) is that it provides us with all the transitions which the two atoms undergo during the collision. Fig. 3.2 illustrates Eq. (3.30) as a transition diagram, where the transitions are not direct, but through the ℓ-th partial wave, which participates as an intermediate process. Thus, the first term, both in Fig. 3.2 and in Eq. (3.30) indicates a direct "open-open" (oo) channel transition and contains, in particular, the description of potential resonances. The second term of Eq. (3.30) is related with transitions into closed channels, which can be split into two processes. As it is shown in Fig. 3.2 the second term of Eq. (3.30) consists of two transition processes, the first describes an "open-closed-open" (oco) channel transition, while the second describes an "open-closed" (oc) channel transition, followed by transitions from *all* closed channels to *all* closed channels (cc) and finally a "closed-open" (co) channel transition. Note that a similar idea has been discussed in [108].

The contribution of the transitions into the closed channels during the two-body collision is significantly affected by the factor $1/(1-i\gamma)$, where the parameter γ includes all the closed channel transitions through an effective bound state which is supported by all the closed channels and for $\gamma \to -i$ the bound state coincides with the threshold yielding a resonant collision process. Indeed, according to MQDT this can be justified since the parameter $\gamma = Tr(\underline{K}^{1D}_{cc,\ell}) \to -i$ is a root of the relation $det(\mathbb{I} - i\underline{K}^{1D}_{cc,\ell}) = 1 - iTr(\underline{K}^{1D}_{cc,\ell}) = 0$ and as we have mentioned above these roots describe the closed channel bound states at given energy E. Thus, we observe that the K-matrix approach provides us with an important insight of CIR physics by linking in a transparent way the physical picture of virtual excitations [9] and the Fano-Feshbach-like scheme [10]. Additionally, an important aspect of the transition diagram (see Fig. 3.2) is that it illustrates in a clear manner the Fano-Feshbach mechanism: the first term represents the continuum (either interacting or non-interacting) and the second term exhibits all the cc transitions, which collectively result in an effective closed-channel bound state and its coupling to the continuum. By applying $\gamma = -i$ for each single ℓ partial wave one obtains the condition for resonant scattering of bosons or spin-polarized fermions

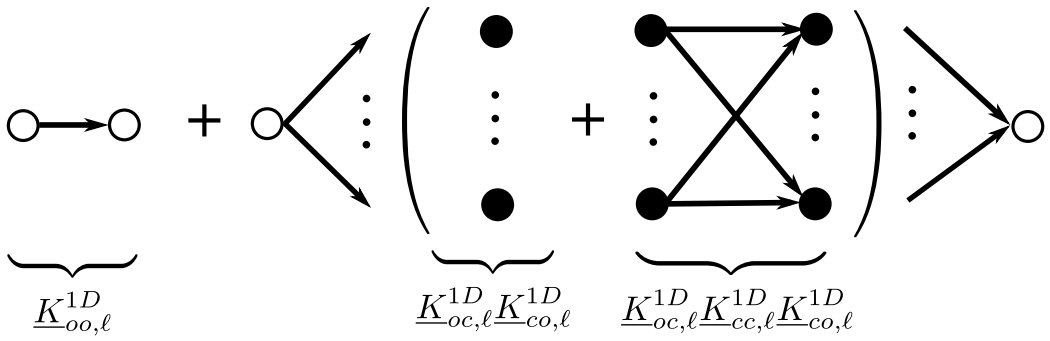

Figure 3.2: A schematic illustration of the transitions into N channels which contribute in the scattering process, corresponding to the K-matrix $\underline{K}^{1D,\ phys}_{oo,\ell}$. The empty (filled) circles indicate the open (closed) channels, the arrows depict the transitions through the ℓ-th partial wave, and the dots denote the $N-3$ channels and their corresponding transitions. Note that $N-3$ indicates the number of the closed channels.

under strong transverse confinement. Thus for $\ell = 0, 1, 2$ one will obtain the same resonance condition as in [9, 107, 35], being in agreement with pseudopotential theory.

The conclusion that all the closed channels collectively support only one bound state unifies the two physical pictures of the virtual excitations with the Fano-Feshbach resonant scenario. This behavior can be understood according to the K-matrix framework by inverting Eq. (3.19):

$$F_\ell(\mathbf{r}) = \sum_n f_n(\mathbf{r})(U^{-1})_{n\ell} \tag{3.31}$$

where the matrix elements $(U^{-1})_{n\ell}$ can be interpreted as the transition amplitudes of the states $f_n(\mathbf{r})$. Evidently, we observe that all these processes collectively result in a single state, $F_\ell(\mathbf{r})\tilde{j}_\ell(kr)P_\ell(\cos\theta)$ which asymptotically vanishes. Thus, indeed it is reasonable to assume that all the virtual excitations support one bound state where its wave function has the form of $F_\ell(\mathbf{r})$. A strong supportive evidence of this behavior is also manifested in the numerical simulations shown in the chapter 2. In Fig. (2.7) of chapter 2 we showed that for a particular ℓ-wave CIR the probability density of the wave function possesses a unique profile. This is approximately similar to the profile of a wave function of the form $\psi(r,\theta) = j_\ell(kr)P_\ell(\cos\theta)$ for each particular ℓ quantum number.

3.3.2 The physical K-matrix for multiple partial waves

Extending K-matrix and the position of coupled ℓ-wave confinement-induced CIRs

Up to now we have been focusing on the case of a single partial wave. By extending the K-matrix $\underline{K}^{3D}$ into an $\ell \times \ell$ diagonal matrix, we take into account all the partial waves compatible with the atomic species, i.e. even (odd) ℓ for bosononic (fermionic)

collisions. In this direction, in the corresponding $\underline{K}_{oo}^{1D,phys}$ we partition the matrices $\underline{K}_{oo}^{1D}$,$\underline{K}_{oc}^{1D}$,$\underline{K}_{co}^{1D}$ and $\underline{K}_{cc}^{1D}$ into sums of their ℓ components. Namely, we have that

$$\underline{K}_{oo}^{1D,\ phys} \equiv \sum_{\ell} \underline{K}_{oo,\ell}^{1D} + i\left(\sum_{\ell} \underline{K}_{oc,\ell}^{1D}\right)\left(\mathbb{I} - i\sum_{\ell} \underline{K}_{cc,\ell}^{1D}\right)^{-1}\left(\sum_{\ell} \underline{K}_{co,\ell}^{1D}\right). \tag{3.32}$$

We remark that each matrix $\underline{K}_{cc,\ell}^{1D}$ is a rank one matrix. Hence, the matrix $\mathbb{I} - i\sum_{\ell} \underline{K}_{cc,\ell}^{1D}$ can be inverted by applying recursively the matrix inversion identity that we used in Eq. (3.29) for each $\underline{K}_{cc,\ell}^{1D}$ according to the following relation:

$$\Bigg(\underbrace{\mathbb{I} - i\sum_{\ell\neq\ell_0} \underline{K}_{cc,\ell}^{1D}}_{\mathfrak{R}_{\ell-1}^{-1}} - i\underline{K}_{cc,\ell_0}^{1D}\Bigg)^{-1} = \mathfrak{R}_{\ell-1}^{-1} + \frac{i}{1 - iTr[\underline{K}_{cc,\ell_0}^{1D}\mathfrak{R}_{\ell-1}^{-1}]}\mathfrak{R}_{\ell-1}^{-1}\underline{K}_{cc,\ell_0}^{1D}\mathfrak{R}_{\ell-1}^{-1}, \tag{3.33}$$

where this recursive procedure allows us to eliminate one $\underline{K}_{cc,\ell}^{1D}$ matrix at each iteration.

Eqs. (3.32) and (3.33) provides us with an extended physical K-matrix, namely $\underline{K}_{oo,phys}^{1D}$ which includes contributions from all the higher partial waves. Consequently, as in the case of the single partial wave by finding the roots of $det\big(\mathbb{I} - i\underline{K}_{cc}^{1D}\big)$, we obtain an approximate expression which provides us with the positions of all the ℓ-wave confinement-induced resonances coupled to each other.

$$1 - i\sum_{\ell=s_0}^{\infty} Tr[\underline{K}_{cc,\ell}^{1D}] - \frac{1}{2}\sum_{\ell=s_0+2}^{\infty}\sum_{\ell'=s_0}^{\ell-2} t_{\ell\ell'} \cong 0, \tag{3.34}$$

$$\begin{aligned} \text{with} \quad & t_{\ell\ell'} = \tan\delta_{\ell}\tan\delta_{\ell'}\sum_{i,j=1}^{\infty}\left(U_{i\ell}U_{j\ell'} - U_{j\ell}U_{i\ell'}\right)^2 \\ \text{and} \quad & Tr[\underline{K}_{cc,\ell}^{1D}] = \tan\delta_{\ell}\sum_{n=1}^{\infty} U_{n\ell}^2 \end{aligned} \tag{3.35}$$

Note that for Eqs. (3.34) and (3.35) the summation with respect to ℓ runs over all the even (odd) ℓ with $s_0 = 0$ ($s_0 = 1$) for the case of bosons (fermions). Furthermore, Eqs. (3.34) and (3.35) are exact for the case of two partial waves. Though, for an amount of partial waves greater than two, this set of equations becomes a good approximation since we have omitted higher-order coupling terms. This is justified since in all the higher-order terms are multiplied with combinations of the phase shifts from higher partial waves, which tend to zero with increasing ℓ.

Transition diagrams: virtual excitations and Fano-Feshbach resonances

In order to give some quantitative results in the following we will focus on low energy bosonic collisions ($q_0 a_{\perp} \ll 1$) considering s- and d-partial waves. Note that a similar

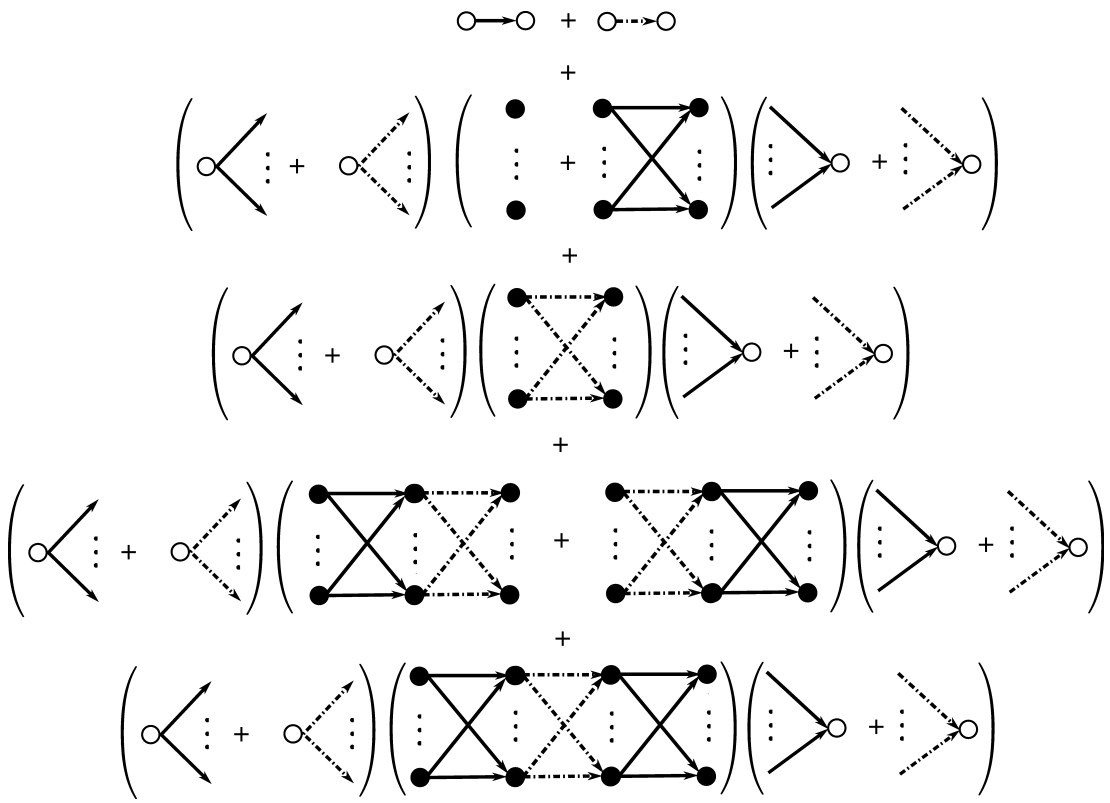

Figure 3.3: A schematic illustration of the transitions into N channels which contribute in the scattering process, for the case of s- and d-wave. The empty (filled) circles indicate the open (closed) channels, the solid-black (dashed-dotted) arrows depict the transitions through the s- (d-) partial wave, while the dots denote the $N-3$ channels and their corresponding transitions.

analysis, as it is presented below, can be done also for the case of spin-polarized fermions which involve p- and f- partial waves.

For the scattering of two bosons the matrix $\underline{K}_{oo}^{1D,\ phys}$ can be written in terms of s- and d-wave K-matrices in a similar way as in Eq. (3.30) yielding the following relation:

$$\begin{aligned}
\underline{K}_{oo}^{1D,\ phys} &= (\underline{K}_{oo,s}^{1D} + \underline{K}_{oo,d}^{1D}) \\
&+ i(\underline{K}_{oc,s}^{1D} + \underline{K}_{oc,d}^{1D})(\mathbb{I} + g_1\underline{K}_{cc,s}^{1D})(\underline{K}_{co,s}^{1D} + \underline{K}_{co,d}^{1D}) \\
&+ ig_2(\underline{K}_{oc,s}^{1D} + \underline{K}_{oc,d}^{1D})\underline{K}_{cc,d}^{1D}(\underline{K}_{co,s}^{1D} + \underline{K}_{co,d}^{1D}) \\
&+ ig_1g_2(\underline{K}_{oc,s}^{1D} + \underline{K}_{oc,d}^{1D})(\underline{K}_{cc,s}\underline{K}_{cc,d}^{1D} \\
&+ \underline{K}_{cc,d}^{1D}\underline{K}_{cc,s}^{1D})(\underline{K}_{co,s}^{1D} + \underline{K}_{co,d}^{1D}) \\
&+ ig_1^2g_2(\underline{K}_{oc,s}^{1D} + \underline{K}_{oc,d}^{1D})\underline{K}_{cc,s}^{1D}\underline{K}_{cc,d}^{1D} \times \\
&\times \underline{K}_{cc,s}^{1D}(\underline{K}_{co,s}^{1D} + \underline{K}_{co,d}^{1D}),
\end{aligned} \tag{3.36}$$

where g_1 and g_2 are defined as follows:

$$g_1 = \frac{i}{1 - iTr[\underline{K}^{1D}_{cc,s}]}, \tag{3.37}$$

and

$$\begin{aligned} g_2 &= i\big(1 - iTr[\underline{K}^{1D}_{cc,s}]\big)/\big(1 - iTr[\underline{K}^{1D}_{cc,s}] - iTr[\underline{K}^{1D}_{cc,d}] \\ - &\quad Tr[\underline{K}^{1D}_{cc,s}]Tr[\underline{K}^{1D}_{cc,d}] + Tr[\underline{K}^{1D}_{cc,d}\underline{K}^{1D}_{cc,s}]\big). \end{aligned} \tag{3.38}$$

Equation (3.36) is illustrated by the transition diagram in Fig. 3.3 which depicts all the possible transitions that can occur during the collision. In this case there are two intermediate transition processes involved, which are related to the s- and d-partial wave indicated by solid and dash-dotted arrows, respectively. Additionally, one can observe in Fig. 3.3 that the first and second simple terms describe direct oo transitions via s- and d-partial waves respectively. The third (fourth) term describes cc transitions via s- (d-) partial waves which are directly coupled to the continuum. The last two terms of the diagram in Fig. 3.3 describe processes combining cc transitions of both types (s- and d-partial waves-mediated) coupled to the continuum. Moreover, in the resonant scattering the factors g_1 and g_2 control the contribution of the cc transitions via s- and d-partial waves, respectively. One can observe that for $g_1 \to \pm\infty$ and $g_2 \to 0$ the resonant scattering is caused by a s-wave CIR, since the cc transitions through s-partial wave become the main resonant mechanism. Additionally, for $g_2 \to \pm\infty$ the resonant scattering is caused by a d-wave CIR, since the cc transitions through the d-partial wave become dominant, i.e. are much larger than the contributions of the transitions mediated by the s-partial wave.

According to Eq. (3.34) the relation which predicts the positions of s- and d-wave CIR reads

$$1 + c_1(k)\frac{a_s(k)}{a_\perp} + c_2(k)\left(\frac{a_d(k)}{a_\perp}\right)^5 + c_3(k)\frac{a_s(k)}{a_\perp}\left(\frac{a_d(k)}{a_\perp}\right)^5 = 0, \tag{3.39}$$

where $a_s(k) = -\tan\delta_{\ell=0}(k)/k$, $a_d^5(k) = -\tan\delta_{\ell=2}(k)/k^5$ are the energy dependent s- and d-wave scattering lengths and $c_1(k)$, $c_2(k)$, $c_3(k)$ are constants related to the Hurwitz zeta functions [109], which depend on the total colliding energy according to

the following relations:

$$\begin{aligned} c_1(k) &= \zeta\left[\frac{1}{2},\frac{3}{2}-\left(\frac{ka_\perp}{2}\right)^2\right] \\ c_2(k) &= 180\zeta\left[-\frac{3}{2},\frac{3}{2}-\left(\frac{ka_\perp}{2}\right)^2\right] \\ &+ 30(ka_\perp)^2\zeta\left[-\frac{1}{2},\frac{3}{2}-\left(\frac{ka_\perp}{2}\right)^2\right] \\ &+ \frac{5}{4}(ka_\perp)^4\zeta\left[\frac{1}{2},\frac{3}{2}-\left(\frac{ka_\perp}{2}\right)^2\right] \\ c_3(k) &= 180\Bigg\{\zeta\left[-\frac{3}{2},\frac{3}{2}-\left(\frac{ka_\perp}{2}\right)^2\right]\times \\ &\times \zeta\left[\frac{1}{2},\frac{3}{2}-\left(\frac{ka_\perp}{2}\right)^2\right]-\zeta\left[-\frac{1}{2},\frac{3}{2}-\left(\frac{ka_\perp}{2}\right)^2\right]^2\Bigg\}. \end{aligned} \tag{3.40}$$

For $q_0 a_\perp \ll 1 \Rightarrow ka_\perp \approxeq \sqrt{2}$ the values of these constants are $c_1 = -1.46035$, $c_2 = -24.3622$ and $c_3 = -1.07986$.

Moreover, the "physical" K-matrix, $\underline{K}_{oo}^{1D,\ phys}$, in the open channels reads

$$\begin{aligned} \underline{K}_{oo}^{1D,\ phys} &= -\frac{1}{q_0 a_\perp}\frac{1}{1+\frac{a_s(k)}{a_\perp}c_1(k)}\Bigg[2\frac{a_s(k)}{a_\perp}+10\frac{a_d^5(k)}{a_\perp^5}\times \\ &\times \frac{[1+(c_1(k)-\frac{c_4(k)}{2})\frac{a_s(k)}{a_\perp}]^2}{1+\frac{a_s(k)}{a_\perp}c_1(k)+\frac{a_d^5(k)}{a_\perp^5}(c_2(k)+c_3(k)\frac{a_s(k)}{a_\perp})}\Bigg], \end{aligned} \tag{3.41}$$

where the constant $c_4(k)$ is given by the relation:

$$\begin{aligned} c_4(k) &= 12\zeta(-1/2,3/2-(ka_\perp/2)^2) \\ &+ (ka_\perp)^2\zeta(1/2,3/2-(ka_\perp/2)^2). \end{aligned} \tag{3.42}$$

In the limit $q_0 a_\perp \ll 1$ the constant c_4 takes the value $c_4 = -5.41533$.

Equation (3.41) encapsulates all the information of two bosons in a harmonic waveguide involving s- and d-partial wave scattering. Note that $\underline{K}_{oo}^{1D,\ phys}$ possesses two singularities and their positions are given by the following relations:

$$a_s(k) = -\frac{a_\perp}{c_1(k)} \text{ and } a_d(k) = \sqrt[5]{-\frac{1+c_1(k)\frac{a_s(k)}{a_\perp}}{c_2(k)+c_3(k)\frac{a_s(k)}{a_\perp}}}\ a_\perp. \tag{3.43}$$

Singularities occur when the s- and d-wave scattering length are approximately half of the length of the harmonic oscillator $a_\perp$ corresponding to the s-wave and d-wave CIR, respectively. Furthermore, one observes that the position of the d-wave CIR directly depends on the ratio $a_s(k)/a_\perp$. Interestingly, the second term in the brackets

of Eq. (3.41), which is related to the d-wave CIR, renders the Fano profile of the s- and d- interfering partial waves, where the nominator describes the width of the d-wave CIR depending strongly on the ratio $a_s(k)/a_\perp$.

The effective 1D Hamiltonian and the transmission coefficient T

As it was shown in [9] the scattering of two bosons in the presence of a harmonic waveguide can be mapped onto an effective 1D Hamiltonian of two bosons which interact via a 1D delta potential, $V_{1D}(z) = g_{1D}\delta(z)$, where $g_{1D} = -\hbar^2/\mu a_{1D}$, with the effective one-dimensional scattering length being defined as $a_{1D} = \frac{a_\perp^2}{2a_s}(-1 + 1.4603\frac{a_s}{a_\perp})$. The coupling strength g_{1D} diverges when $a_{1D} \to 0$ at the position of the s-wave CIR.

This idea can be extended in such a way that the d-wave CIR is also included in g_{1D}. The latter will permit us to define the effective one dimensional length and the transmission coefficient T. According to Eq. (3.26) the *physical* K-matrix and the corresponding scattering wave function in the asymptotic regime, $|\mathbf{r}| \to \infty$, are related as follows:

$$\Psi^{phys}(z,\rho) = \big[\cos(q_0|z|) - \underline{K}_{oo}^{1D}\sin(q_0|z|)\big]\Phi_0(\rho) \tag{3.44}$$

where Ψ^{phys} is the physical wave function and $\Phi_0(\rho)$ is the eigenfunction of the two-dimensional harmonic oscillator for $n = 0$, i.e. the lowest transversal channel. Note that $\Psi^{\rm phys}$ consists only of the real part of the total wave function in the asymptotic regime. Thus, in order to relate the coupling constant g_{1D} to the $\underline{K}_{oo}^{1D,phys}$ matrix we map the relative Hamiltonian H of the two bosons in the waveguide onto an effective one-dimensional (1D) Hamiltonian where they interact via a 1D δ function, as mentioned above. This is permitted since the relative Hamiltonian H asymptotically is fully separable, and all the relevant scattering information is imprinted in the z-component of the wave function. Consequently, by imposing the boundary condition of the δ function we determine the prefactor g_{1D} such that the real part of the wave function of the effective 1D Hamiltonian is the same as the z-dependent part of $\Psi^{\rm phys}$. Thus the effective coupling constant g_{1D} becomes $g_{1D} = -\frac{\hbar^2 q_0}{\mu}\underline{K}_{oo}^{1D,\ phys}$ where the effective 1D scattering length a_{1D} given by the following expression:

$$\begin{aligned}\frac{1}{a_{1D}} &= -\frac{1}{1+\frac{a_s}{a_\perp}c_1}\Bigg[2\frac{a_s(k)}{a_\perp^2} \\ &+ 10\frac{a_d^5(k)}{a_\perp^6}\frac{[1+(c_1-\frac{c_4}{2})\frac{a_s(k)}{a_\perp}]^2}{1+\frac{a_s(k)}{a_\perp}c_1+\frac{a_d^5(k)}{a_\perp^5}(c_2+c_3\frac{a_s(k)}{a_\perp})}\Bigg].\end{aligned} \tag{3.45}$$

In addition, the corresponding transmission coefficient T of the effective 1D Hamiltonian reads

$$T = \frac{1}{1+\frac{\mu^2 g_{1D}^2}{\hbar^4 q_0^2}} = \frac{1}{1+(\underline{K}_{oo}^{1D,phys})^2}. \tag{3.46}$$

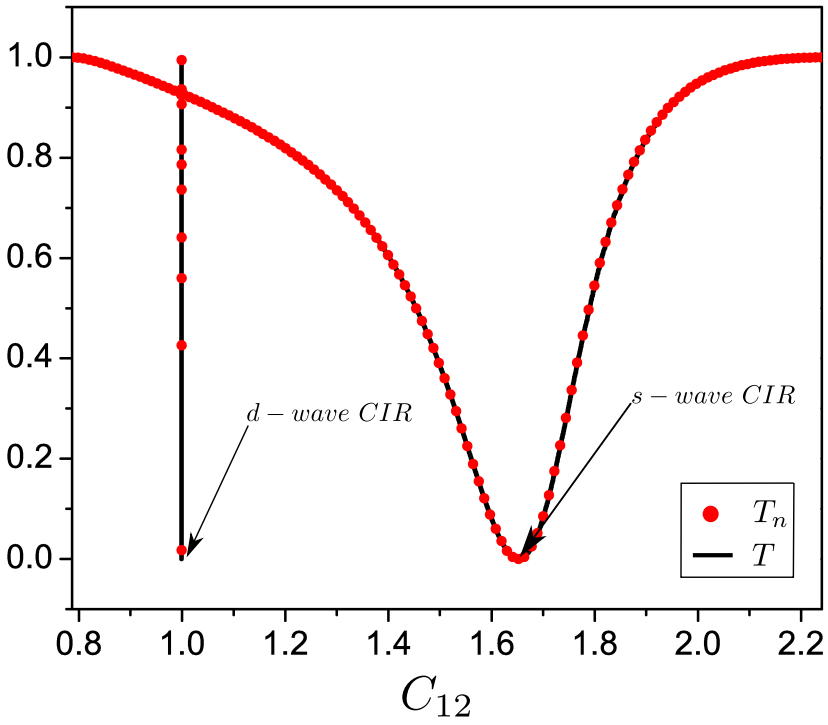

Figure 3.4: The numerical (red circles) and analytical (solid black line) calculated transmission coefficient T as a function of C_{12} parameter with transversal confinement $\omega_\perp = 2 * 10^{-4}$.

3.3.3 The validity of the treatment: analytics vs exact numerical calculations

In this section we compare the analytical results of the previous subsection with the corresponding numerical data. This comparison is based on Cs atom collisions representing an ideal system for such a study with a rich spectrum of resonances [97, 98].

First we evaluate the s- and d-wave energy-dependent scattering lengths by solving numerically the free space scattering of two Cs atoms interacting via a Lennard-Jones potential, $V_{sh}(r) = \frac{C_{12}}{r^{12}} - \frac{C_6}{r^6}$. The dispersion coefficient C_6 has been taken from [97], where the van der Waals length is $\ell_{vdW} = (2\mu C_6/\hbar^2)^{1/4} = 202\ a_0$ (a_0 is the Bohr radius) and C_{12} is a free parameter, which controls the values of the s- and d-wave scattering lengths. Then we use the scattering lengths as an input in Eq. (3.41), leading to a parametrization of the K-matrix $\underline{K}_{oo}^{1D,\ phys}$ in terms of C_{12}.

Moreover, the numerical simulations of Cs-Cs collisions in the harmonic waveguide are based on [14, 34, 110], where we employ the units $m_{\rm Cs}/2 = \hbar = \omega_0 = 1$, with $m_{\rm Cs}$ being the mass of the Cs atom and $\omega_0 = 2\pi \times 10$ MHz. The longitudinal energy is set to $\varepsilon_\parallel = 2 \times 10^{-6}$ and the transversal energy is varied within the interval $2 \times 10^{-4} \leq \varepsilon_\perp \leq 8 \times 10^{-4}$, corresponding to the experimentally accessible range 4π kHz $\leq \omega_\perp \leq 16\pi$ kHz for the waveguide confinement frequency. Additionally, the corresponding range of

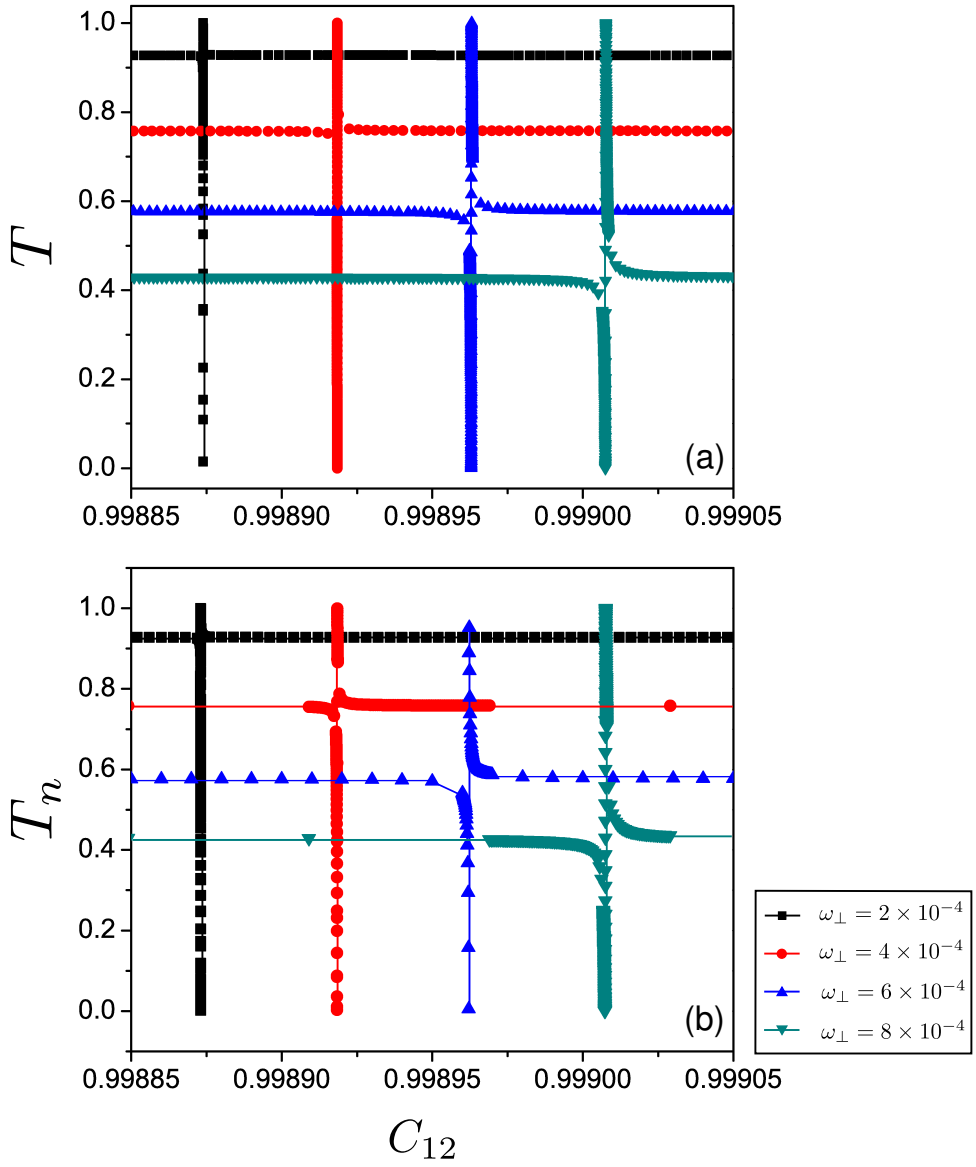

Figure 3.5: A comparison plot for (a) analytically calculated transmission coefficient T and (b) numerically calculated transmission coefficient T_n of d-wave CIR for several confinement frequencies $\omega_\perp$.

harmonic oscillator length is 5176 $a_0 \leq a_\perp \leq$ 2588 a_0, fulfilling thus the criterion of the harmonic oscillator length being much larger than the range of the interatomic potential, $a_\perp \gg \ell_{vdW}$.

In Fig. 3.4 the transmission coefficient T is illustrated as function of the C_{12} parameter for a relatively weak confinement frequency, namely $\omega_\perp = 2 * 10^{-4}$. The Fig. 3.4 depicts the s- and d-wave CIR, where their position is indicated by the zeros of the

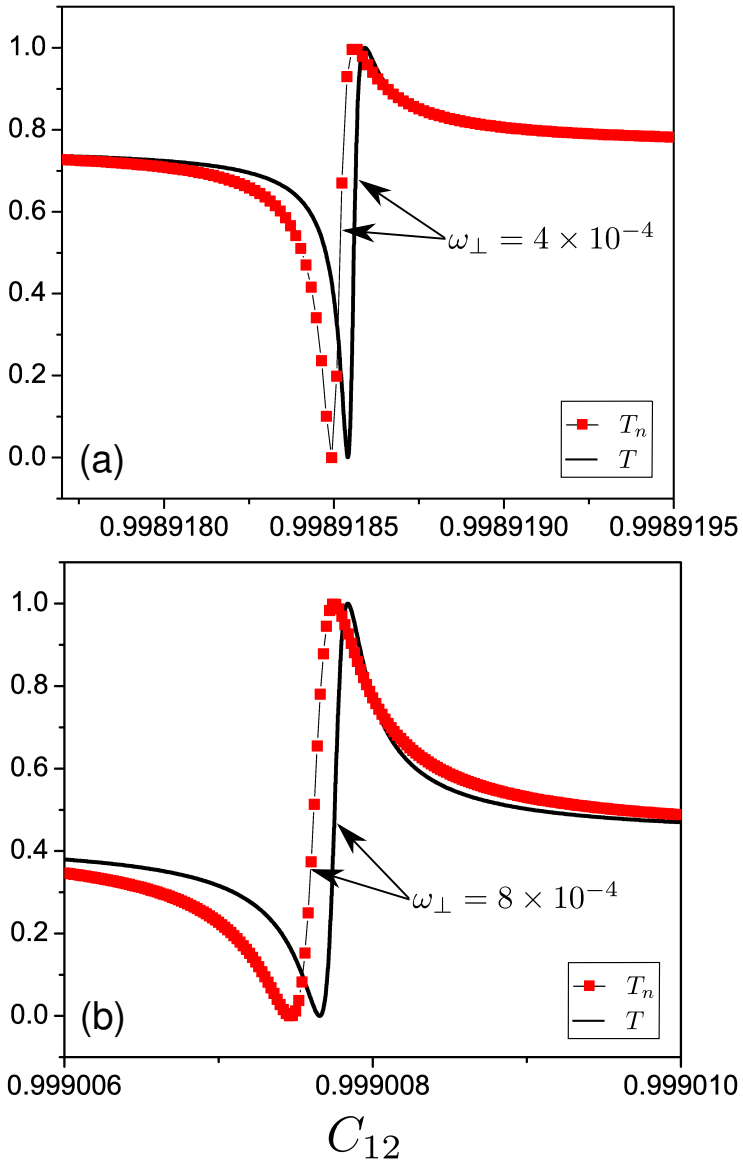

Figure 3.6: A high resolution comparison of analytical results (solid line) with numerical data (red squares) for the d-wave CIR for two different confinement frequencies, $\omega_\perp = 4 \times 10^{-4},\ 8 \times 10^{-4}$ in (a),(b) respectively.

transmission coefficient $T = 0$. We observe that the analytical results, indicated by the black solid line, predict the effect of s- and d-wave CIR. Comparing these results with the exact numerical calculation being indicated by the red circles we observe an excellent agreement at this particular confinement frequency. More specifically, the analytical calculations capture exactly the position and the width of s-wave CIR. Due to the narrow width of the d-wave CIR a more detailed analysis is needed in much

smaller scales than this of Fig. 3.4.

In Fig. 3.5 (a,b) we present the analytically and numerically calculated transmission coefficients, T and T_n respectively, for several confinement frequencies in the vicinity of the d-wave CIR. Notably, the agreement of the numerical with the analytical calculations is excellent for all confinement frequencies. Moreover, the analytical results capture the shift of the d-wave CIR with increasing confinement frequency and the effect of the strong asymmetric Fano-lineshape of the transmission spectrum T. The latter occurs, due to the interference of s- and d-wave CIRs, where, as it is indicated in Eq. (3.41), the broad s-wave CIR serves as a background and the narrow d-wave CIR couples to it. One should note that this difference in the widths of the two resonances is attributed to the centrifugal term, which is absent in the case of s-wave CIR. Furthermore, we present in Fig. 3.6 a high resolution plot for two confinement frequencies again comparing the analytical with the numerical results. Even in this fine scale of the C_{12} parameter the analytical calculations follow the numerical ones both qualitatively and quantitatively. The small deviations can be explained by the fact that the criterion $a_\perp \gg \ell_{vdW}$ is not strictly fulfilled for large confinement frequencies and consequently the analytical results become less accurate. Indeed, one can observe that these small deviations in Fig. 3.6 (b), which refer to the case of strong confinement, become less pronounced in the case of intermediate confinement addressed in Fig. 3.6 (a).

Fig. 3.7 demonstrates the origin of s- and d-wave CIR. For that purpose we compare the transmission coefficient T (see Figs. 3.7 (a) and (c)) with the contourplot of the expression $|\det(\mathbb{I} - i\underline{K}_{cc}^{1D})|$ (see Fig. 3.7(b)). The transmission coefficient T and the relation $|\det(\mathbb{I} - i\underline{K}_{cc}^{1D})|$ both depend on the total energy $E = \hbar^2 k^2/2\mu$ and the ratios $a_s/a_\perp$, $(a_d/a_\perp)^5$. More specific, in Fig. 3.7 (b) for a given energy equal to the total colliding energy E the quantity $|\det(\mathbb{I} - i\underline{K}_{cc}^{1D})|$ has two zeros whose position is indicated in the contourplot by the dark shaded areas (dashed circles), where the positions of the zeros correspond to two different pairs of ratios $(a_s/a_\perp, (a_d/a_\perp)^5)$. The latter means that the closed channels possess two distinct bound states with energy equal to the total energy E at the corresponding values of the pairs $(a_s/a_\perp, (a_d/a_\perp)^5)$, where one bound state is related to the s-wave ($(a_d/a_\perp)^5 \approx 0$) and the other one is related to the d-wave. On the other hand, in Figs. 3.7(a) and (c) the transmission coefficient T of the open channel at the same energy E possesses two zeros which correspond to resonant scattering. The position of the d-wave CIR is in Fig. 3.7(a) at the point $a_s/a_\perp = 0.02$ and in Fig. 3.7(c) at the point $(a_d/a_\perp)^5 = 0.04$. Respectively, the position of the s-wave CIR is in Fig. 3.7(a) (see also the inset plot on a logarithmic scale) at the point $a_s/a_\perp = 0.68$ and in Fig. 3.7(c) at the point $(a_d/a_\perp)^5 \approx 0$. Thus, we observe an exact matching of the pairs $(a_s/a_\perp, (a_d/a_\perp)^5)$ at $T = 0$, denoted by the dotted vertical and horizontal lines in Fig. 3.7(b), with the pairs of $(a_s/a_\perp, (a_d/a_\perp)^5)$ obtained from the zeros of the relation $|\det(\mathbb{I} - i\underline{K}_{cc}^{1D})|$. The latter means that the s- and d-wave confinement-induced resonances occur due to the corresponding s- and d-wave bound states of the closed channels, which couple to the continuum of the open channel. Furthermore, due to the harmonic confinement, s- and d-wave CIR are coupled together rendering interference effects, i.e. a strong asymmetric Fano-lineshape of the

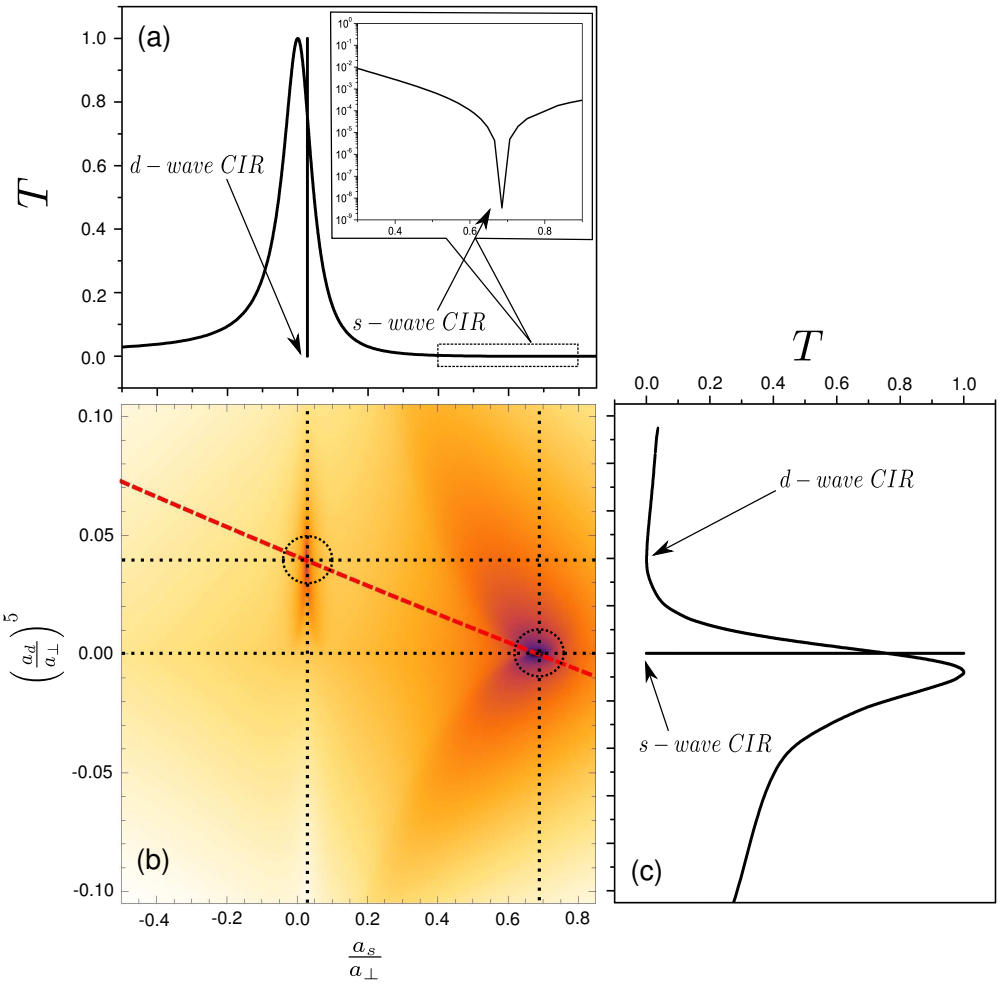

Figure 3.7: (a) Transmission coefficient T as a function of the $a_s/a_\perp$ parameter, (b) contourplot of the quantity $|\det(\mathbb{I} - i\underline{K}^{1D}_{cc})|$ versus the parameters $a_s/a_\perp$ and $(a_d/a_\perp)^5$ and (c) transmission coefficient T as a function of the $(a_d/a_\perp)^5$. In (b) the black dotted lines indicate the position of the resonance with respect to the subfigures (a) and (c), the black dotted circles indicate the positions of the zeros of $|\det(\mathbb{I}-i\underline{K}^{1D}_{cc})|$ and the red dashed line shows the positions of the resonances for an arbitrary short-range interatomic potential. The inset of (a) refers to the dashed boxed area and depicts on a logarithmic scale the second zero of the transmission coefficient (s-wave CIR).

transmission coefficient T, as it is depicted in Fig. 3.7(a) and (c). Finally, in Fig. 3.7(b) the red dashed line indicates the position of the d-wave CIR for any short-range interatomic potential according to Eq. (3.39).

3.4 Brief Summary and Conclusions

In this chapter we developed a non-perturbative theoretical framework which permits us to explore two-body scattering within a harmonic waveguide taking into account all possible partial wave excitations. Our analysis is based on the assumption that the range of the interatomic interactions is smaller than the length scale of the harmonic confinement, imposing thus two regimes of distinct symmetries, i.e. spherical for $|\mathbf{r}| \to 0$ and cylindrical for $|\mathbf{r}| \to \infty$. This length scale separation yields two approximate symmetries in configuration space: a spherical symmetry close to the origin of the scattering event and a cylindrical one in the asymptotic regime. Furthermore, the well separated length scales leads to the existence of an nonorthogonal local frame transformation. The local frame transformation permits us to interrelate the spherical symmetric solutions with the cylindrical ones. Therefore, by means of this transformation we are able to "propagate" the scattering information which is encapsulated in the K^{3D} matrix outwards to the asymptotic regime.

In addition, we demonstrated that the K-matrix approach can be generalized in order to include contributions from the higher partial waves in the presence of the harmonic confinement. The expansion over ℓ-partial waves leads to an extension of CIR physics, where more $\ell \neq 0$-wave CIRs emerge being coupled to the broad s-wave CIR predicted in [9]. Furthermore, we obtain analytically the positions of all ℓ-wave confinement-induced resonances (Eqs. (3.34, 3.35)). This general result refers both to fermionic and bosonic collisions. Note that it can be easily extended for more than one open channel taking into account inelastic processes as well. Additionally, we have demonstrated that the K-matrix approach can provide us with a unique insight into the underling physics of scattering in confined geometries (Eqs. (3.30, 3.36)). More specifically, we show that the "physical" 1D K-matrix, $K_{oo}^{1D,\ phys}$, can be expanded in a Dyson-like form of equations, where each term describes all possible transitions which occur during the collision process. The latter permits us to classify and thoroughly analyze all couplings which are induced by the presence of higher ℓ-partial waves. Moreover, this scheme allows to unravel the connection of the two interpretations for the CIR effect introduced in [9, 10]: All the possible transitions through each ℓ-partial wave into the closed channels act in a collective way yielding an effective ℓ-wave bound state supported by all closed channels being coupled to the continuum of the open channel. The latter yields an asymmetric Fano-lineshape in the transmission coefficient T. Additionally, we implement the extended analytical model in the case of two-body bosonic collisions in the presence of a harmonic waveguide with the scattering process involving only s- and d-partial waves, where we observe an excellent agreement between the analytical and numerical results. Furthermore, we analyze the d-wave CIR being coupled to the s-wave CIR, where both resonances depict an asymmetric Fano-lineshape in the transmission spectrum. A similar behavior is expected also for the case of spin-polarized fermionic collisions involving p- and f-partial waves and their couplings. Nevertheless, we should mention that for higher partial waves ($\ell \geq 4$) the widths of the corresponding ℓ-wave CIRs become very narrow, due to the pronounced

centrifugal barrier which the atoms have to tunnel through in order to perform a ℓ-partial wave collision. Finally, within the framework of the K-matrix approach the origin of the narrow ℓ-wave resonances in the presence of confinement has shown to be of Fano-Feshbach type.

Chapter 4

Dipolar scattering in confined geometries

Recent experimental advances allowed the realization of dense ultracold polar molecule gases [45, 46, 47]. This was achieved using traps of reduced dimensionality, where the extra handling parameters of the confinement yield the control of external and internal degrees of freedom of the polar molecules. This controllability results in the suppression of the chemical reactions which can be induced during collisional events, going a step towards the Bose-Einstein condensation of ground-state polar molecules. In contrast to the case of atomic collisions, polar molecules interact via dipole-dipole interaction (DDI), which are intrinsically different than those of neutral atoms, since they posses a long-range character and are anisotropic. The extensive theoretical study of free-space dipolar collisions [111, 112, 113, 114, 115, 116, 117, 119] combined with the effects of the reduced dimensionality has opened new avenues of dipolar many-body phases [120, 121], such as dipolar crystals [122]. In view of the substantial theoretical effort made on confined dipolar scattering [123, 124, 38, 125, 126, 39], the need for a rigorous understanding of the role of anisotropic forces in CIRs becomes evident.

In this chapter, we present a nonperturbative theoretical framework which incorporates generic anisotropic interactions that allows us to study dipolar collisions in the presence of a harmonic transversal confinement. The approach we employ here mainly consists of a generalization of the K-matrix theory presented in chapter 3, where are consistently taken into account higher angular momentum states and their couplings as well. These ℓ-wave states are firstly coupled due to the anisotropic nature of the DDI and secondly by the harmonic confinement, which leads to a rich resonance structure of ℓ-wave dipolar confinement-induced resonances (DCIRs). These resonances appear in the vicinity of shape resonances which are properly taken into account within the K-matrix approach going beyond the effective one-dimensional pseudopotential theory [38]. Interestingly, this interplay between the confinement and the DDI leads to an intricate dependence of the s-wave DCIRs positions on the dipolar interaction strength. The derived resonance condition reveals in detail the impact of the DDI anisotropy on the CIR effect and provides the necessary tool for the experimental control of the dipo-

lar collisions in quasi-one-dimensional (Q1D) traps. We remark that this sensitivity of the s-wave DCIRs on the strength of dipolar interactions has been observed, so far, numerically [38, 39]. The exact knowledge of the positions of DCIRs can be utilized for the realization of a dipolar version of the (super-) Tonks-Girardeau gas [11, 12], providing different dynamics in the collective oscillations of the many-body phase [127]. Notably, the present theoretical treatment can equally be applied to other collisional systems either of bosonic or fermionic symmetry where anisotropic forces dominate, such as metastable alkaline-earth-metal atoms in magnetic fields which interact with quadrupole-quadrupole interactions [128], or rare-earth atoms, e.g. Dy, Er [129, 130].

4.1 K-matrix approach for dipolar collisions

4.1.1 Hamiltonian and the partitioning of the configuration space

In the following, we consider a system of two bosonic, nonreactive polar molecules which collide in a Q1D waveguide. They are treated as perfect dipoles fully polarized by an external electric field along the waveguide axis $\hat{z}$. The transversal confinement is induced by a two-dimensional (2D) harmonic potential which still permits a separation of the center of mass and relative degrees of freedom. The physics of the collisional processes is then completely described by the relative Hamiltonian expressed in cylindrical coordinates $\mathbf{r} = (\rho, \phi, z)$

$$H = -\frac{\hbar^2}{2\mu}\nabla^2 + \frac{\mu}{2}\omega_\perp^2\rho^2 + V_{\rm int}(\mathbf{r}), \tag{4.1}$$

where μ denotes the reduced mass and $\omega_\perp$ is the confinement frequency.

The interaction potential is given by the following relation:

$$V_{\rm int}(\mathbf{r}) = V_{\rm sh}(\mathbf{r}) + \frac{d^2}{r^3}[1 - 3(\hat{z}\cdot\hat{r})^2], \tag{4.2}$$

where the short-range term $V_{\rm sh}$ is modeled by a Lennard-Jones (LJ) 12-6 potential, $V_{\rm sh}(\mathbf{r}) = \frac{C_{12}}{r^{12}} - \frac{C_6}{r^6}$. The second term describes the DDI where d is the induced dipole moment.

The justification of the LJ-potential for the short-range behavior of the two nonreactive molecules lies in the separation of the energy scales for elastic ultracold collisions and inelastic *chemical* processes [39]. The ranges of the LJ and DDI potentials are $l_{\rm vdW} = (2\mu C_6/\hbar^2)^{\frac{1}{4}}$ and $l_d = \mu d^2/\hbar^2$, respectively. As in Refs.[33, 35], we consider the confining oscillator length $a_\perp \equiv \sqrt{\hbar/\mu\omega_\perp}$ to be the larger length scale, i.e. $a_\perp \gg l_{\rm vdW}, l_d$.

This condition separates the configuration space into three domains with respect to the relative distance r:

(I) $l_d,\ l_{\rm vdW} < r \ll a_\perp$: At small separation distances the interactions $V_{\rm int}$(r) dominate, so that the dipoles effectively experience a free-space collision of total energy $E = \hbar^2k^2/2\mu$, with the according symmetry imposed. In this region, the corresponding wave function can thus be efficiently expanded in the ℓ-wave angular momentum

eigenstates. Note that, due to the azimuthal rotational symmetry of H, the quantum number m is conserved, and will here be fixed to $m = 0$. On the contrary, the angular momentum ℓ is not conserved due to the anisotropy of the DDI, which couples states with $\Delta\ell = \ell - \ell' = 2$. The scattering information of V_{int} is then imprinted in a free-space K-matrix of tridiagonal and symmetric form in ℓ-representation, with entries for even ℓ due to bosonic symmetry; considering up to g-wave contributions, namely $\ell = 4$, it reads

$$\underline{K}^{\text{3D}} = \begin{pmatrix} K_{ss} & K_{sd} & 0 \\ K_{ds} & K_{dd} & K_{dg} \\ 0 & K_{gd} & K_{gg} \end{pmatrix}. \tag{4.3}$$

Since the waveguide confinement is not experienced in this region, the entries of $\underline{K}^{\text{3D}}$ are a measure of the distortion of the wave function due to the presence of V_{int}.

(II) $a_\perp \ll r \to \infty$: At large separations the cylindrical confinement prevails, such that the wave function decomposes into the radial eigenmodes n of the transversal 2D harmonic oscillator. These are regarded as asymptotic channels of the scattering process, which is described by the corresponding K-matrix in one dimension, $\underline{K}^{\text{1D}}$.

(III) $l_d,\ l_{\text{vdW}} \ll r \ll a_\perp$: At intermediate separation distances there is, in general, an admixture of ℓ-wave states from V_{int} and n-mode states from the confinement. However, in this particular domain, both the interaction and confining potentials essentially vanish, so that the corresponding scattering solutions can be efficiently matched. Therefore, a non-orthogonal *local frame transformation* $\underline{U}$ exists [103], which enables the projection of the wave function of domain (I) onto that of domain (II). In particular, $\underline{U}$ transforms the corresponding K-matrices into one another: $\underline{K}^{1D} = \underline{U}^T\ \underline{K}^{3D}\ \underline{U}$ with its elements being $(\underline{K}^{1D})_{nn'} = \sum_{\ell\ell'} U^T_{n\ell}(\underline{K}^{3D})_{\ell\ell'}U_{\ell'n'}$. Note that both $\underline{K}^{3D}$ and $\underline{K}^{1D}$ depend on the total energy E. We recall that the matrix elements of the local frame transformation U with the azimuthal quantum number being $m = 0$ have the following explicit form:

$$U_{\ell n} = \frac{\sqrt{2}(-1)^{d_0}}{a_\perp}\sqrt{\frac{2\ell+1}{kq_n}}P_\ell\left(\frac{q_n}{k}\right), \tag{4.4}$$

where q_n refers to the momentum along the longitudinal axis, the quantity d_0 is $\ell/2$ ($(\ell-1)/2$) for bosons (fermions). q_n is defined by the following relation of the total colliding energy E:

$$\frac{E}{\hbar\omega_\perp} = \frac{(ka_\perp)^2}{2} = 2n + 1 + \frac{(q_n a_\perp)^2}{2}. \tag{4.5}$$

4.1.2 Single mode regime and the physical K-matrix

In the following, we consider low-energy scattering in the asymptotic transversal ground state $n = 0$, following the criterion $q_0 a_\perp \ll 1$ for the relative longitudinal wave vector q_0 which is considered to be small and finite. The total collision energy, in domain II, is $E = \hbar^2k^2/2\mu = \hbar\omega_\perp + \hbar^2q_0^2/2\mu$, so that only the first channel ($n = 0$) is energetically open (o), while higher channels ($n > 0$) remain closed (c), since $E < \hbar\omega_\perp(2n+1)$.

The asymptotic components of the wave function in the c-channels, however, contains exponential divergences, rendering the scattering *unphysical*. This behavior is remedied in the framework of multichannel quantum defect theory (MQDT) by imposing the physically acceptable boundary conditions in c-channels [105], yielding a *physical* K-matrix given by

$$\underline{K}_{oo}^{1D,\ phys} = \underline{K}_{oo}^{1D} + i\underline{K}_{oc}^{1D}(\mathcal{I} - i\underline{K}_{cc}^{1D})^{-1}\underline{K}_{co}^{1D}, \tag{4.6}$$

where $\mathcal{I}$ is the identity matrix. The roots of $\det(\mathcal{I} - i\underline{K}_{cc}^{1D}) = 0$ provide the bound states in the c-channels which energetically lie in the continuum of the o-channels.

By expressing Eq. (4.6) in terms of (ℓ, ℓ')-pairs of the angular momentum states we get the following relation:

$$\underline{K}_{oo}^{1D,\ phys} = \sum_{\ell\ell'} \underline{K}_{oo}^{1D,\ell\ell'} + i\sum_{\ell\ell'} \underline{K}_{oc}^{1D,\ell\ell'} \left(\mathcal{I} - i\sum_{\ell\ell'} \underline{K}_{cc}^{1D,\ell\ell'}\right)^{-1} \sum_{\ell\ell'} \underline{K}_{co}^{1D,\ell\ell'}, \tag{4.7}$$

where $\underline{K}_{oo}^{1D,\ell\ell'}$ refers to the open-open channel transitions, where its matrix element is defined as $(\underline{K}_{oo}^{1D,\ell\ell'})_{00} = (U^T)_{0\ell}K_{\ell\ell'}^{3D}U_{\ell'0}$ with $K_{\ell\ell'}^{3D}$ being the corresponding matrix element of $\underline{K}^{3D}$. $\underline{K}_{oc}^{1D,\ell\ell'}$ ($\underline{K}_{co}^{1D,\ell\ell'}$) refers to open-closed (closed-open) transitions and each one is a single row- (column-) matrix, where its entries are defined as $(\underline{K}_{oc}^{1D,\ell\ell'})_{0n} = (U^T)_{0\ell}K_{\ell\ell'}^{3D}U_{\ell'n}$ ($(\underline{K}_{co}^{1D,\ell\ell'})_{n0} = (U^T)_{n\ell}K_{\ell\ell'}^{3D}U_{\ell'0}$). $\underline{K}_{cc}^{1D,\ell\ell'}$ refers to closed-closed transitions, and the matrix elements of $\underline{K}_{cc}^{1D,\ell\ell'}$ are given by $(\underline{K}_{cc}^{1D,\ell\ell'})_{nn'} = (U^T)_{n\ell}K_{\ell\ell'}^{3D}U_{\ell'n'}$. We remark that each matrix $\underline{K}_{cc}^{1D,\ell\ell'}$ is a rank one matrix. The matrix $\mathcal{I} - i\sum_{\ell\ell'}\underline{K}_{cc}^{1D,\ell\ell'}$ is inverted analytically where for each $\underline{K}_{cc}^{1D,\ell\ell'}$ rank one matrix we use recursively the inversion identity for rank one matrices of Ref. [106]. Note that the $\underline{K}_{oo}^{1D,\ phys}$ in Eq. (4.7) constitutes the Dyson-like form of the physical K matrix.

After performing all the corresponding matrix multiplications Eq. (4.7) then reads

$$\underline{K}_{oo}^{1D,\ phys} = -\frac{\boldsymbol{\alpha}\cdot\boldsymbol{\xi}}{q_0 a_\perp(1 + \boldsymbol{\alpha}\cdot\boldsymbol{\mathcal{R}})}, \tag{4.8}$$

where the scalar products are short-hand for summed coefficients of the $\boldsymbol{\alpha}, \boldsymbol{\xi}$ and $\boldsymbol{\mathcal{R}}$. $\boldsymbol{\xi}$ and $\boldsymbol{\mathcal{R}}$ contain traces $\sum_n U_{n\ell}^T U_{\ell' n}$ over the c-channels n, yielding combinations of the Hurwitz ζ-function for each (ℓ, ℓ')-pair. $\boldsymbol{\alpha}$ consists of single-term combinations of $\bar{a}_{\ell\ell'} \equiv a_{\ell\ell'}/a_\perp$, where $a_{\ell\ell'} = -K_{\ell\ell'}/k$ are generalized, energy dependent scattering lengths for dipolar collisions in free-space [115]. Due to Eq. (4.9) we remark that $\boldsymbol{\alpha}$ contains up to g-wave $\bar{a}_{\ell\ell'}$-terms. Eq. (4.8) therefore encapsulates directly the impact of the anisotropy of the DDI on the confined scattering: $\underline{K}_{oo}^{1D,\ phys}$ is determined by the dipole-induced $\bar{a}_{\ell\ell'}$-terms contained in $\boldsymbol{\alpha}$, which are simultaneously weighted by the coupling due to the confinement via $\boldsymbol{\xi}$ and $\boldsymbol{\mathcal{R}}$.

The explicit form of $\boldsymbol{\alpha}\cdot\boldsymbol{\xi}$ and $\boldsymbol{\alpha}\cdot\boldsymbol{\mathcal{R}}$

Here for reasons of completeness we provide the explicit form of Eq. (4.8). Namely, the scalar product $\boldsymbol{\alpha}\cdot\boldsymbol{\mathcal{R}}$ has the following form:

$$
\begin{aligned}
\boldsymbol{\alpha}\cdot\boldsymbol{\mathcal{R}} &= \bar{a}_{ss}\mathcal{R}_1+\bar{a}_{dd}\mathcal{R}_2+\bar{a}_{gg}\mathcal{R}_3+\bar{a}_{sd}\mathcal{R}_4+\bar{a}_{dg}\mathcal{R}_5+\bar{a}_{sd}^2\mathcal{R}_6+\bar{a}_{dg}^2\mathcal{R}_7+\bar{a}_{ss}\bar{a}_{gg}\mathcal{R}_8\\
&+ \bar{a}_{ss}\bar{a}_{dg}\mathcal{R}_9+\bar{a}_{ss}\bar{a}_{dd}\mathcal{R}_{10}+\bar{a}_{gg}\bar{a}_{sd}\mathcal{R}_{11}+\bar{a}_{dd}\bar{a}_{gg}\mathcal{R}_{12}+\bar{a}_{sd}\bar{a}_{dg}\mathcal{R}_{13}\\
&+ (\bar{a}_{ss}\bar{a}_{dg}^2+\bar{a}_{gg}\bar{a}_{sd}^2-\bar{a}_{ss}\bar{a}_{dd}\bar{a}_{gg})\mathcal{R}_{14}, \qquad (4.9)
\end{aligned}
$$

with $\bar{a}_{\ell\ell'}\equiv a_{\ell\ell'}/a_\perp$ with $a_{\ell\ell'}=-K_{\ell\ell'}/k$ being generalized, energy dependent scattering lengths for dipolar collisions in free-space [115] encapsulating the scattering information of the short-range and the dipole-dipole interactions. The coefficients $\mathcal{R}_i$, $i=1,\ldots,14$, are the components of the vector $\boldsymbol{\mathcal{R}}$ and are defined by the following:

$$
\begin{aligned}
\mathcal{R}_1 &= b_1;\quad \mathcal{R}_2=\frac{b_2}{(ka_\perp)^4};\quad \mathcal{R}_3=\frac{b_6}{(ka_\perp)^8};\quad \mathcal{R}_4=\frac{2b_3}{(ka_\perp)^2};\quad \mathcal{R}_5=\frac{2b_4}{(ka_\perp)^6};\\
\mathcal{R}_6 &= \frac{b_3^2-b_1b_2}{(ka_\perp)^4};\quad \mathcal{R}_7=\frac{b_4^2-b_6b_2}{(ka_\perp)^{12}};\quad \mathcal{R}_8=\frac{b_1b_6-b_5^2}{(ka_\perp)^8};\quad \mathcal{R}_9=\frac{2(b_1b_4-b_3b_5)}{(ka_\perp)^6};\\
\mathcal{R}_{10} &= -\frac{b_3^2-b_1b_2}{(ka_\perp)^4};\quad \mathcal{R}_{11}=\frac{2(b_3b_6-b_4b_5)}{(ka_\perp)^{10}};\quad \mathcal{R}_{12}=-\frac{b_4^2-b_6b_2}{(ka_\perp)^{12}}; \qquad (4.10)\\
\mathcal{R}_{13} &= \frac{2(b_3b_4-b_2b_5)}{(ka_\perp)^8};\quad \mathcal{R}_{14}=\frac{b_1(b_4^2-b_6b_2)+b_3(b_3b_6-b_4b_5)-b_5(b_3b_4-b_2b_5)}{(ka_\perp)^{12}};
\end{aligned}
$$

where the b_i's, with $i=1,\ldots,6$, are constants, given by

$$
\begin{aligned}
b_1 &= \zeta\Big(\frac{1}{2},\epsilon\Big);\quad b_2=180\zeta\Big(-\frac{3}{2},\epsilon\Big)+30(ka_\perp)^2\zeta\Big(-\frac{1}{2},\epsilon\Big)+\frac{5}{4}(ka_\perp)^4\zeta\Big(\frac{1}{2},\epsilon\Big)\\
b_3 &= 2\sqrt{5}\Big[3\zeta\Big(-\frac{1}{2},\epsilon\Big)+\frac{(ka_\perp)^2}{4}\zeta\Big(\frac{1}{2},\epsilon\Big)\Big]\\
b_4 &= 6\sqrt{5}\Big[210\zeta\Big(-\frac{5}{2},\epsilon\Big)+\frac{125(ka_\perp)^2}{2}\zeta\Big(-\frac{3}{2},\epsilon\Big)+\frac{39(ka_\perp)^4}{8}\zeta\Big(-\frac{1}{2},\epsilon\Big)\\
&+ \frac{3(ka_\perp)^6}{24}\zeta\Big(\frac{1}{2},\epsilon\Big)\Big]\\
b_5 &= 210\zeta\Big(-\frac{3}{2},\epsilon\Big)+45(ka_\perp)^2\zeta\Big(-\frac{1}{2},\epsilon\Big)+\frac{3(ka_\perp)^4}{8}\zeta\Big(\frac{1}{2},\epsilon\Big)\\
b_6 &= 90\Big[490\zeta\Big(-\frac{7}{2},\epsilon\Big)+210(ka_\perp)^2\zeta\Big(-\frac{5}{2},\epsilon\Big)+\frac{555(ka_\perp)^4}{20}\zeta\Big(-\frac{3}{2},\epsilon\Big)\\
&+ \frac{45(ka_\perp)^6}{40}\zeta\Big(-\frac{1}{2},\epsilon\Big)+\frac{9(ka_\perp)^8}{640}\zeta\Big(\frac{1}{2},\epsilon\Big)\Big], \qquad (4.11)
\end{aligned}
$$

here $\zeta(\cdot,\cdot)$ denotes the Hurwitz zeta function and $\epsilon=3/2-(ka_\perp/2)^2$.

Similarly, the scalar product $\boldsymbol{\alpha}\cdot\boldsymbol{\xi}$ results in the following expression:

$$
\begin{aligned}
\boldsymbol{\alpha}\cdot\boldsymbol{\xi} &= \bar{a}_{ss}\xi_1+\bar{a}_{dd}\xi_2+\bar{a}_{gg}\xi_3+\bar{a}_{sd}\xi_4+\bar{a}_{dg}\xi_5+\bar{a}_{sd}^2\xi_6+\bar{a}_{dg}^2\xi_7+\bar{a}_{ss}\bar{a}_{gg}\xi_8\\
&+ \bar{a}_{ss}\bar{a}_{dg}\xi_9+\bar{a}_{ss}\bar{a}_{dd}\xi_{10}+\bar{a}_{gg}\bar{a}_{sd}\xi_{11}+\bar{a}_{dd}\bar{a}_{gg}\xi_{12}+\bar{a}_{sd}\bar{a}_{dg}\xi_{13}\\
&+ (\bar{a}_{ss}\bar{a}_{dg}^2+\bar{a}_{gg}\bar{a}_{sd}^2-\bar{a}_{ss}\bar{a}_{dd}\bar{a}_{gg})\xi_{14}, \qquad (4.12)
\end{aligned}
$$

with ξ_i, $i = 1, \ldots, 14$, being the components of the vector $\boldsymbol{\xi}$ and are defined as follows:

$$\begin{aligned}
\xi_1 &= 2;\ \ \xi_2 = \frac{10}{(ka_\perp)^4};\ \ \xi_3 = \frac{81}{2(ka_\perp)^8};\ \ \xi_4 = \frac{4\sqrt{5}}{(ka_\perp)^2};\ \ \xi_5 = \frac{18\sqrt{5}}{(ka_\perp)^6};\\
\xi_6 &= \frac{-2b_2 + 4\sqrt{5}b_3 - 10b_1}{(ka_\perp)^4};\ \ \xi_7 = \frac{18\sqrt{5}b_4 - 10b_6 - \frac{81}{2}b_2}{(ka_\perp)^{12}};\ \ \xi_8 = \frac{\frac{81}{2}b_1 - 18b_5 + 2b_6}{(ka_\perp)^8}\\
\xi_9 &= \frac{18\sqrt{5}b_1 - 18b_3 + 4b_4 - 4\sqrt{5}b_5}{(ka_\perp)^6};\ \ \xi_{10} = \frac{10b_1 + b_2 - 4\sqrt{5}b_3}{(ka_\perp)^4};\\
\xi_{11} &= \frac{81b_3 - 18b_4 - 18\sqrt{5}b_5 + 4\sqrt{5}b_6}{(ka_\perp)^{10}};\ \ \xi_{12} = \frac{\frac{81}{2}b_2 - 18\sqrt{5}b_4 + 10b_6}{(ka_\perp)^{12}};\\
\xi_{13} &= \frac{-18b_2 + 18\sqrt{5}b_3 + 4\sqrt{5}b_4 - 20b_5}{(ka_\perp)^8};\\
\xi_{14} &= \Big[\frac{81}{2}(b_3^2 - b_1b_2) + 18(b_2b_5 - b_3b_4) + 2(b_4^2 - b_2b_6) + 4\sqrt{5}(b_3b_6 - b_4b_5)\\
&+ 10(b_5^2 - b_1b_6) + 18\sqrt{5}(b_1b_4 - b_3b_5)\Big]/(ka_\perp)^{12},
\end{aligned} \tag{4.13}$$

with the constants b_i, $i = 1, \ldots, 6$, given in Eq. (4.11).

Note that in the low-energy regime, $q_0 a_\perp \ll 1$, the dimensionless total energy becomes $\frac{(ka_\perp)^2}{2} = 1 + \frac{(q_0 a_\perp)^2}{2} \approx 1$.

4.2 Dipolar confinement-induced resonances

The resonant behavior arises in the form of poles of $\underline{K}_{oo}^{1D,\,phys}$, given by the roots of the equation

$$1 + \boldsymbol{\alpha} \cdot \boldsymbol{\mathcal{R}} = 0. \tag{4.14}$$

These coincide with the zeros of $\det(\mathcal{I} - i\underline{K}_{cc}^{1D}) = 0$ in Eq. (4.6), which demonstrates that the origin of the resonance structure is a Fano-Feshbach mechanism. Note that the resonance condition, Eq. (4.14), can be met in multiple ways by allowing either one of the $\bar{a}_{\ell\ell'}$-terms to be dominant.

It is thus evident that due to the presence of the DDI within the waveguide, different ℓ-wave states from the domain (I) contribute to this resonance mechanism. The ℓ-wave labeling is still used in the sense that a particular partial wave dominates over the others, although they are coupled together due to DDI, which leads to broad s-wave and narrow ($\ell > 0$)-wave DCIRs with corresponding positions in the parameter space, e.g. l_d, l_{vdW}, $a_\perp$, determined by Eq. (4.14). Note that this difference of the widths arises from the free-space dipolar scattering, where within the adiabatic approximation of the two-body dynamics [117] the s-wave adiabatic channel possesses an effective $-1/r^4$ potential tail, while each $\ell > 0$ state exhibits a repulsive barrier leading to increasingly narrower resonances with increasing ℓ-wave character.

We will now focus on the s-wave DCIRs, which are of immediate experimental relevance. Hence, we isolate the free-space a_{ss} dipolar scattering length on the left hand side of Eq. (4.14), and obtain the corresponding resonance condition $\bar{a}_{ss}(ka_\perp, d) = \mathcal{F}(\{\bar{a}_{\ell\ell'}(ka_\perp, d)\}, \{\mathcal{R}_i(ka_\perp)\})$, where

$$\mathcal{F} = -\frac{1+\bar{a}_{dd}(\mathcal{R}_2+\bar{a}_{gg}\mathcal{R}_{12})+\bar{a}_{gg}(\mathcal{R}_3+\bar{a}_{sd}\mathcal{R}_{11})+\bar{a}_{sd}(\mathcal{R}_4+\bar{a}_{dg}\mathcal{R}_{13})+\bar{a}_{dg}(\mathcal{R}_5+\bar{a}_{dg}\mathcal{R}_7)+\bar{a}_{sd}^2(\mathcal{R}_6+\bar{a}_{gg}\mathcal{R}_{14})}{\mathcal{R}_1+\bar{a}_{dd}\mathcal{R}_{10}+\bar{a}_{gg}\mathcal{R}_8+\bar{a}_{dg}\mathcal{R}_9+(\bar{a}_{dg}^2-\bar{a}_{dd}\bar{a}_{gg})\mathcal{R}_{14}}, \tag{4.15}$$

with the $\mathcal{R}_i$ ($i = 1 \ldots 14$) being the components of $\boldsymbol{\mathcal{R}}$. Originating from the poles of $\underline{K}_{oo}^{1D,\,phys}$ in Eq. (4.8), the quantity $\mathcal{F}$ now embodies the interplay between the DDI anisotropy and the confinement. Note that in general $\bar{a}_{ss}(ka_\perp, d)$ and $\mathcal{F}(\{\bar{a}_{\ell\ell'}(ka_\perp, d)\}, \{\mathcal{R}_i(ka_\perp)\})$ depend differently on the dipole moment d; thus their equality provides a transcendental equation being fulfilled for particular values of d in the parameter space.

The s-wave DCIRs appear in the vicinity of the free-space resonances which are s-wave dominated, i.e. near the broad divergences of the a_{ss} dipolar scattering length, where all the higher $a_{\ell\ell'}$ scattering lengths are non-resonant. Additionally, as was shown in Ref.[115, 124] within the Born approximation (BA) the non-resonant $a_{\ell\ell'}$ terms, except for the ones with $\ell = \ell' = 0$, are proportional to the dipolar length l_d. Consequently, this universal, i.e. V_{sh}-independent, behavior of the higher $a_{\ell\ell'}$ terms leads to the following simplification of Eq. (4.15):

$$\mathcal{F}_{\mathrm{BA}} = -\frac{1 + \eta_1\bar{l}_d + \eta_2\bar{l}_d^2 + \eta_3\bar{l}_d^3}{\sigma_0 + \sigma_1\bar{l}_d + \sigma_2\bar{l}_d^2}, \tag{4.16}$$

where $\bar{l}_d \equiv l_d/a_\perp$ and the η_j and σ_j consist of combinations of $\mathcal{R}_i$'s. In the considered low-energy limit $q_0 a_\perp \ll 1$, they acquire the values $\eta_1 \approx 1.844$, $\eta_2 \approx -1.119$, $\eta_3 \approx 0.013$, $\sigma_0 \approx -1.46$, $\sigma_1 \approx 2.008$ and $\sigma_2 \approx 0.046$. For $l_d = 0$, the resonance condition, $\bar{a}_{ss} = \mathcal{F}_{\mathrm{BA}}$, reduces to $\bar{a}_s = -1/\sigma_0 = 0.68$, as expected for the s-wave CIR [9].

The explicit form of the η- and σ-constants expressed in terms of the components of $\boldsymbol{\mathcal{R}}$ take the following form:

$$\begin{aligned}
\eta_1 &= -\frac{2\mathcal{R}_2}{21} - \frac{2\mathcal{R}_3}{77} - \frac{\sqrt{5}}{105}(7\mathcal{R}_4 + \mathcal{R}_5) \\
\eta_2 &= \frac{2\sqrt{5}\mathcal{R}_{11}}{1155} + \frac{4\mathcal{R}_{12}}{1617} + \frac{1}{2205}(7\mathcal{R}_{13} + 49\mathcal{R}_6 + \mathcal{R}_7) \\
\eta_3 &= -\frac{2\mathcal{R}_{14}}{3465} \\
\sigma_0 &= \mathcal{R}_1 \\
\sigma_1 &= -\frac{2\mathcal{R}_{10}}{21} - \frac{2\mathcal{R}_8}{77} - \frac{\sqrt{5}}{105}\mathcal{R}_9 \\
\sigma_2 &= -\frac{\mathcal{R}_{14}}{495}
\end{aligned} \tag{4.17}$$

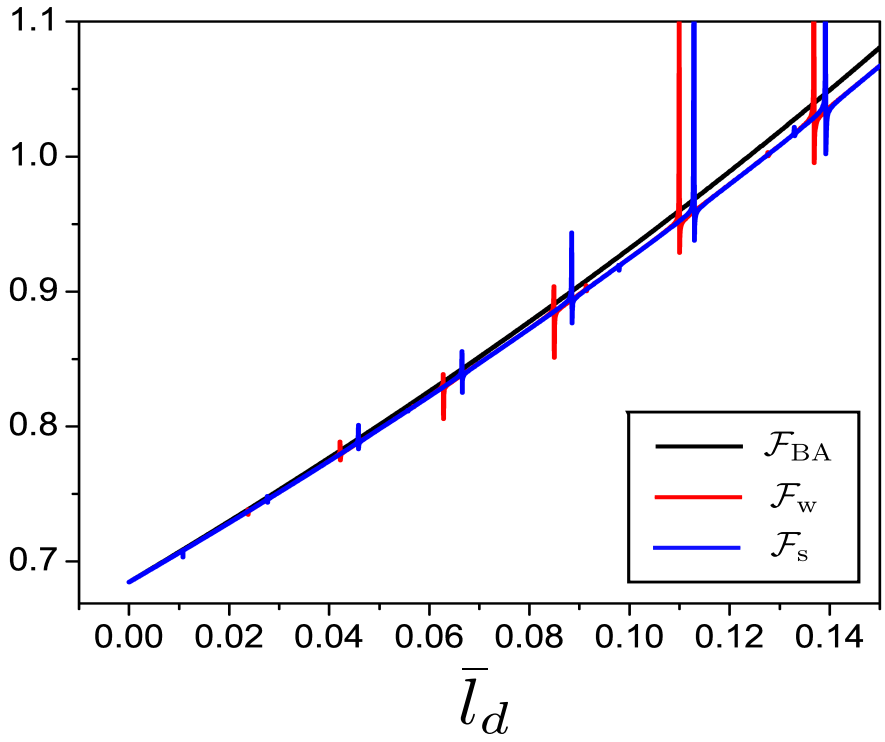

Figure 4.1: $\mathcal{F}$ versus $\bar{l}_d \equiv l_d/a_\perp$. The black line refers to $\mathcal{F}_{BA}$ (Eq. (4.16)), whereas $\mathcal{F}_{\rm w}$ (red line) and $\mathcal{F}_{\rm s}$ (blue line) refer to Eq. (4.15) where the terms $a_{\ell\ell'}$ are numerically calculated for a LJ potential that possesses for $d = 0$ a weakly or a strongly s-wave bound state, respectively.

4.3 Discussion

The validity of the Born approximation

The analytical results from the BA, Eq. (4.16), are compared in Fig.4.1 to those of Eq. (4.15), in which the $a_{\ell\ell'}$ are calculated numerically from the dipolar free-space problem [131]. We see that, whereas the BA breaks down close to free-space resonances ($a_{\ell\ell'} \to \infty$, $\ell,\ \ell' \geq 0$) as expected [49], $\mathcal{F}_{\rm BA}$ is in good agreement with the non-resonant parts of $\mathcal{F}$; these are also the regimes of interest here, since the s-wave DCIRs occur away from $a_{\ell\ell'}$, $\ell,\ \ell' \geq 0$ free-space resonances.

To study the universal aspects of $\mathcal{F}$, we consider for $d = 0$ the two limiting cases of a weakly and a strongly s-wave bound state in the LJ potential, yielding $a_s \gg l_{\rm vdW}$ and $a_s \ll l_{\rm vdW}$, respectively. We observe in Fig. 4.1 that $\mathcal{F}_{\rm s}$ (strongly bound-blue line) and $\mathcal{F}_{\rm w}$ (weakly bound-red line) practically coincide everywhere apart from the positions of the narrow resonant features. The non-universality of these resonant features mainly arises from the coupling term a_{sd}, which is strongly affected by the non-universal and strongly resonant behavior of a_{ss}. However, the distance between

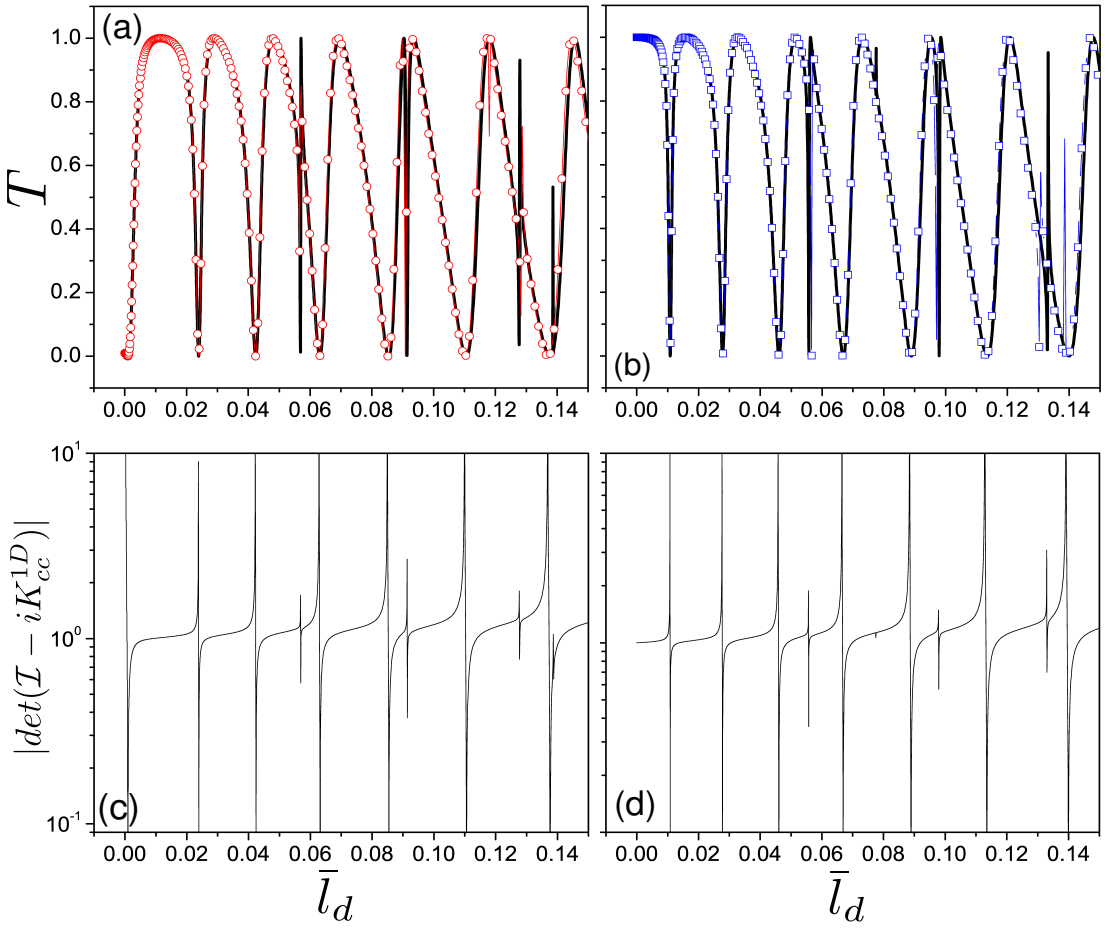

Figure 4.2: The transmission T: analytical results (solid line) and numerical calculations for (a) $a_s \gg l_{\rm vdW}$ ($-\circ-$), (b) $a_s \ll l_{\rm vdW}$ ($-\square-$). (c) and (d) show the corresponding quantity $|det(\mathcal{I} - iK^{1D}_{cc})|$, for the parameter values of (a) and (b), respectively.

the corresponding divergences in $\mathcal{F}_{\rm s}$ and $\mathcal{F}_{\rm w}$ decreases as $\bar{l}_d$ increases. This is because, as the DDI becomes stronger, it dominates the short-range LJ interaction and eventually shields it completely, thereby restoring the universal behavior of a_{ss}.

Analytics-numerics

We now investigate the resonant structure of the transmission coefficient T for confined dipolar scattering, which we derive analytically in terms of the physical K-matrix as $T = 1/[1+(\underline{K}^{1D,\ phys}_{oo})^2]$[1] . Note that the numerically calculated $\boldsymbol{\alpha}$ from the unconfined problem is used as an input in Eq. (4.8), as before. The transmission is shown in Fig.4.2

[1]For further details on the derivation and the construction of an effective one-dimensional Hamiltonian see the corresponding part in subsection 3.3.2.

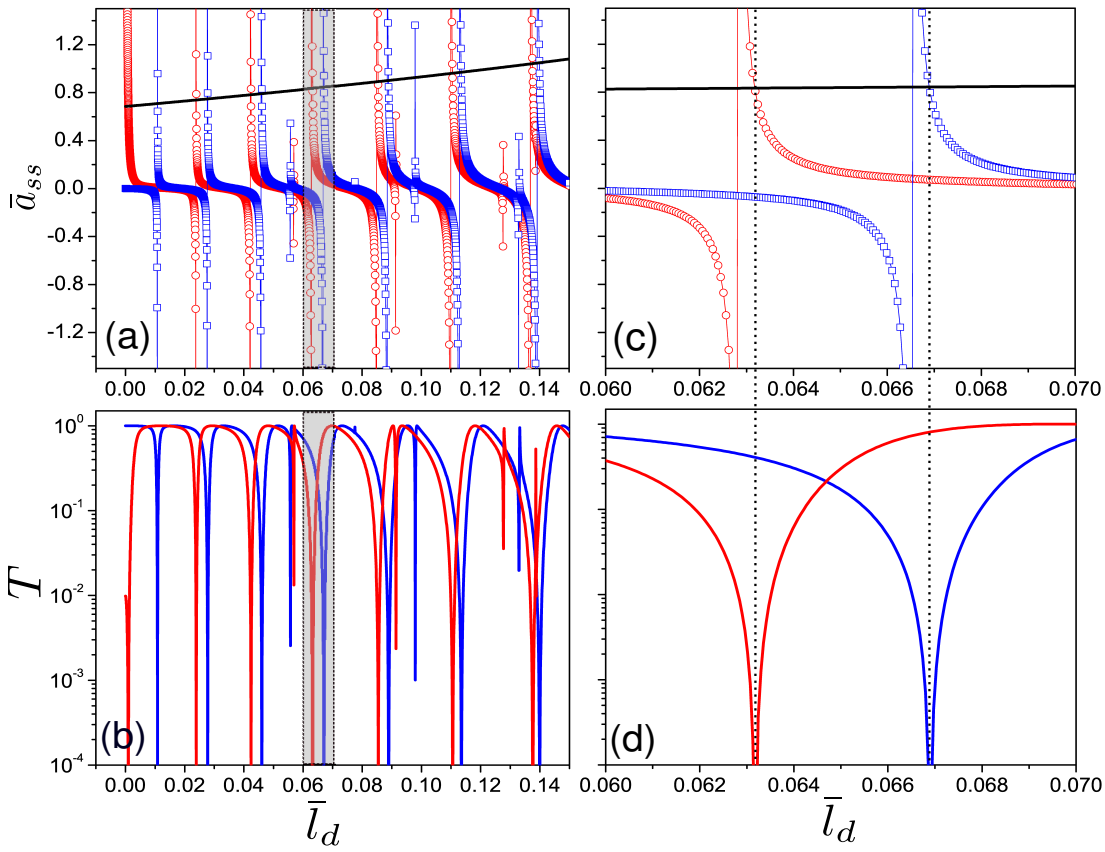

Figure 4.3: (a) $\bar{a}_{ss}$ depicted for $a_s \gg l_{\mathrm{vdW}}$ ($-\bigcirc-$) and $a_s \ll l_{\mathrm{vdW}}$ ($-\square-$), whereas the black line shows the quantity $\mathcal{F}_{BA}$, (b) the analytically calculated transmission T for $a_s \gg l_{\mathrm{vdW}}$ (red line) and $a_s \ll l_{\mathrm{vdW}}$ (blue line). (c) and (d) represent magnifications of the gray shaded areas of (a) and (b), respectively.

as a function of $\bar{l}_d$, again for the cases of (a) a weakly and (b) a strongly bound s-wave state in the LJ potential at $d = 0$, each featuring sequences of s- and higher partial waves ($\ell > 0$) DCIRs. As mentioned previously, the latter are much narrower due to the presence of the repulsive barrier. These results are compared to exact numerical calculations of T (red circles and blue squares in Fig.4.2 (a) and (b), respectively) based on a scheme presented in Ref. [110]. An excellent agreement is observed. Moreover, Fig.4.2 (c) and (d) show the corresponding expression $|det(\mathcal{I}-iK_{cc}^{1D})|$, which is observed to tend to zero exactly at the positions of $T \approx 0$. This indeed illustrates that the ℓ-wave DCIRs fulfill a Fano-Feshbach scenario.

s-wave dipolar confinement-induced resonances

Fig.4.3 (a) shows a graphical solution of the resonance condition for the positions of the s-wave DCIRs. There the dipolar scattering within the waveguide becomes

resonant for the values of $\bar{l}_d$ where $\bar{a}_{ss} = \mathcal{F} \simeq \mathcal{F}_{\mathrm{BA}} > 0$. We focus on the broad divergences of $\bar{a}_{ss}$ related to s-wave dominated dipolar free-space resonances, whose width increases with $\bar{l}_d$, since the DDI becomes more attractive. The intersections of $\mathcal{F}_{\mathrm{BA}}$ and $\bar{a}_{ss}$ in Fig.4.3 (a) are seen to occur exactly at the zeros $T(\bar{l}_d) = 0$ of the transmission in Fig.4.3 (b), as clearly demonstrated for the magnified grey shaded areas in Fig.4.3 (c) and (d). This striking coincidence demonstrates the high accuracy of the derived resonance condition for s-wave DCIRs, for both limiting cases $a_s \ll l_{\mathrm{vdW}}$ and $a_s \gg l_{\mathrm{vdW}}$.

This accurate prediction of the s-wave DCIRs is retained over the whole range of the DDI strengths, from the non-universal to the universal regime ($\bar{l}_d > 0.11$) of the s-wave dominated dipolar free-space resonances. In the universal regime the short-range physics represented by V_{sh} indeed becomes irrelevant, in the sense that the positions of the s-wave DCIRs (intersections of $\bar{a}_{ss}$ and $\mathcal{F}_{\mathrm{BA}}(\bar{l}_d)$) for different strengths of V_{sh} to a good approximation coincide in the $(\bar{a}_{ss}, \bar{l}_d)$-plane.

Fig.4.3 (a) comprises the most intriguing difference of DCIRs compared to well-established CIRs with *isotropic* interactions: In contrast to the case of CIRs, the positions of s-wave DCIRs, measured in values of $\bar{a}_{ss}$, increases for increasing interaction strength of the DDI potential, or, equivalently, for an increasing number of s-wave dominated dipolar free-space resonances which have become bound within $V_{\mathrm{int}}(\mathbf{r})$. Therefore, in the presence of a DDI the confinement-induced shift of free-space resonances is no longer constant, but increases for successive resonances passing the open channel threshold. This behavior arises from the anisotropic nature of the DDI, which mixes higher partial ℓ-waves more strongly for larger l_d, and is enhanced via their recoupling by the confinement, yielding substantial contributions to the positions of the s-wave DCIRs.

4.4 Concluding remarks

In conclusion, we have extended the K-matrix formalism to treat dipolar collisions and include higher partial waves in the presence of a harmonic Q1D confinement leading to the prediction of ℓ-wave DCIRs. In particular, we analyzed in detail the case of s-wave DCIRs and derive analytically the corresponding resonance condition in the form $\bar{a}_{ss} = \mathcal{F}_{\mathrm{BA}}$, containing explicitly the dependence on the DDI strength. Apart from providing an essential ingredient for the resonant control of nonreactive polar molecule gases in Q1D, this result sheds light on the physics underlying the DCIR effect: We demonstrate how the DDI couples the ℓ-wave states of the short-range potential, which are in turn mixed by the confinement. As a result of this interplay between DDI and confinement, the positions of the s-wave DCIRs, measured in values of $\bar{a}_{ss}$, were shown to shift for increasing strength of the interaction potential, in contrast to the case of mere s-wave CIRs. We remark that in the case of fermionic dipolar collisions we expect the appearance of corresponding DCIRs, which may exhibit universal characteristics even for weak dipole moments as BA indicates [115]. In addition, for non-polarized dipoles including the azimuthal ϕ dependence in our framework may emerge ℓ-wave DCIRs which split into components of the azimuthal quantum number m [132]. The theoretical advance presented here, combined with MQDT theory [133], may pave the way for new insights on reactive polar molecule collisions in quasi-2D [45]. Furthermore, we remark that the s-wave dominated dipolar free-space resonances can be induced either by strong dc-electric or laser fields [111, 112, 116]. This together with the tunability of the confinement frequency provides us with excellent tools for probing s-wave DCIRs, which experimentally can be identified by their shifts for successive free-space dipolar resonances (see Fig.4.3(a)). Notably, the density of the s-wave DCIRs does not depend on the changes of the short-range physics, though is strongly affected by the density of the free-space resonances as Fig.4.3(a) indicates. Hence, for a spectrum of free-space resonances of a certain density the corresponding DCIRs might be experimentally resolvable, since their width increases as $\bar{l}_d$ increases (see Fig.4.2(a)-(b)).

Chapter 5

Conclusions and outlook

Conclusive remarks and perspectives have been included in each chapter of the present thesis. In this chapter we will only summarize the very basic aspects and provide a more general outlook.

The main purpose of this thesis is the development of a non-perturbative theoretical framework for multichannel collisions in the presence of external confining potentials. This theoretical treatment permits us to obtain a substantial physical insight on the collisional properties of confinement-induced processes which either involve isotropic or anisotropic interactions including contributions from higher angular momentum states. Furthermore, this method avoids the limitations of pseudopotential theory as we have discussed in chapter 2.4, allowing us to obtain quantitative results which describe the corresponding resonant phenomena. These quantitative results, i.e. the resonance conditions, may pave the way to design and manipulate new exotic many-body phases of effective one-dimensional strongly correlated gases yielding new properties.

In particular, we have investigated the case of higher partial wave scattering of neutral atoms within a harmonic waveguide. The contributions from all the higher partial waves during the atom-atom collisions yield mutually coupled ℓ-wave CIRs, which fulfill a Fano-Feshbach scenario. This leads to an extension of the concept of CIR physics beyond the previous studies [9, 33] showing a much richer resonance structure in the transmission spectrum. The underlying physics of this particular collisional system has been demonstrated in chapter 3 where the Dyson-like form of the physical 1D K-matrix, $K_{oo}^{1D,\,phys}$, provided us with a classification of the virtual transitions that the colliding atoms undergo. The corresponding transition diagrams permit us to analyze thoroughly all the couplings induced by the presence of higher partial waves. Moreover, this scheme allows us to unravel the connection of the two interpretations for the CIR effect introduced in [9, 10], where all the possible transitions through each ℓ-partial wave into the closed channels act in a collective way yielding an effective ℓ-wave bound state supported by all closed channels. it is this effective ℓ-wave bound state supported by all closed channels that becomes coupled to the continuum of the open channel leading to an ℓ-wave CIR. Finally, we remark that the analytically derived resonance conditions for the ℓ-wave CIRs show how different ℓ-wave interactions can

be manipulated by tuning of the transversal confinement.

The robustness of the K-matrix approach allows us to include apart from higher angular momentum states, the couplings between them as well. This extension essentially enables us to study the collisional properties of systems which interact with anisotropic forces. More specifically, in chapter 4 we considered a system of bosonic dipoles which collide within a harmonic waveguide leading to the prediction of ℓ-wave DCIRs. Furthermore, we focused on the case of s-wave DCIRs and derive analytically the corresponding resonance condition going beyond the previous studies [38]. The extended K-matrix formalism permitted us to unravel the impact of the anisotropic nature of the dipolar forces on CIR physics yielding DCIRs whose their positions are sensitive on the strength of dipolar interactions, in contrast to the case of mere CIRs. This sensitivity arises due the coupling of the ℓ-wave states of the short-range potential by the dipole-dipole interactions, which are in turn mixed by the confinement. We remark that the resonance condition of the ℓ-wave DCIRs shows explicitly how this type of resonances can be manipulated. The latter is achieved either by adjusting the transversal confinement frequency or by tuning the the strength of dipole-dipole interactions via an external electric field.

The general scheme of the K-matrix formalism opens new research options in order to study more complicated colliding systems in the presence of external potentials providing new insights and a plethora of new effects. Such collisional systems are the rare-earth atoms (e.g. Er, Dy) which have recently attracted a lot of scientific interest or alkaline-earth-metal atoms in magnetic fields which interact with quadrapole-quadrapole interactions. We have also (chapter 4.4) discussed that by including a ϕ azimuthal dependence in the K-matrix approach collisions of non-polarized dipoles can be investigated as well. This will allow for studying collisions of light (heavy) atoms which interact with spin-spin (second order spin-orbit) interactions. In addition, this method can be directly applied also in the case where the two particles, i.e. atoms or dipoles, can occupy after the collision a transversally excited state of the confining potential. Such collisions will involve more than one open channel and therefore inelastic processes could be investigated as well. Another research option constitutes the extension of the concept of local frame transformation in other types of transverse confining potentials such as the two-dimensional anisotropic harmonic oscillator. This extension combined with MQDT theory [133], will allow us to investigate rigorously collisions of reactive polar molecules in quasi-2D traps which is expected provide new insights and complement the recent experimental observations [45].

Appendix A

Computational methods

A.1 Two-body collisions with or without external confining potentials

A.1.1 Hamiltonians, Schrödinger equation and boundary conditions

Hereafter we will discuss the numerical methods which we have implemented in order to treat the scattering problem either in free space or in the presence of a transverse harmonic confinement[1] . Throughout this appendix we assume that the corresponding Hamiltonians possess azimuthal symmetry. This imposes that the dependence on the angle ϕ can be neglected and consequently the corresponding Schrödinger equations can be reduced into two-dimensional differential equations.

For the cases of two-body collisions either with or without external confinement, we have the following generic Hamiltonian in the relative degree of freedom:

$$H = -\frac{\hbar^2}{2\mu}\left\{\frac{d^2}{dr^2} + \frac{1}{r^2}\frac{d}{dx}[(1-x^2)\frac{d}{dx}]\right\} + V(\mathbf{r}), \tag{A.1}$$

where $x = \cos\theta$, μ is the reduced mass and the potential term $V(\mathbf{r})$ is given by the relations

$$\text{(I) For free-space collisions: } V(\mathbf{r}) = \frac{C_{12}}{r^{12}} - \frac{C_6}{r^6} \tag{A.2}$$

$$\text{(II) For collisions in the waveguide: } V(\mathbf{r}) = \frac{C_{12}}{r^{12}} - \frac{C_6}{r^6} + \frac{\mu\omega_\perp}{2}r^2(1-x^2),$$

where in the case (II) the term $\omega_\perp$ is the transversal confinement frequency. Note that Eqs. (A.1) and (A.2) are expressed in spherical coordinates. The corresponding Schrödinger equation reads

$$-\frac{\hbar^2}{2\mu}\left\{\frac{d^2}{dr^2} + \frac{1}{r^2}\frac{d}{dx}[(1-x^2)\frac{d}{dx}]\right\}\Psi(r,x) + V(\mathbf{r})\Psi(r,x) = E\Psi(r,x), \tag{A.3}$$

[1]For additional details on the numerical methods see Ref.[110].

where E is the total colliding energy.

The wave function $\Psi(r,x)$ close to the origin for both potentials of Eq. (A.2) has to vanish, namely we have that

$$\text{For } |\mathbf{r}| \to 0: \quad \Psi(r,x) \to 0 \tag{A.4}$$

In the asymptotic region, $|\mathbf{r}| \to \infty$, the boundary conditions then read: (I) For free-space collisions:

$$\Psi(r,x) = r(\cos(krx) + f(\theta)e^{ikr}), \tag{A.5}$$

where k is the wave vector defined by $k = \sqrt{2\mu E/\hbar^2}$. (II) For collisions in the waveguide:

$$\Psi(r,x) = r(\cos(q_0 rx) + fe^{iq_0 r|x|})\phi_{n=0,m=0}(r\sqrt{1-x^2}), \tag{A.6}$$

where $\phi_{n=0,m=0}(r\sqrt{1-x^2})$ is the ground state of the two-dimensional harmonic oscillator expressed in spherical coordinates, and n, m are the principal and the azimuthal quantum number respectively. These quantum numbers define the eigenspectrum of the two-dimensional harmonic oscillator, namely $E_\perp = \hbar\omega_\perp(2n+|m|+1)$. We consider the case of one energetically open channel, namely $n=0$, and the azimuthal quantum number is set to zero. The quantity q_0 is the wave vector in the z-direction and it is defined by the relation $E = \hbar\omega_\perp + \hbar^2 q_0^2/2\mu$, where E is the total colliding energy.

We remark that the wave functions of Eqs. (A.5) and (A.6) possess bosonic symmetry. In order to describe fermionic collisions one has to substitute the first terms of Eqs. (A.5) and (A.6) with $\sin(krx)$ and $\sin(q_0 rx)$ respectively.

In the following we will present the discretization of the angular and the radial part of the wave function, as well as the solution of the two-dimensional Schrödinger equation with the help of an implicit LU decomposition. These steps are equally applicable to the case of collisions with or without external confining potential.

A.1.2 Discretization of the angular part of the wave function

We discretize the angular variable $x = \cos\theta \to x_j = \cos\theta_j, \quad j = 1,\ldots,N_\theta$, where N_θ is the total amount of angular grid points. These N_θ angular grid points are defined by the nodes of the Legendre polynomial $P_{N_\theta}(x)$ of N_θ-oder. Then with the help of the Gaussian integration, the integrals over the angle θ take the following form:

$$\int F(\cos\theta)d\theta \approx \sum_{j=1}^{N_\theta} F(\cos\theta_j)w_j, \tag{A.7}$$

where the quantity w_j is the weight of the Gauss quadrature.

The completeness and the orthogonality relations of the *normalized* Legendre polynomials on the angular grid read

$$\text{Completeness: } \sum_{\ell=0}^{N_\theta-1} P_\ell(x_j)P_\ell(x_{j'})\sqrt{w_j w_{j'}} = \delta_{j,j'}, \quad j,\ j' = 1,2,\dots N_\theta \tag{A.8}$$

$$\text{Orthogonality: } \sum_{j=1}^{N_\theta} P_\ell(x_j)P_{\ell'}(x_j)w_j = \delta_{\ell,\ell'}, \quad \ell,\ \ell' = 0,2,\dots N_\theta - 1$$

We are thus able to project the wave function Ψ on the angular grid according to the following Anstice:

$$\Psi(r,x_j) = \sum_{\ell=0}^{N_\theta-1}\sum_{j'=1}^{N_\theta} P_\ell(x_j)P_\ell(x_{j'})\sqrt{w_j}u_{j'}(r) \tag{A.9}$$

A.1.3 Discretization of the radial part of the wave function

In scattering problems the wave function at small separation distances r possesses a rapid oscillatory behavior, especially for interatomic potentials which have a large amount of bound states close to threshold. On the other hand, at large distances the wave function oscillates with large period $\sim 2\pi/k$, where k is the wave vector of the total colliding energy. This behavior of the wave function at small and large separation distances means that in order to describe it accurate enough on a radial grid we need more grid points at small r than in the asymptotic region. Therefore, in order to assure fast convergence we have to use a quasi-uniform grid for the radial part of the wave function. This is achieved by the following relation:

$$r = r_{max}\frac{e^{r_s\xi}-1}{e^{r_s}-1}, \tag{A.10}$$

where $\xi \in [0,1]$, $r \in [0, r_{max}]$, and r_s is a parameter that controls the density of grid points at small r. r_{max} is the maximum value of distance r, where we assume that the asymptotic region starts.

Then, Eq. (A.3) in the quasi-uniform representation takes the following form:

$$-\frac{\hbar^2}{2\mu}\left\{f_1^2(\xi)\frac{d^2}{d\xi^2} + 2f_2(\xi)\frac{d}{d\xi} + \frac{1}{r^2(\xi)}\frac{d}{dx}[(1-x^2)\frac{d}{dx}]\right\}\Psi(\xi,x) + V(\xi)\Psi(\xi,x) = E\Psi(\xi,x), \tag{A.11}$$

where the functions $f_1(\xi)$ and $f_2(\xi)$ are defined by the relations

$$f_1(\xi) = \frac{e^{r_s}-1}{r_s[r_{max} + r(\xi)(e^{r_s}-1)]} \quad \text{and} \quad f_2(\xi) = -r_s f_1^2(\xi) \tag{A.12}$$

Since we have introduced the quasi-uniform radial representation, we can now proceed to its discretization. This is done by discretizing equidistantly the ξ variable, namely we take

$$\xi \to \xi_i, \quad \text{where} \quad \xi_i - \xi_{i-1} = 1/N_r, \tag{A.13}$$

where $N_r + 1$ is the total amount of radial grid points.

With the help of Eq. (A.13), Eq. (A.10) the radial variable r becomes discretized as well, $r \to r_i$, providing a quasi-uniform radial grid.

A.1.4 B-splines basis

One might observe that in this discrete representation the potential term in Eq. (A.11) simply becomes $V(r) \to V(r_i)$. However, in order to approximate the derivatives $d^2/d\xi^2$, $d/d\xi$ we have to expand the radial part of the wave function $\Psi(\xi, x)$ on a B-splines basis set [78]. From Eq. (A.9) we have that the radial part is described by $u_j(r_i) \equiv u_j(\xi_i)$, and by using a 5th-order B-splines we obtain

$$u_j(\xi_i) = \sum_{k=i}^{i+4} B_k(\xi_i) C_{k,j}, \tag{A.14}$$

where the coefficients $C_{k,j}$ are the unknowns and $B_k(\xi_i)$ are piecewise polynomials of ξ_i.

Then according to Eq. (A.14) the derivatives with respect to ξ_i obtain the following form:

$$\left.\frac{du_j(\xi)}{d\xi}\right|_{\xi=\xi_i} = \sum_{k=i}^{i+4} \left.\frac{dB_k(\xi)}{d\xi}\right|_{\xi=\xi_i} C_{k,j} \quad \text{and} \quad \left.\frac{d^2u_j(\xi)}{d\xi^2}\right|_{\xi=\xi_i} = \sum_{k=i}^{i+4} \left.\frac{d^2B_k(\xi)}{d\xi^2}\right|_{\xi=\xi_i} C_{k,j}, \tag{A.15}$$

where the terms $\frac{dB_k(\xi)}{d\xi}$ and $\frac{d^2B_k(\xi)}{d\xi^2}$ are well known functions.

Having projected the radial part of the wave function on the quasi-uniform radial grid the total wave function is given by the relation

$$\Psi(\xi_i, x_j) = \sum_{\ell=0}^{N_\theta - 1} \sum_{j'=1}^{N_\theta} P_\ell(x_j) P_\ell(x_{j'}) \sqrt{w_{j'}} \sum_{k=i}^{i+4} B_k(\xi_i) C_{k,j'}. \tag{A.16}$$

A.1.5 Projecting the Schrödinger equation on a mathematical grid

In the following we substitute the ansatz of the total wave function [Eq. (A.16)] in the Schrödinger equation (Eq. A.11)). Then for each term of Eq. (A.11) we obtain

- $$-\frac{\hbar^2}{2\mu}\left\{ f_1^2(\xi)\frac{d^2}{d\xi^2} + 2f_2(\xi)\frac{d}{d\xi}\right\}\Psi(\xi,x)\Big|_{(\xi,x)=(\xi_i,x_j)} =$$

$$= -\frac{\hbar^2}{2\mu}\sum_{k=i}^{i+4}\sum_{j'=1}^{N_\theta}\left\{ f_1^2(\xi_i)\left.\frac{d^2B_k(\xi)}{d\xi^2}\right|_{\xi=\xi_i} + 2f_2(\xi_i)\left.\frac{dB_k(\xi)}{d\xi}\right|_{\xi=\xi_i}\right\}\frac{C_{k,j'}\delta_{j,j'}}{\sqrt{w_{j'}}} \tag{A.17}$$

- $$-\frac{\hbar}{2\mu r^2(\xi)}\frac{d}{dx}[(1-x^2)\frac{d}{dx}]\Psi(\xi,x)\Big|_{(\xi,x)=(\xi_i,x_j)} =$$

$$= -\frac{\hbar}{2\mu r^2(\xi_i)}\sum_{k=i}^{i+4}\sum_{\ell=0}^{N_\theta-1}\sum_{j'=1}^{N_\theta}\ell(\ell+1)P_\ell(x_j)P_\ell(x_{j'})\sqrt{w_j}B_k(x_i)C_{k,j'} \tag{A.18}$$

- $[V(\xi) - E]\Psi(\xi, x)\Big|_{(\xi,x)=(\xi_i,x_j)} =$

$$= [V(\xi_i) - E] \sum_{k=i}^{i+4} \sum_{j'=1}^{N_\theta} B_k(x_i) \frac{C_{k,j'}\delta_{j,j'}}{\sqrt{w_{j'}}} \tag{A.19}$$

With the help of Eqs. (A.17), (A.18) and (A.19), the Schrödinger equation takes the following form:

$$\begin{aligned} &\sum_{k=i}^{i+4} \sum_{j'=1}^{N_\theta} \Bigg\{ -\frac{\hbar^2}{2\mu} \left[f_1^2(\xi_i) \frac{d^2 B_k(\xi)}{d\xi^2}\Big|_{\xi=\xi_i} + 2 f_2(\xi_i) \frac{dB_k(\xi)}{d\xi}\Big|_{\xi=\xi_i} \right] \\ + \quad & [V(\xi_i) - E] B_k(x_i) \Bigg\} [\sqrt{w_{j'}} C_{k,j'}] \delta_{j,j'} - \frac{\hbar}{2\mu r^2(\xi_i)} \sum_{k=i}^{i+4} \sum_{j'=1}^{N_\theta} \Bigg[\sum_{\ell=0}^{N_\theta - 1} \ell(\ell+1) \\ & P_\ell(x_j) \sqrt{w_j} P_\ell(x_{j'}) \sqrt{w_{j'}} \Bigg] B_k(x_i) [\sqrt{w_{j'}} C_{k,j'}] = 0. \end{aligned} \tag{A.20}$$

Hence, Eq. (A.20) can be rewritten in a matrix form as follows:

$$\sum_{s=1}^{5} (\underline{H}_i^{(s)} + \underline{L}_i^{(s)}) \overrightarrow{D}_{s+i-1} = 0 \quad \text{for } i = 1, \ldots, N_r + 1, \tag{A.21}$$

where the matrix $\underline{H}_i^{(s)}$ is diagonal and the matrix $\underline{L}_i^{(s)}$ is a symmetric one. Both matrices have dimensions $N_\theta \times N_\theta$. The vector $\overrightarrow{D}_k$ contains the unknowns $\sqrt{w_j} C_{k,j}$ for $j = 1, \ldots, N_\theta$ and $k = 1, \ldots, N_r + 5$.

Eq. (A.21) implies that we have a system of $N_r + 1$ matrix equations with $N_r + 5$ unknown vectors. In order to be solvable such a system, we need 4 additional matrix equations. These additional matrix equations can be constructed by the boundary conditions of the wave function. For $|\mathbf{r}| \to 0$ we have

$$\underline{B}_1 \overrightarrow{D}_1 + \underline{B}_2 \overrightarrow{D}_2 + \underline{B}_3 \overrightarrow{D}_3 + \underline{B}_4 \overrightarrow{D}_4 + \underline{B}_5 \overrightarrow{D}_5 = 0. \tag{A.22}$$

$$\underline{R}_2 \overrightarrow{D}_2 + \underline{R}_3 \overrightarrow{D}_3 + \underline{R}_4 \overrightarrow{R}_4 + \underline{R}_5 \overrightarrow{D}_5 + \underline{R}_6 \overrightarrow{D}_6 = 0, \tag{A.23}$$

where the matrices $\underline{B}_k$ ($\underline{R}_k$) are given by the relations $\underline{B}_k^{(i)} = B_k(\xi_1)\mathcal{I}$ ($\underline{R}_k^{(i)} = B_k(\xi_2)\mathcal{I}$), with $\mathcal{I}$ the identity matrix. For $|\mathbf{r}| \to \infty$ we have

$$\sum_{k=N_r-1}^{N_r+3} B_k(\xi_{N_r-1}) \overrightarrow{D}_k = \overrightarrow{g}_{N_r-1} \tag{A.24}$$

$$\sum_{k=N_r}^{N_r+4} B_k(\xi_{N_r}) \overrightarrow{D}_k = \overrightarrow{g}_{N_r} \tag{A.25}$$

$$\sum_{k=N_r+1}^{N_r+5} B_k(\xi_{N_r+1})\overrightarrow{D}_k = \overrightarrow{g}_{N_r+1} \tag{A.26}$$

where the elements of the vector $\overrightarrow{g}_i$ are given by the relations:
-For free-space collisions:

$$g_{i,j} = \sqrt{w_j} r_{N_r-1}(\cos(k r_{N_r-1} x_j + f e^{-ikr_{n_r-1}|x_j|}). \tag{A.27}$$

-For collisions within the waveguide:

$$g_{i,j} = \sqrt{w_j} r_{N_r-1}(\cos(k_0 r_{N_r-1} x_j + f e^{-ik_0 r_{n_r-1}|x_j|})\phi_{n=0,m=0}(r_{N_r-1}\sqrt{1-x_j^2}). \tag{A.28}$$

Eqs. (A.24)-(A.26) contain the scattering amplitude f which is unknown. Combining Eq. (A.24) with (A.25) and Eq. (A.25) with (A.26) we eliminate the scattering amplitude arriving at the following set of matrix equations:

$$\sum_{k=N_r-1}^{N_r+4} \underline{T}_k \overrightarrow{D}_k = \overrightarrow{p}_{N_r} \tag{A.29}$$

$$\sum_{k=N_r}^{N_r+5} \underline{T}_k \overrightarrow{D}_k = \overrightarrow{p}_{N_r+1} \tag{A.30}$$

A.1.6 LU decomposition: An implicit algorithm

Eqs. (A.21), (A.22), (A.23), (A.29) and (A.30) form a set of $N_r + 5$ matrix equations for the $N_r + 5$ unknown vectors $\overrightarrow{D}_q$ $(q = 1, \ldots, N_r + 5)$.

$$\begin{aligned}
&\underline{B}_1\overrightarrow{D}_1 + \underline{B}_2\overrightarrow{D}_2 + \underline{B}_3\overrightarrow{D}_3 + \underline{B}_4\overrightarrow{D}_4 + \underline{B}_5\overrightarrow{D}_5 = 0\\
&\underline{R}_2\overrightarrow{D}_2 + \underline{R}_3\overrightarrow{D}_3 + \underline{R}_4\overrightarrow{R}_4 + \underline{R}_5\overrightarrow{D}_5 + \underline{R}_6\overrightarrow{D}_6 = 0\\
&\sum_{s=1}^{5}(\underline{H}_i^{(s)} + \underline{L}_i^{(s)})\overrightarrow{D}_{s+i-1} = 0 \quad \text{for } i = 1, \ldots, N_r + 1\\
&\sum_{k=N_r-1}^{N_r+4} \underline{T}_k \overrightarrow{D}_k = \overrightarrow{p}_{N_r}\\
&\sum_{k=N_r}^{N_r+5} \underline{T}_k \overrightarrow{D}_k = \overrightarrow{p}_{N_r+1}.
\end{aligned}$$

In order to solve this system, we have to transform it into a band structured set of matrix equations. For this reason we have to eliminate the first two matrix equations in the spirit of *Gauss elimination* yielding the following system of matrix equations:

$$\underline{\alpha}_1 \overrightarrow{D}_4 + \underline{\alpha}_2 \overrightarrow{D}_5 + \underline{\alpha}_3 \overrightarrow{D}_6 = 0 \tag{A.31}$$

$$\underline{\beta}_1 \overrightarrow{D}_4 + \underline{\beta}_2 \overrightarrow{D}_5 + \underline{\beta}_3 \overrightarrow{D}_6 + \underline{\beta}_4 \overrightarrow{D}_7 = 0 \tag{A.32}$$

$$\sum_{s=1}^{5} (\underline{H}_i^{(s)} + \underline{L}_i^{(s)}) \overrightarrow{D}_{s+i-1} = 0 \quad \text{for } i = 4, \ldots, N_r + 1 \tag{A.33}$$

$$\sum_{k=N_r-1}^{N_r+4} \underline{T}_k \overrightarrow{D}_k = \overrightarrow{p}_{N_r} \tag{A.34}$$

$$\sum_{k=N_r}^{N_r+5} \underline{T}_k \overrightarrow{D}_k = \overrightarrow{p}_{N_r+1}. \tag{A.35}$$

For this system we can apply the following ansatz for the unknown vectors $\overrightarrow{D}_i$ (for $i = 1, \ldots, N_r + 5$):

$$\overrightarrow{D}_i = \underline{U}_i \overrightarrow{D}_{i+1} + \underline{Y}_i \overrightarrow{D}_{i+2}, \tag{A.36}$$

Substituting now Eq. (A.36) in the matrix equations of (A.33) we get recursive relations for the matrices $\underline{U}_i$ and $\underline{Y}_i$ which read

$$\underline{U}_i = -\left\{ \left[\underline{O}_{i-2}^{(1)} \underline{U}_{i-2} + \underline{O}_{i-2}^{(2)} \right] \underline{U}_{i-1} + \underline{O}_{i-2}^{(1)} \underline{Y}_{i-2} + \underline{O}_{i-2}^{(3)} \right\}^{-1} \times \tag{A.37}$$

$$\times \left\{ \left[\underline{O}_{i-2}^{(1)} \underline{U}_{i-2} + \underline{O}_{i-2}^{(2)} \right] \underline{Y}_{i-1} + \underline{O}_{i-2}^{(4)} \right\} \tag{A.38}$$

$$\underline{Y}_i = \left\{ \left[\underline{O}_{i-2}^{(1)} \underline{U}_{i-2} + \underline{O}_{i-2}^{(2)} \right] \underline{U}_{i-1} + \underline{O}_{i-2}^{(1)} \underline{Y}_{i-2} + \underline{O}_{i-2}^{(3)} \right\}^{-1} \underline{O}_{i-2}^{(5)}. \tag{A.39}$$

From the matrix equations (A.31) and (A.32) we can define explicitly the matrices $\underline{U}_4$ and $\underline{Y}_4$. Then all the $\underline{U}_i$ and $\underline{Y}_i$ matrices can be calculated from the recursive relations of Eqs. (A.38) and (A.39).

Applying now Eq. (A.36) in the matrix equations (A.34) and (A.35) we can calculate the vectors $\overrightarrow{D}_{N_r+4}$ and $\overrightarrow{D}_{N_r+5}$. Hereafter, with the help of Eq. (A.36) we can calculate all the vectors $\overrightarrow{D}_i$. This allows us to deduce the wave function according to Eq. (A.16). Since the wave function is known over all the mathematical grid we can now calculate the scattering amplitude f for collisions with or without external confinement. This is done by dividing Eqs. (A.25) and (A.26) and solving with respect to the unknown f.

Acknowledgements

First and foremost, I would like to thank and acknowledge my advisor Prof. Peter Schmelcher for introducing me into the field of ultracold atoms and in particular in their collisional aspects. Among other things, Peter has taught me how to think critically about physics and how to pursue creative ideas about my work in a beneficial way both to me and for the scientific community. His encouragement, invaluable advices and ideas provided the necessary ingredients in order to realize this thesis.

I would also like to thank Prof. Vladimir S. Melezhik. It was a pleasure for me to collaborate with Vladimir, who taught me a lot of things regarding physics and in particular for introducing me in the amazing world of numerical methods which constitute the backbone of this thesis. I am also grateful to him and his family for the warm hospitality that they have provided me during my visits in Dubna.

A heartly thank goes to my teacher Prof. Fotis K. Diakonos for his patience, his willingness and his creative intuition in physics which inspired me and taught me how to be an efficient physicist from my undergraduate years until now. Without him this thesis would not have been carried out.

I would also like to thank Prof. Hossein Sadeghpour, for his warm hospitality and stimulated discussions during my visit in ITAMP. I am thankful and grateful to Prof. Panagiotis Kevrekidis for his fruitful discussions on the non-linear partial differential equations and Bose-Einstein condensation, for his comments and for his help.

I am heartly thankful to my friend Christian Morfonios for his unmatched goodness and immense help that he has been providing me these 5 years. I am also thankful to him for teaching me how to perceive the right physical questions, for the endless discussions that we had regarding physics and for the proof reading of this thesis. I would like to thank my friend Yiannis Brouzos for our chess games and for our extended discussions about physics or not. Sincerely I am grateful to Yiannis, Christian, Alexandros Karlis and Marios Tsatsos for supporting me in all difficult moments of these five years.

From here I would like to thank also my colleges Bernd, Mikhael, Florian, Christoph, Stefan, Lushuai, Budha, Markus, Jan, Sven, Benno, Andrea, Thomas, Benjamin, Fabian, Franjeska, Andreas, Alexandra, Simos which I had the honor to meet and made my life more joyful in and out of the office. Especially, I would like to thank Alexandra Zampetaki, Benjamin Hess and Sven Krönke for proof reading my thesis and help me with their wise comments.

Outside the world of physics I had the chance to meet Marko, Yihuee, Marlen, Nina, Magi, Aliki, Efi, Dimitris(x2),Johannes, Angelo, Jasi, Kathrin, Monica, Zaloren, Elina, Nena and many others. I am grateful to these bright people who spared their joy with me. My family has also played a crucial role in the duration of my studies providing me support and encouragement to keep pursuing my dreams and my thoughts. Consequently a simple "thank you" cannot match all these. I owe them everything.

Finally, I would like to thank Eleni for her love and support. She inspires a joy and a confidence that penetrates deeply into my life.

Bibliography

[1] C. J. Pethick and H. Smith, *Bose-Einstein condensation in dilute gases* (Cambridge University Press, 2008); L. Pitaevskii and S. Stringari, *Bose-Einstein Condensation* (Oxford University Press, 2003); F. Dalfovo, S. Giorgini, L. P. Pitaevskii and S. Stringari, Rev. Mod. Phys. **71**, 463 (1999); A. J. Leggett, Rev. Mod. Phys. **73**, 307 (2001).

[2] S. N. Bose, Z. Phys. 26, 178 (1924); A. Einstein, *Sitzungsberichte der Preussischen Akademie der Wissenschaften, Physikalisch-mathematische Klasse* (1924), p. 261; (1925), p. 3.

[3] M. H. Anderson , J. R. Ensher, M. R. Matthews, C. E. Wieman and E. A. Cornell, Science **269**, 198 (1995); C. C. Bradley, C. A. Sackett, J. J. Tollett and R. G. Hulet, Phys. Rev. Lett. **75**, 1687 (1995); K. B. Davis, M.-O. Mewes, M. R. Andrews, N. J. van Druten, D. S. Durfee, D. M. Kurn and W. Ketterle, Phys. Rev. Lett. **75**, 3969 (1995).

[4] C. Chin, R. Grimm, P. Julienne, and E. Tiesinga, Rev. Mod. Phys. **82**, 1225-1286 (2010).

[5] I. Bloch, J. Dalibard and W. Zwerger, Rev. Mod. Phys. **80**, 885 (2008); M. Lewenstein, A. Sanpera, V. Ahufinger, B. Damski, A. Sen and U. Send, Adv. Phys. **56**, 243 (2007). M. Lewenstein, A. Sanpera and V. Ahufinger, *Ultracold Atoms in Optical Lattices: Simulating quantum many-body systems* (Oxford University Press, 2012); K. Bongs and K. Sengstock, Rep. Prog. Phys. **67**, 907 (2004); D. C. McKay and B. DeMarco, Rep. Prog. Phys. **74**, 054401 (2011).

[6] M. A. Cazalilla, R. Citro, T. Giamarchi, E. Orignac and M. Rigol, Rev. Mod. Phys. **83**, 1405 (2011); A. Imambekov, T. L. Schmidt and L. I. Glazman, Rev. Mod. Phys. **84**, 1253-1306 (2012); T. Giamarchi, *Quantum Physics in One Dimension* (Oxford University Press, 2003); E. H. Lieb, R. Seiringer, J. Yngvanson, Commun. Math. Phys. **244**, 347 (2004); E. B. Kolomeisky and J. P. Straley, Rev. Mod. Phys. **68**, 175 (1996);

[7] S. Giorgini, L. P. Pitaevskii and S. Stringari, Rev. Mod. Phys. **80**, 1215 (2008).

[8] L. Tonks, Phys. Rev. **50**, 955 (1936); M. Girardeau, J. Math. Phys. (N.Y.) **1**, 516 (1960); A. Lenard, **7**, 1268 (1966).

[9] M. Olshanii, Phys. Rev. Lett. **81**, 938 (1998).

[10] T. Bergeman, M.G. Moore and M. Olshanii, Phys. Rev. Lett. **91**, 163201 (2003).

[11] T. Kinoshita, T. Wenger and D. S. Weiss, Science **305**, 1125 (2004); B. Paredes, A. Widera, V. Murg, O. Mandel, S. Fölling, I. Cirac, G. V. Shlyapnikov, T. W. Hänsch and I. Bloch, Nature **429**, 277 (2004).

[12] E. Haller, M. Gustavsson, M.J. Mark, J.G. Danzl, R. Hart, G. Pupillo, and H.C. Nägerl, Science **325**, 1224 (2009).

[13] M. G. Moore, T. Bergeman, and M. Olshanii, J. Phys. IV 116, 69 (2004).

[14] S. Saeidian, V.S. Melezhik and P. Schmelcher, Phys. Rev. A **77**, 042721 (2008).

[15] S. Saeidian, V. S. Melezhik, and P. Schmelcher, Phys. Rev. A **86**, 062713 (2012).

[16] V.S. Melezhik and P. Schmelcher, Phys. Rev. A **84**, 042712 (2011).

[17] V. Peano, M. Thorwart, C. Mora, and R. Egger, New J. Phys. **7**, 192 (2005).

[18] S. Sala, P.-I. Schneider and A. Saenz, Phys. Rev. Lett. **109**, 073201 (2012).

[19] S.G. Peng, H. Hu, X.J. Liu and P.D. Drummond, Phys. Rev. A **84**, 043619 (2011).

[20] V.S. Melezhik, and P. Schmelcher, New J. Phys. **11**, 073031 (2009).

[21] J.I. Kim, J. Schmiedmayer, and P. Schmelcher, Phys. Rev. A **72**, 042711 (2005).

[22] P.O. Fedichev, M.J. Bijlsma, and P. Zoller, Phys. Rev. Lett. **92**, 080401 (2004).

[23] X. Cui, Y. Wang, and F. Zhou, Phys. Rev. Lett. **104**, 153201 (2010).

[24] C. Mora, R. Egger, A.O. Gogolin, and A.Komnik, Phys. Rev. Lett. **93**, 170403 (2004).

[25] C. Mora, R. Egger, and A.O. Gogolin, Phys. Rev. A **71**, 052705 (2005).

[26] C. Mora, A. Komnik, R. Egger, and A.O. Gogolin, Phys. Rev. Lett. **95**, 080403 (2005).

[27] D.S. Petrov and G.V. Shlyapnikov, Phys. Rev. A **64**, 012706 (2001).

[28] Z. Idziaszek and T. Calarco, Phys. Rev. Lett. **96**, 013201 (2006).

[29] Y. Nishida, and S. Tan, Phys. Rev. A **82**, 062713 (2010).

[30] C. Zhang, and C. H. Greene, arXiv:1304.8094v1 (2013).

[31] J.I. Kim, V.S. Melezhik, and P. Schmelcher, Phys. Rev. Lett. **97**, 193203 (2006); Rep. Progr. Theor. Phys. Supp. **166**, 159 (2007).

[32] V.S. Melezhik, J.I. Kim, and P. Schmelcher, Phys. Rev. A **76**, 053611 (2007).

[33] B.E. Granger, and D. Blume, Phys. Rev. Lett. **92**, 133202 (2004).

[34] P. Giannakeas, V. S. Melezhik and P. Schmelcher, Phys. Rev. A **84**, 023618 (2011).

[35] P. Giannakeas, V.S. Melezhik, and P. Schmelcher, Phys. Rev. A **85**, 042703 (2012).

[36] P. Giannakeas, F. K. Diakonos and P. Schmelcher, Phys. Rev. A **86**, 042703 (2012).

[37] P. Giannakeas, V.S. Melezhik, and P. Schmelcher, arXiv:1302.5632v1 (2013).

[38] S. Sinha and L. Santos, Phys. Rev. Lett. **99**, 140406 (2007).

[39] T. M. Hanna, E. Tiesinga, W. F. Mitchell, and P. S. Julienne, Phys. Rev. A **85**, 022703 (2012).

[40] E. Haller *et. al.*, Phys. Rev. Lett. **104**, 153203 (2010).

[41] S. Sala, G. Zürn, T. Lompe, A. N. Wenz, S. Murmann, F. Serwane, S. Jochim, and A. Saenz, arXiv:1303.1844v1 (2013).

[42] B. Fröhlich *et al.*, Phys. Rev. Lett. **106**, 105301 (2011).

[43] K. Günter, T. Stoferle, H. Moritz, M. Kohl,T. Esslinger, Phys. Rev. Lett. **95**, 230401 (2005);H. Moritz, T. Stöferle, K. Günter, M. Köhl, and T. Esslinger, Phys. Rev. Lett. **94**, 210401 (2005).

[44] G. Lamporesi, J. Catani1, G. Barontini, Y. Nishida, M. Inguscio, and F. Minardi1, Phys. Rev. Lett. **104**, 153202 (2010).

[45] K.-K. Ni *et. al.*, Science **322**, 231 (2008).

[46] S. Ospelkaus *et. al.*, Phys. Rev. Lett. **104**, 030402 (2010).

[47] S. Ospelkaus *et. al.*, Science **327**, 853 (2010).

[48] L.D. Landau and E.M. Lifshitz, *Quantum Mechanics, Course of Theoretical Physics, Volume 3* (Pergamon Press, Oxford, 1977).

[49] J.R. Taylor, *Scattering Theory: The Quantum Theory of Nonrelativistic Collisions* (Dover Publications, Inc., New York, 1972).

[50] H. Friedrich, *Theoretical Atomic Physics* (Springer, Heidelberg, 1994).

[51] C. Cohen-Tannoudji and D. Guéry-Odelin, *Advances in Atomic Physics: An Overview* (World Scientific Publishing, Singapore, 2011).

[52] A.G. Sitenko, *Scattering Theory* (Springer-Verlag, Heidelberg, 1991).

[53] P.G. Burke, *R-matrix Theory of Atomic Collisions* (Springer-Verlag, Heidelberg, 2011).

[54] J.M. Blatt, J.D. Jackson, Phys. Rev. **76**, 18 (1949).

[55] H.A. Bethe, Phys. Rev. **76**, 38 (1949).

[56] B. Gao, Phys. Rev. A **80**, 012702 (2009).

[57] U. Fano, Nuovo Cimento **12**, 154-161 (1935).

[58] U. Fano, Phys. Rev. **124**, 1866 (1961).

[59] U. Fano, G. Pupillo, A. Zannoni, and C. W. Clark, J. Res. Natl. Inst. Stand. Technol. **110**, 583-587 (2005).

[60] H. Feshbach, Ann. Phys.(N.Y.) **5**, 357-390 (1958).

[61] H. Feshbach, Ann. Phys.(N.Y.) **19**, 287-313 (1962).

[62] S. Inouye, M.R. Andrews, J. Stenger, H.-J. Miesner, D.M. Stamper-Kurn, and W. Ketterle, Nature **392**, 151 (1998).

[63] M. Theis, G. Thalhammer, K. Winkler, M. Hellwig, G. Ruff, R. Grimm, and J.H. Denschlag, Phys. Rev. Lett. **93**, 123001 (2004).

[64] T. Köhler, K. Góral and P.S. Julienne, Rev. Mod. Phys. **78**, 1311 (2006).

[65] H. Bethe and R. Peierls, Proc. R. Soc. A **148**, 146 (1935).

[66] J. Dalibard, "Collisional dynamics of ultra-cold atomic gases", in *Bose-Einstein Condensation in Gases*, ed. M. Inguscio, S. Stringari, and C.E. Wieman, pp. 321-349 (IOS Press, Amsterdam, 1999).

[67] E. Fermi, Nuovo Cimento, **11**, 157 (1934).

[68] K. Huang and C. N. Yang, Phys. Rev. **105**, 767 (1957).

[69] K. Huang, *Statistical Mechanics*, (John Wiley & Sons, New York, 1963).

[70] V. A. Yurovski, M. Olshanii and D.S. Weiss, *Collisions, Correlations, and Integrability in Atom Waveguides*, Advances in Atomic, Molecular, and Optical Physics, **55**, 61 (2008).

[71] V. Dunjko, M. G. Moore, T. Bergeman, and M. Olshanii, Confinement-Induced Resonances, Advances in Atomic, Molecular, and Optical Physics, **60**, 461 (2011).

[72] E. Tiesinga, C.J. Williams, F.H. Mies, and P.S. Julienne, Phys. Rev. A **61**, 063416 (2000).

[73] C. Ticknor, C.A. Regal, D.S. Jin, and J.L. Bohn, Phys. Rev. A **69**, 042712 (2004).

[74] A. M. Rey, R. Sensarma, S. Fölling, M. Greiner, E. Demler, and M. D. Lukin, Europhys. Lett. **87**, 60001 (2009).

[75] B. Deb and J. Hazra, Phys. Rev. Lett. **103**, 023201 (2009).

[76] W. Hofstetter, J. I. Cirac, P. Zoller, E. Demler, and M. D. Lukin, Phys. Rev. Lett. **89**, 220407 (2002).

[77] V.S. Melezhik, J. Comput. Phys. **92**, 67 (1991).

[78] Carl de Boor, *A Practical Guide to Splines*, Springer (1978).

[79] E.T.Y. Lee, Computing **29**, 365 (1982).

[80] A. Derevianko, J.F. Babb, A. Dalgarno, Phys. Rev. A **63**, 052704 (2001).

[81] S.G. Porsev and A. Derevianko, Phys. Rev. A **65**, 020701(R) (2002).

[82] R. Stock, A. Silberfarb, E.L. Bolda, and I.H. Deutsch, Phys. Rev. Lett. **94**, 023202 (2005).

[83] B.E. Londono, J.E. Mahecha, E. Luc-Koenig, and A. Crubellier, Phys. Rev. A **82**, 012510 (2010).

[84] M. Marinescu, Phys. Rev. A **50**, 3177 (1994).

[85] T. Busch, B.-G. Englert, K. Rzazewski, and M. Wilkens, Found. Phys. **28**, 549 (1998).

[86] A. Derevianko, Phys. Rev. A **72**, 044701 (2005).

[87] Z. Idziaszek, Phys. Rev. A **79**, 062701 (2009).

[88] F. Stampfer and P. Wagner, J. Math. Anal. Appl. **342**, 202 (2008).

[89] L. Pricoupenko, Phys. Rev. Lett. **96**, 050401 (2006).

[90] K. Huang, Int. J. Mod. Phys. A **4**, 1037 (1989).

[91] Y. N. Demkov and G. F. Drukarev, Sov. Phys. JETP **54**, 650 (1981).

[92] M. V. Frolov, N.L. Manakov, E. A. Pronin, and A. F. Starace, Phys. Rev. Lett. **91**, 053003 (2003).

[93] D. Blume, and C.H. Greene, Phys. Rev. A **65**, 043613 (2002).

[94] E. L. Bolda, E. Tiesinga, and P. S. Julienne, Phys. Rev. A **66**, 013403 (2002).

[95] T. M. MacRobert, *Spherical Harmonics*, (Dover Publications, New York, 1948).

[96] T. M. Apostol, *The American Mathematical Monthly*, Vol. 106, No. 5, 409-418 (1999).

[97] C. Chin *et al.*, Phys. Rev. A **70**, 032701 (2004).

[98] M. Mark *et al.*, Phys. Rev. A **76**, 042514 (2007).

[99] J.P. Connerade, *Highly Excited Atoms* (Cambridge University Press, 1998).

[100] D. Harmin, Phys. Rev. Lett. **49**, 128 (1982).

[101] D. Harmin, Phys. Rev. A **26**, 2656 (1982); Comments At. Mol. Phys. **15**, 281 (1985).

[102] U. Fano, Phys. Rev. A **24**, 619 (1981).

[103] C. H. Greene, Phys. Rev. A **36**, 4236 (1987).

[104] I.S. Gradshteyn and I.M. Ryzhik, *Table of Integrals, Series, and Products*, 4th ed. (Academic, New York, 1965).

[105] M. Aymar, C.H. Greene, and E. Luc-Koenig, Rev. Mod. Phys. **91**, 1015 (1996).

[106] K.S. Miller, Mathematics Magazine **54**, 67 (1981).

[107] A. Imambekov, A.A. Lukyanov, L.I. Glazman, and V. Gritsev, Phys. Rev. Lett. **104**, 040402 (2010).

[108] G. Alber and P. Zoller, Phys. Rep. **199**, 231 (1991).

[109] *Handbook of Mathematical Functions*, M. Abramowitz and I.E. Stegun (Department of Commerce, Washington, DC, 1972), 10th ed.

[110] *Multi-channel Computations in Low-Dimensional Few-Body Physics*, V. S. Melezhik, Lecture Notes in Computer Science, 2012, Volume 7125, Mathematical Modeling and Computational Science, Pages 94-107.

[111] M. Marinescu, L. You, Phys. Rev. Lett. **81**, 4596 (1998).

[112] V. S. Melezhik, and Chi-Yu Hu, Phys. Rev. Lett. **90**, 083202 (2003).

[113] C. Ticknor, Phys. Rev. Lett. **100**, 133202 (2008).

[114] Y. Wang and C.H. Greene, Phys. Rev. A **85**, 022704 (2012).

[115] J. L. Bohn, M. Cavagnero, and C. Ticknor, New J. Phys. **11**, 055039 (2009).

[116] B. Deb, and L. You, Phys. Rev. A **64**, 022717 (2001).

[117] V. Roudnev and M. Cavagnero, Phys. Rev A **79**, 014701 (2009).

[118] V. Roudnev and M. Cavagnero, J. Phys. B **42**, 044017 (2009).

[119] S. Yi and L. You, Phys. Rev. A **63**, 053607 (2001).

[120] M. Baranov, Phys. Rep. **464**, 71 (2008).

[121] M. L. Wall, L. D. Carr, arXiV: 1303.1230 (2013).

[122] H.P. Bücler, E. Demler, M. Lukin, A. Micheli, N. Prokof'ev, G. Pupillo, and P. Zoller, Phys. Rev. Lett. **98**, 060404 (2007).

[123] K. Kanjilal, and D. Blume, Phys. Rev. A **78**, 040703(R) (2008).

[124] K. Kanjilal, J. L. Bohn, and D. Blume, Phys. Rev. A **75**, 052705 (2007).

[125] C. Ticknor, Phys. Rev. A **81**, 042708 (2010).

[126] J. P. D'Incao, and C. H. Greene, Phys. Rev. A **83**, 030702(R) (2011).

[127] P. Pedri *et al.*, Phys. Rev. A **77**, 015601 (2008).

[128] A. Derevianko, S. G. Porsev, S. Kotochigova, E. Tiesinga, and P.S. Julienne, Phys. Rev. Lett. **90**, 063002 (2003).

[129] M. Lu *et al.*, Phys. Rev. Lett. **107**, 190401 (2011).

[130] K. Aikawa, A. Frisch, M. Mark, S. Baier, A. Rietzler, R. Grimm, and F. Ferlaino, Phys. Rev. Lett. **108**, 210401 (2012).

[131] V.S. Melezhik, J. Comp. Phys. **92**, 67 (1991).

[132] C. Ticknor, C.A. Regal, D.S. Jin, and J.L. Bohn, Phs. Rev. A **69**, 0421712 (2004).

[133] B.P. Ruzik, C.H. Greene, and J.L. Bohn, Phys. Rev. A **87**, 032706 (2013).